Reaction Engineering Characterization of Biocatalytic Organoborane Synthesis

Vom Promotionsausschuss der
Technischen Universität Hamburg

zur Erlangung des akademischen Grades

Doktor-Ingenieur (Dr.-Ing.)

genehmigte Dissertation

von
Jens Hennig

aus
Hagen

2023

1. Gutachter:	Prof. Dr. rer. nat. Andreas Liese
2. Gutachter:	Prof. Dr.-Ing. Ralf Pörtner
Prüfungsvorsitz:	Prof. Dr.-Ing. Michael Schlüter

Tag der mündlichen Prüfung: 21.11.2022

ORCID-iD (Jens Hennig): https://orcid.org/0000-0003-1186-1976
DOI: https://doi.org/10.15480/882.8633

Acknowledgements

First of all, I would like to express my gratitude to Prof. Andreas Liese for his valuable supervision and unconditional support and trust as well as for the opportunity to do my PhD in his institute. His commitment to interdisciplinary collaboration and teamwork has been a constant inspiration to me.

I would like to thank Prof. Ralf Pörtner for reviewing my thesis as second examiner as well as for the possibility to use the DASGIP reactors. Furthermore, I would like to thank Prof. Michael Schlüter for chairing the examination.

I would like to thank Dr. Ayad Dawood for his supervision as group leader and versatile and fruitful discussions.

I am truly grateful to the entire ITB team for any kind of support, cordial interaction and the everlasting joy in research and collaboration.

Special gratitude to Hassan Raza, Kyungjoo Park, and Saskia Klinger for their extraordinary cooperation and tireless efforts in the lab during their theses.

Furthermore, I would like to thank Lena Wriede, Eric Guachamin, Jeremy Elizaga, Loredana Perbandt, and Ragna Baur for their important hands-on support during their internships.

Great thanks are also due to Prof. Frances Arnold, Dr. Xiongyi Huang, Dr. Sabine Brinkmann-Chen, Dr. Nicholas Porter and Dr. Kari Hernandez for providing the enzyme variant Rma cytc BOR^{R1}, versatile discussions and scientific exchange and support.

In particular, I would like to thank Marlene, Daniela and Johannes for reviewing this thesis including valuable critics and helpful comments.

The deepest gratitude, however, belongs to my family, especially my parents, my grandparents as well as Thorben and Lea, for their unconditional, sacrificial support, motivation and love. Without them, the path to completing this thesis would not have been possible and I would not have been the person I am today. This is for you.

Per aspera ad astra.

Abstract

Organoboranes (OBs) are characterized by a heteroatomic carbon-boron bond, that provides these compounds with beneficial chemical properties. Thus, they are widely spread platform chemicals, serving as precursors for applications in nowadays pharmacy, agriculture and organic chemistry. Although different synthesis routes are applied industrially, all of them are dealing with limitations as being environmentally hazardous and enantioselectively hindered. Recently, a promising heme-enzyme based technique for biocatalytic OB synthesis was presented, which demands for expanded research to establish an efficient alternative for a green OB production.

This thesis presents multi-disciplinary developments of the promising approach of biocatalytic borylation driven by cytochrome c (Cytc) harboured in *E. coli*. The heme-enzyme catalyzes the model reaction of a *N*-heterocyclic carbene borane (NHCB) and the diazo compound ethyl 2-diazopropanoate (DAC) towards the corresponding OB product. Therefore, crucial substrate properties were studied to locate suitable operation windows regarding pH and temperature. Tests quantified the decay of DAC under the influence of temperature and UV-light as well as its hydrolysis in water. Those results enabled a kinetic characterization to describe the reaction kinetics by setting up a mathematical model derived from the Michaelis-Menten theory. Here, based on experimental data, a numerical fitting with non-linear regression in Matlab calculated the kinetic parameters v_{max}, $K_{m,NHCB}$, $K_{m,DAC}$, $K_{i,NHCB}$ and K_{dea}. The evaluation of the overall substrate-surplus inhibited double-substrate Michaelis-Menten model was executed with a simulation of the reaction process and its comparison with experimental data. To overcome found reversible and irreversible substrate inhibitions, a reaction engineering investigation tested different operation modes. Moreover, these studies additionally targeted the enhancement of the process parameters space-time yield, total turnover number and product concentration, to develop further benefits of the heme-driven synthesis compared to its chemical counterparts. Mentioning only one result, the product concentration was multiplied to a multi-gram-scale.

Concluding, this thesis gives close insights into the development of a novel biocatalytic reaction by kinetic characterization as well as reaction engineering, guiding this greener approach to an industrially relevant alternative.

Kurzfassung

Organoborane (OBs) zeichnen sich durch eine heteroatomare Kohlenstoff-Bor-Bindung aus, die diesen Verbindungen vorteilhafte chemische Eigenschaften verleiht. Daher sind sie weit verbreitete Plattformchemikalien, die als Vorstufen für Anwendungen in der heutigen Pharmazie, Landwirtschaft und organischen Chemie dienen. Obwohl verschiedene Synthesewege industriell genutzt werden, haben alle mit Einschränkungen zu kämpfen, da sie umweltschädlich sind und die Enantioselektivität beeinträchtigen. Kürzlich wurde eine vielversprechende, auf Häm-Enzymen basierende Technik für die biokatalytische OB-Synthese vorgestellt, die weitere Forschung erfordert, um eine effiziente Alternative für eine umweltfreundliche OB-Produktion zu schaffen.

In dieser Arbeit werden vielseitige Weiterentwicklungen des vielversprechenden Ansatzes der biokatalytischen Borylierung mit Hilfe von Cytochrom c (Cytc) in *E. coli* vorgestellt. Das Häm-Enzym katalysiert die Modellreaktion eines *N*-heterozyklischen Carbenborans (NHCB) und der Diazoverbindung Ethyl-2-diazopropanoat (DAC) zum entsprechenden OB-Produkt. Hierfür wurden entscheidende Substrateigenschaften untersucht, um geeignete Betriebsbereiche hinsichtlich pH-Wert und Temperatur zu finden. In Tests wurde der Zerfall von DAC unter dem Einfluss von Temperatur und UV-Licht sowie seine Hydrolyse in Wasser quantifiziert. Diese Ergebnisse ermöglichten eine kinetische Charakterisierung zur Beschreibung der Reaktionskinetik durch Aufstellung eines mathematischen Modells, welches von der Michaelis-Menten-Theorie abgeleitet wurde. Auf der Grundlage der experimentellen Daten wurden durch eine numerische Anpassung mit nichtlinearer Regression in Matlab die kinetischen Parameter v_{max}, $K_{m,NHCB}$, $K_{m,DAC}$, $K_{i,NHCB}$ und K_{dea} berechnet. Die Bewertung des gesamten Substratüberschuss-inhibierten Doppelsubstrat-Michaelis-Menten-Modells wurde mit einer Simulation des Reaktionsprozesses im Vergleich zu experimentellen Daten durchgeführt. Um die gefundenen reversiblen und irreversiblen Substrathemmungen zu überwinden, wurden in einer reaktionstechnischen Untersuchung verschiedene Betriebsmodi getestet. Darüber hinaus zielten diese Studien auf die Verbesserung der Prozessparameter Raum-Zeit-Ausbeute, Gesamtumsatzzahl und Produktkonzentration ab, um weitere Vorteile der Häm-getriebenen Synthese im Vergleich zu ihren chemischen Pendants zu entwickeln. Um nur ein Ergebnis zu nennen: Die Produktkonzentration konnte auf eine Multi-Gramm-Skala vervielfacht werden.

Zusammenfassend lässt sich sagen, dass diese Arbeit einen Einblick in die Entwicklung einer neuartigen biokatalytischen Reaktion durch kinetische Charakterisierung sowie Reaktionstechnik gibt und diesen umweltfreundlicheren Ansatz zu einer industriell relevanten Alternative macht.

Contents

1 Introduction and Theoretical Background **1**

1.1 Organoboranes - Properties and Applications . . . 3
1.1.1 Chemical Synthesis Routes . . . 4
1.1.2 Alternative Synthesis Routes - Help from Nature? . . . 6
1.1.2.1 Cytochrome c Driven Biocatalytic Borylation . . . 7
1.2 Kinetic Characterization . . . 11
1.2.1 Michaelis-Menten Theory . . . 12
1.2.2 Inhibitions . . . 14
1.2.3 Kinetic Parameter Estimation . . . 14
1.3 Reaction Engineering . . . 15
1.3.1 Operation Modes . . . 16
1.4 Aim of the Thesis . . . 19

2 Materials and Methods **21**

2.1 Chemicals . . . 21
2.2 Buffers, Stocks and Media . . . 21
2.2.1 Buffers . . . 21
2.2.2 Stock Solutions . . . 22
2.2.3 Cultivation Media . . . 23
2.3 Strains and Plasmids . . . 23
2.4 Cultivation . . . 24
2.5 Cytochrome c Purification . . . 24
2.6 Cytochrome c Immobilization . . . 24
2.7 *N*-Heterocyclic Carbene Borane Synthesis . . . 25
2.8 Chemical Organoborane Synthesis . . . 26
2.9 Biocatalytic Organoborane Synthesis . . . 26
2.9.1 Batch Mode . . . 26
2.9.2 Fed-Batch Mode . . . 27
2.9.3 Continuous Mode . . . 28
2.10 Analytics . . . 29
2.10.1 Cell Concentration . . . 29
2.10.2 Cytochrome c Concentration . . . 29
2.10.3 Protein Concentration . . . 30
2.10.4 Protein Mass . . . 30
2.10.5 Substrate and Product Concentration . . . 30

2.11 Calculations 32

3 Results **33**

3.1 Starting Material Investigation 33
3.1.1 *N*-Heterocyclic Carbene Borane 33
3.1.2 Ethyl 2-Diazopropanoate 35
3.1.2.1 Hydrolysis 35
3.1.2.2 Water-Induced Decay 36
3.1.2.3 Temperature-Induced Decay 38
3.1.2.4 UV-Light-Induced Decay 41
3.2 Kinetic Characterization 42
3.2.1 Temperature Screening 42
3.2.2 pH Screening 44
3.2.3 Determination of Kinetic Parameters 46
3.2.3.1 Michaelis-Menten Kinetics 46
3.2.3.2 Inhibition and Deactivation Studies 51
3.2.3.3 Reaction Simulation for Parameter Evaluation 54
3.3 Reaction Engineering 57
3.3.1 Batch Mode 57
3.3.1.1 Application of Cytc 57
3.3.1.2 Varying Cytc Concentration 59
3.3.2 Fed-Batch Mode 61
3.3.2.1 Varying Cytc Concentration 62
3.3.2.2 Supplementation With Glucose 66
3.3.2.3 Scale-Up to 150 mL 67
3.3.2.4 Scale-Up to 500 mL 72
3.3.3 Continuous Mode 77
3.3.3.1 CSTR Characterization 77
3.3.3.2 Continuous OB Synthesis 80
3.3.4 Process Parameter Comparison 82

4 Discussion and Outlook **85**

4.1 Starting Material Investigation 85
4.2 Kinetic Characterization 86
4.3 Reaction Engineering 91

5 Summary **98**

6 Supplementary Information **100**

6.1 Materials and Methods 100

6.2 Results 101

6.3 Discussion and Outlook 105

List of Figures

1.1 Applications of OB in different fields of modern industry. 2
1.2 Chemical OB synthesis routes. 4
1.3 Natural occurring boron-containing antibiotics based on boric acid 6
1.4 Cytc catalyzed model reaction of biocatalytic borylation for OB synthesis . . 8
1.5 Final OB products of via enzyme-driven biocatalytic borylation with Cytc BOR^{R1} based on varying structures for NHCB and DAC 10
1.6 Deactivation mechanism of heme-harbouring P450 by DAC. 11
1.7 Main operation modes used in biochemical and chemical engineering shown for a stirred tank reactor. 17

2.1 Experimental setup for small scale biocatalytic OB synthesis 27
2.2 Experimental setup for small scale biocatalytic OB synthesis in fed-batch mode. 28
2.3 Experimental setup for small scale biocatalytic OB synthesis in continuous mode. 29
2.4 Calibration curves of NHCB and OB for GC analysis and the applied temperature profile with typical retention times. 31

3.1 Titration of NHCB with HCl 34
3.2 pH change due to addition of pure MeCN (A) or MeCN with DAC in phosphate buffer. 36
3.3 EL formation over time in phosphate buffer under anaerobic conditions. . . . 37
3.4 Absorption spectra of DAC recorded with UV-Vis spectrophotometry and the calibration based on peak height at λ_{max}. 38
3.5 Absorption spectra of DAC recorded with UV-Vis spectrophotometry to identify diazo group specific absorption peaks in the UV range. 39
3.6 Change of absorption spectra of DAC recorded with UV-Vis spectrophotometry in the fingerprint-region due to decomposition caused by incubation at elevated temperatures. 40
3.7 Change of absorption spectra of DAC recorded with UV-Vis spectrophotometry in fingerprint-region due to decomposition caused by incubation under UV-light. 41
3.8 Temperature screening for Cytc BOR^{R1} hosted in *E. coli* BL21 DE3 catalyzing biocatalytic borylation. 43
3.9 PH screening for Cytc BOR^{R1} hosted in *E. coli* BL21 DE3 catalyzing biocatalytic borylation. 45

3.10 Michaelis-Menten plots for biocatalytic borylation for NHCB and DAC, catalyzed by Cytc BOR^{R1} harboured in *E. coli* BL21 DE3. 47
3.11 Numerically fitted Michaelis-Menten plots for biocatalytic borylation catalyzed by Cytc BOR^{R1} harboured in *E. coli* BL21 DE3 for NHCB and DAC, based on experimental data to determine kinetic parameters v_{max}, $K_{m,NHCB}$, $K_{m,DAC}$ and $K_{i,NHCB}$. 48
3.12 Ratio of numerically fitted $K_{i,NHC}$ and $K_{m,NHC}$ as wells as K_{cat} for biocatalytic borylation catalyzed by Cytc BOR^{R1} harboured in *E. coli* BL21 DE3. 50
3.13 Influence of pre-incubation with DAC and NHCB on the initial reaction rate of biocatalytic borylation catalyzed by Cytc BOR^{R1} harboured in *E. coli* BL21 DE3. 52
3.14 Influence of different OB contents on the initial reaction rate of biocatalytic borylation catalyzed by Cytc BOR^{R1} harboured in *E. coli* BL21 DE3. 53
3.15 Simulation of biocatalytic OB synthesis catalyzed by Cytc BOR^{R1} harboured in *E. coli* BL21 DE3 according to numerically estimated kinetic parameters. 55
3.16 Simulation of biocatalytic OB synthesis catalyzed by Cytc BOR^{R1} harboured in *E. coli* BL21 DE3 according to manually adapted kinetic parameters. . . . 56
3.17 Product formation of biocatalytic OB synthesis catalyzed by Cytc BOR^{R1} as free enzyme or immobilized on silica beads compared to Cytc in whole cells in batch mode. 58
3.18 Product formation of biocatalytic OB synthesis catalyzed by Cytc BOR^{R1} harboured in *E. coli* BL21 DE3 at OD 5 and OD 15 in batch mode. 59
3.19 Process parameters OB_{final} and TTN in dependence of Cytc concentration of biocatalytic OB synthesis catalyzed by Cytc BOR^{R1} harboured in *E. coli* BL21 DE3 at OD 5, 15 and 30 in batch mode. 61
3.20 OB_{final} in dependence of the dilution rate for biocatalytic OB synthesis catalyzed by Cytc BOR^{R1} harboured in *E. coli* BL21 DE3 at OD 5 in fed-batch mode. 63
3.21 OB_{final} in dependence of the dilution rate for biocatalytic OB synthesis catalyzed by Cytc BOR^{R1} harboured in *E. coli* BL21 DE3 at OD 15 in fed-batch mode. 64
3.22 OB_{final} in dependence of the dilution rate for biocatalytic OB synthesis catalyzed by Cytc BOR^{R1} harboured in *E. coli* BL21 DE3 at OD 30 in fed-batch mode. 65

3.23 TTN in dependence of the dilution rate for biocatalytic OB synthesis catalyzed by Cytc BOR^{R1} harboured in *E. coli* BL21 DE3 at different ODs in fed-batch mode. 66
3.24 OB_{final} and TTN in dependence of the dilution rate for biocatalytic OB synthesis catalyzed by Cytc BOR^{R1} harboured in *E. coli* BL21 DE3 at OD 5 in fed-batch mode with additional glucose. 67
3.25 OB formation as function of time in biocatalytic borylation catalyzed by Cytc BOR^{R1} harboured in *E. coli* BL21 DE3 at OD 5 in fed-batch mode in with 150 mL reaction volume. 68
3.26 OB formation over time in biocatalytic borylation catalyzed by Cytc BOR^{R1} harboured in *E. coli* BL21 DE3 at OD 15 in fed-batch mode in with 150 mL reaction volume. 69
3.27 OB formation over time in biocatalytic borylation catalyzed by Cytc BOR^{R1} harboured in *E. coli* BL21 DE3 at OD 30 in fed-batch mode in with 150 mL reaction volume. 70
3.28 OB formation over time in biocatalytic borylation catalyzed by Cytc BOR^{R1} harboured in *E. coli* BL21 DE3 at OD 30 in fed-batch mode in with 150 mL reaction volume and a substrate concentration of 20 mM. 71
3.29 OB formation over time in biocatalytic borylation catalyzed by Cytc BOR^{R1} harboured in *E. coli* BL21 DE3 at OD 5 in fed-batch mode in with 500 mL reaction volume. 73
3.30 OB formation over time in biocatalytic borylation catalyzed by Cytc BOR^{R1} harboured in *E. coli* BL21 DE3 at OD 30 in fed-batch mode in with 500 mL reaction volume and a substrate concentration of 20 mM. 74
3.31 OB formation over time in biocatalytic borylation catalyzed by Cytc BOR^{R1} harboured in *E. coli* BL21 DE3 at OD 30 in fed-batch mode in with 500 mL reaction volume and a substrate concentration of overall 40 mM. 75
3.32 Specific molar OB synthesis depending on different activity loadings. 76
3.33 Cumulative RTD of a CSTR with NHCB as tracer as a jump function at the reactor inlet to determine the residence time τ. 78
3.34 Cumulative RTD of a CSTR for different dilution rates with NHCB as tracer as a jump function at the reactor inlet. 79
3.35 Conversion of NHCB to OB for different τ for biocatalytic borylation catalyzed by Cytc BOR^{R1} harboured in *E. coli* BL21 DE3 at OD 5 in a CSTR depending on the number of residence times θ. 80

3.36 Molar OB synthesis n_{OB} and STY for different τ for biocatalytic borylation catalyzed by Cytc BOR^{R1} harboured in *E. coli* BL21 DE3 at OD 5 in a CSTR depending on the number of residence times θ. 81
3.37 Evolution of OB_{final} and TTN within this thesis for biocatalytic borylation catalyzed by Cytc BOR^{R1} harboured in *E. coli* BL21 DE3. 83

4.1 Presumable plots of experimental data for the determination of a mathematical expression of K_{dea} in dependency of DAC content. 90
4.2 Derivation of optimal operating points of substrate concentrations for biocatalytic borylation in a CSTR. 95

6.1 Plasmid card of pEC86 with Cytc maturation genes ccmABCDEFGH and a Chl-resistance. 100
6.2 DASGIP reactor setup for biocatalytic borylation in 150 mL and 500 mL scale. 100
6.3 Calibration curve of EL for GC analysis. 101
6.4 Mixing time in dependence of stirrer revolutions in a 500 mL DASGIP reactor. 105
6.5 ^{1}H-NMR spectra of OB synthesized at the Institute of Technical Biocatalysis. 106
6.6 ^{1}H-NMR spectra of OB synthesized at the California Institute of Technology. 107
6.7 ^{1}H-NMR spectra of NHCB synthesized at the Institute of Technical Biocatalysis. 108
6.8 Flowchart of a desired continuous process for biocatalytic borylation of OB. . 109
6.9 Expression of Cytc BOR^{R1} in *E. coli* BL21 DE3 under presence of either DAC, NHCB or MeCN. 109

List of Tables

2.1 Composition of the M9-N buffer for OB synthesis. 21
2.2 Composition of buffers for affinity chromatography. 21
2.3 Composition of SDS running-buffer. 22
2.4 Antibiotica stocks 22
2.5 Inducer stocks 22
2.6 Substrate stocks 23

3.1 Numerically estimated kinetic parameters for Cytc-driven biocatalytic borylation. 49
3.2 Overview of all collected data of reaction engineering experiments for biocatalytic borylation. 84

6.1 Ratio of peak heights of $\lambda_{DAC,1}$ and $\lambda_{DAC,12}$ for different temperatures within fingerprint region of DAC in UV-spectroscopy. 101

List of Symbols

Symbol	Unit	Parameter
$\oslash_i$	mm	inner diameter
D	h^{-1}	dilution rate
$\varepsilon_{550-535}$	$mM^{-1}{\cdot}cm^{-1}$	extinction coefficient for Cytc
θ	-	number of residence times
$\lambda_{DAC,1}$	nm	primary fingerprint wavelenght of DAC
$\lambda_{DAC,2}$	nm	secondary fingerprint wavelenght of DAC
λ_{max}	nm	wavelength with maximum absorption
τ	min	residence time
E	-	free enzyme Cytc
EP	-	enzyme-product complex
EP_2	-	enzyme-secondary-product complex (Cytc-OB)
ES	-	enzyme-substrate complex
ES_1	-	enzyme-primary-substrate complex (Cytc-DAC)
F	-	activated enzyme (Cytc-carbene)
FP_1	-	activated enzyme-primary-product complex (Cytc-carbene-N_2)
FS_2	-	activated enzyme-secondary-substrate complex (Cytc-carbene-NHCB)
K_i	mM	inhibition constant
$K_{i,NHCB}$	mM	inhibition constant for NHCB
K_m	mM	Michaelis-Menten constant
$K_{m,DAC}$	mM	Michaelis-Menten constant for DAC

$K_{m,NHCB}$	mM	Mmichaelis-Menten constant for NHCB
M_{Cytc}	g·mol^1	molar mass of Cytc
M_{OB}	g·mol^1	molar mass of OB
OB_{final}	mM	final OB concentration
P	-	free product
P_1	-	primary free Product (N_2)
P_2	-	secondary free Product (OB)
Q	$L \cdot h^{-1}$	feed rate
T	°C	temperature
t_{Feed}	min	feed time
$t_{Incubation}$	min	incubation time
$t_{Reaction}$	min	reaction time
V_{Feed}	L	feed volume
$V_{Reaction}$	L	reaction volume
S	-	free substrate
S_1	-	primary free substrate (DAC)
S_2	-	secondary free substrate (NHCB)
v	$U \cdot mg_{Cytc}^{-1}$	reaction rate
v_{max}	$U \cdot mg_{Cytc}^{-1}$	maximum reaction rate

Abbreviations

AC	Affinity chromatography
5-ALA	5-Aminolevulinic acid
Amp	Ampicillin
Ar	Argon (molecular)
$CaCl_2$	Calcium cloride
CFE	Cell free extract
Chl	Chloramphenicol
Cytc	Cytochrome c
DAC	Ethyl-2-diazopropanoate
DI	Deionized
DO	Dissolved oxygen
DOE	Design of experiments
FPCP	French pressure cell press
GC	Gas chromatography
H_2	Hydrogen (molecular)
HB	Hyper broth
IPTG	Isopropyl β-D-1-thiogalactopyranoside
KH_2PO_4	Monopotassium phosphate
LB	Lysogeny broth
MeCN	Acetonitrile
$MgSO_4$	Magnesium sulfate
N_2	Nitrogen (molecular)
Na_2HPO_4	Disodium phosphate
NaCl	Sodium cloride
NHCB	*N*-Heterocyclic carbene borane
Ni-NTA	Nickel-nitrilotriacetic acid
OB	Organoborane
OB_{final}	Final organoborane concentration
r.t.	Room temperature
RTD	Residence time distribution

SDS-PAGE	Sodium dodecyl sulfate polyacrylamide gel electrophoresis
STY	Space-time yield
TMB	1,2,3-Trimethoxybenzene
TTN	Total turnover number

1 Introduction and Theoretical Background

Biotechnology has been applied by mankind, even if unknown, already thousands of years ago [1]. Since then microorganisms and enzymes facilitated the production of bread and alcoholic beverages like beer and wine, which built the foundation for the modern industrial processes [1, 2]. Nowadays, the industrial utilization of biotechnology ranges from fine chemicals synthesis for pharmaceuticals, over cosmetics and food to the processing of sustainable energy sources like biogas and hydrogen [3, 4, 5, 6].

Biotechnological processes are considered to be particularly future-oriented, due to the increasing interest in sustainability to preserve our planet and to reduce the anthropogenic pressure on nature [7]. Moreover, they shall pave the way to a climate-neutral economy [8]. Therefore, biotechnological processes state an essential contributor to meet the sustainable development goals 12 and 13 by the United Nations to "ensure sustainable consumption and production patterns" and to "combat climate change and promoting developments into renewable energy" [9].

One important step towards these goals is to exchange aged, fossil fuel driven and environmentally offensive chemical syntheses with bio-based approaches [10]. Here, biocatalytic processes deliver important benefits in contrast to their chemical analogues. The utilization of renewable raw materials and waste-streams support a circular economy and efficient biocatalysts provide outstanding catalytic performance under mild reaction conditions to reduce the energy consumption and waste production [11, 10]. Engines of those biocatalytic processes are enzymes, which are expressed in microorganisms and catalyze a diverse repertoire of reactions with remarkable enantio-, regio- and chemoselectivity [12, 13]. Thus, these biomolecules embody the most important ingredient for the replacement of chemical processes.

An important example for environmentally offensive syntheses is the chemical production of organoboranes (OBs) or organoborane compounds. These building blocks are characterized by a carbon-boron heteroatomic bond, that provides them with advantageous chemical properties to state OBs as multifaceted tool in present organic chemistry [14, 15]. Particularly organoboronic acids and organoboronic esters are required frequently with an annual tonnage of tens of metric tons as building blocks for applications in pharmacy, agriculture and organic chemistry [16, 17, 18](Fig. 1.1). Although their synthesis is well established, it is associated with heavy metal contaminations and a meagre selectivity for more complex OB products [19, 20]. Thus, chemical OB synthesis offers a good target to exchange an

environmentally questionable chemical process with green enzyme-driven sustainability and precision.

Initial steps have already been taken along this path with heme enzymes, which have yielded promising results towards selectivity and moles of OB formed per mole biocatalyst, known as total turnover number (TTN) [21]. However, this approach was only demonstrated in an analytical scale and with low final product concentrations. Therefore, further research is needed to guide the novel approach of biocatalytic borylation on the way towards an industrially relevant alternative for a green synthesis of OBs.

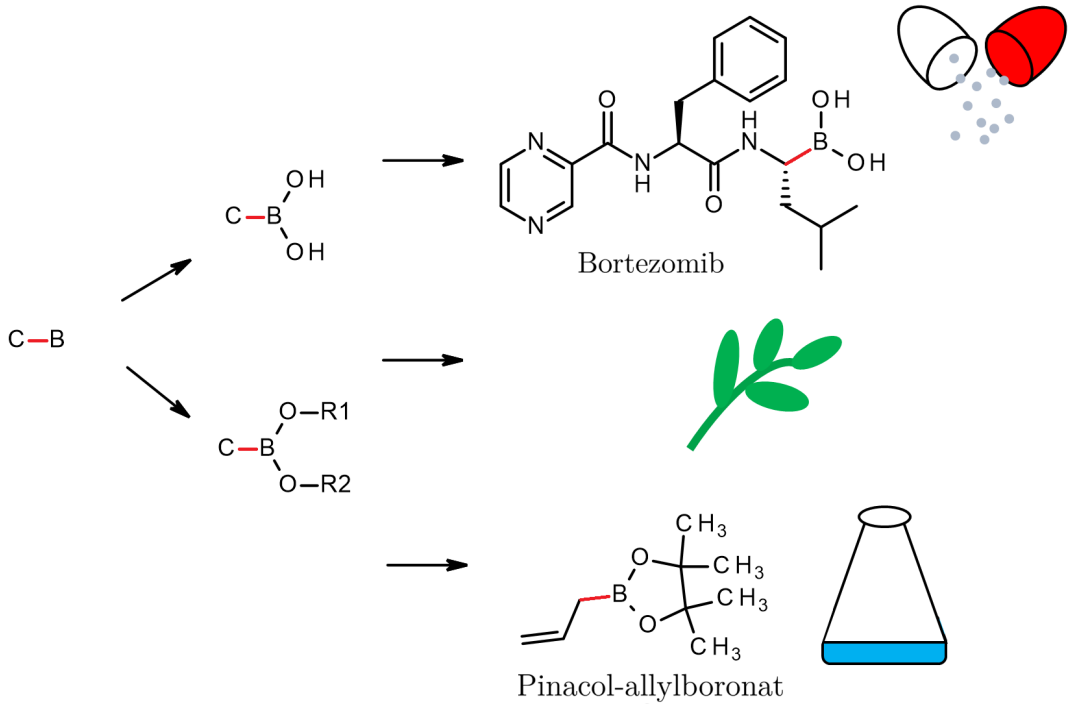

Figure 1.1: Applications of OB in pharmacy, organic chemistry and agriculture via the precursors organoboronic acids and esters.

1.1 Organoboranes - Properties and Applications

Organoboranes are molecules, which originate from an organic compound and a boron derivative and are thereby characterized by a carbon-boron heteroatomic bond [14]. This detail leads to interesting chemical properties of OBs.

In particular, boron is a key factor in the organoboron chemistry. It has three valence electrons and prefers to form three covalent bonds, leading to common products like boric acid, boron trifluoride or the OB trimethylborane. As a result, the boron provides only six bonding electrons, which classify electron-deficient trivalent OBs as remarkably reactive [15]. This is also the reason, why OBs are categorized as strong electrophiles. Furthermore, OBs can be oxidized easily to the corresponding alcohol, where oxygen or hydrogen peroxide is commonly utilized as oxidating agent [22]. Interestingly, OBs are also generally stable due to the low difference in electronegativity of boron and carbon. With respect to the need for green and sustainable products, it is furthermore beneficial, that primary OBs like organoboronic acids and organoboronic esters can be degraded to boric acid, which states these compounds as environmental-friendly, while possessing a minor toxicity [23].

The mentioned advantageous chemical properties assign OB as an important chemical platform, which justifies the intensive research and development since their initial application 60 years ago [23]. Thus, it is no surprise, that OBs deliver a tremendous repertoire of applications in modern organic chemistry, agriculture and pharmacy [18]. Here, the aforementioned organoboronic acids and organoboronic esters embody frequently used starting materials and reaction intermediates in diverse chemical syntheses, e.g. boronic acid pinacol esters, which are well established substrates for C-H coupling reactions [24]. Perhaps the most famous example however, is the Nobel Prize awarded Suzuki-Miyaura cross-coupling reaction, in which OB and halides are connected with palladium catalysts to form carbon-carbon single bonds [25]. With further functionalizations, industrial applications range from antioxidants to rocket fuel supplements and complex biologically active pharmaceutic agents [26]. The latter are carried by anti-microbial, anti-androgenic and anti-oncogenic effects [27]. The anti-cancer drug Bortezombid, marketed as Velcade, is here only one of numerous entries on this list.

Out of all possible applications, the use as a catalyst is the most essential use of OBs. This is a result of the described reactivity on the one hand and the excellent functional-group tolerance on the other hand, stating a unique pattern in the organometallic family compared to other members, like organozinc or organomagnesium compounds [28]. Especially, the ease of oxidating OBs with oxygen leads to carbon-centred radicals, that are common for

polymerization initialization of olefines [29][30].

Considering the applications and properties given above, OB are multifaceted chemical exemplars with an immense annual tonnage, thus, they are definitely worth to study.

1.1.1 Chemical Synthesis Routes

Although it was demonstrated that OB have various applications in diverse fields of modern industry, their production, however, is comparably single-sided - chemical synthesis. Overall, there are three main methods for chemical OB formation, which are applied at industrial scale (Fig. 1.2).

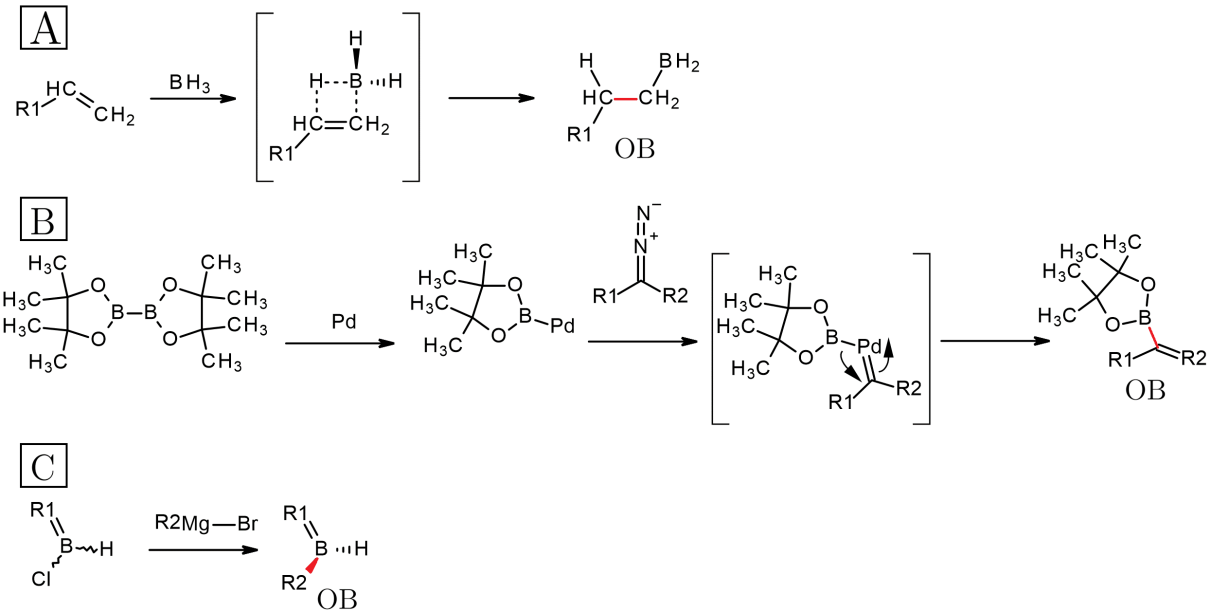

Figure 1.2: Examples for chemical OB synthesis routes. Hydroboration with BH_3 via a transition state (A), borylation from pinacol esters with a transition metal catalyst and a carbene precursor (B) and Grignard reaction using a Grignard reagent (C).

The most common way for OB synthesis is via hydroboration. As the name states, a hydrogen-boron bond is required, usually provided by boranes (BH_3), which favourably connect with carbon-oxygen, carbon-nitrogen or carbon-carbon double bonds, as well as carbon-carbon triple bonds [31]. The reaction with alkenes are following a *syn*-addition and surpass a transition state, where the carbon-hydrogen bond and the carbon-boron bond are formed nearly simultaneously, as the hydrogen and the boron are facing the same side of the double bond (Fig. 1.2A). For asymmetric alkenes, the *anti*-Markovnikov product is preferred, where the boron is bound to the less substituted carbon [32]. This reaction is often employed as an

intermediate step to form alcohols with hydrogen peroxide driven oxidation as already mentioned [22]. More interesting than the mechanism, at least from an engineering point of view, are the advantages and disadvantages regarding process parameters. Here, hydroboration is in general a relatively selective technique if the *anti*-Markovnikov product is targeted, since 94 % selectivity can be reached without further efforts [33]. However, this is only the case if simple boranes are utilized and if the attacked olefin is small and sterically unhindered. The selectivity as well as the reaction rate are seriously reduced, if di- or tri-alkyl boranes are to be produced. Furthermore, more sterically bulky compounds, such as styrene, are known to lead to racemic mixtures of isomers indicating a poor regioselectivity [20]. Regarding the reaction conditions, most hydroborations can be carried out at room temperature [34]. But its high exothermicity is challenging to handle, especially in larger scales, which complicates the control of the reaction rate itself [35].

Borylation is another commonly applied method for the synthesis of OBs. The reaction is catalyzed by transition-metal catalysts to insert boron into aliphatic and aromatic carbon-hydrogen bonds, connections, which are not covered by hydroboration [36]. The general formula $(RO)_2B\text{-}B(OR)_2$ indicates essential boron-containing substrates for this reaction, where frequently employed catechol and pinacol diboranes follow these rule [37]. Borylation is carried out via a transmetalation step and can be accomplished under photochemical and thermal reaction conditions, where mainly rhodium, iridium-, palladium- or rhenium-based catalysts are applied as illustrated in figure 1.2B [38, 39]. Photochemical approaches can be executed at room temperature, but take up to several days to reach acceptable yields above 50 %. In contrast, thermal motivated reactions need less time, but require elevated temperatures around 100 to 160 °C to reach comparable yields [39]. Although borylation is able to synthesize OBs, all procedures described, result in boronic esters as final product. To receive boronic acids, however, additional steps are required [40]. Despite being a well established technique throughout the last decades, borylation deals with heavy metal contaminations as well as environmentally offensive syntheses [19, 41]. This needs to be overcome with respect to the demands for greener processes in the future.

The third reaction, which can be applied for OB formation, is the Grignard reaction (Fig. 1.2C). This process is based on a substance - the Grignard reagent - which consists of alkyl, allyl, vinyl or aryl groups connected to magnesium halides [42, 43]. It is used for the formation of carbon-boron, carbon-carbon, carbon-phosphorus, carbon-silicon or carbon-tin bonds [44]. For carbon-boron bond creation, borate esters or boroxines are chosen typically [45]. The reaction is driven by a nucleophilic attack from the carbon in the Grignard reagent on the electrophilic boron via a ring-assembled intermediate state [46]. The yields for borox-

ine based syntheses reach yields between 21 - 62 %, which are still higher, than those in syntheses with borate esters as starting material. One advantage of this method is the low reaction temperature of 25 °C [45].

1.1.2 Alternative Synthesis Routes - Help from Nature?

It was demonstrated, that boron has unique chemical characteristics, making it useful for many different reactions, for example to produce OB. Thus, it is a legit conclusion, that boron containing compounds are widely spread even in nature.

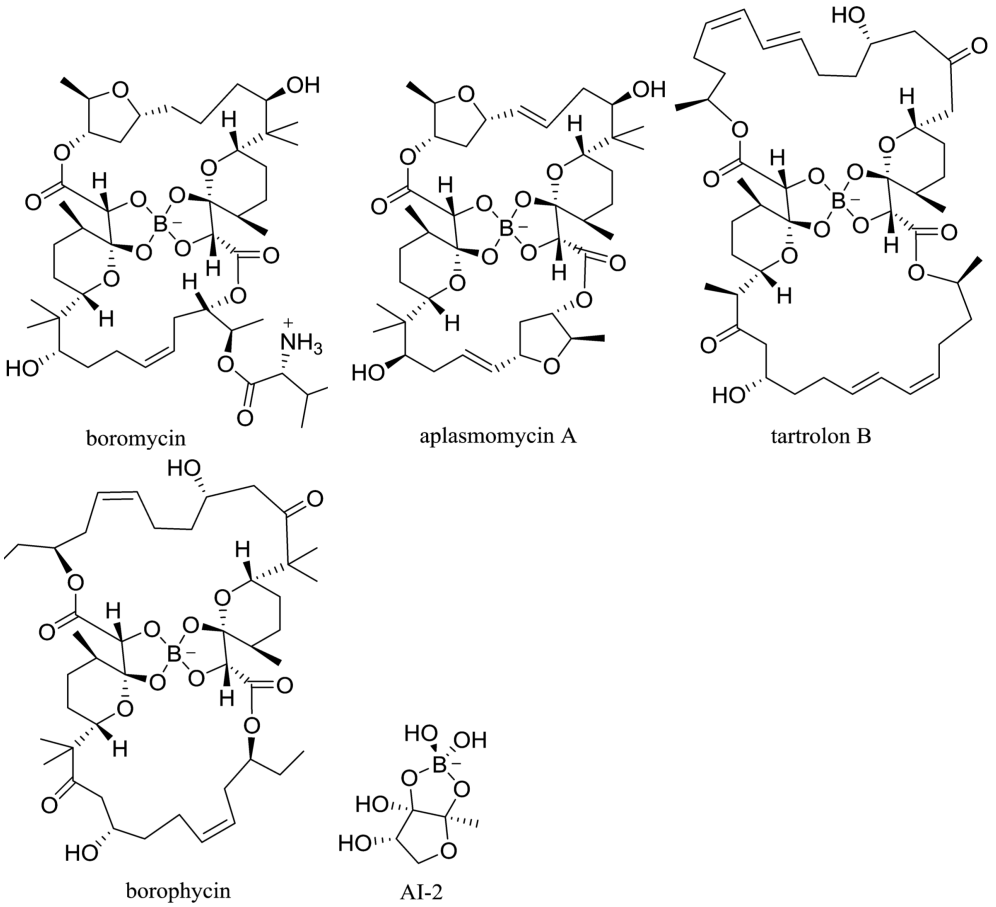

Figure 1.3: Natural occurring boron-containing antibiotics based on boric acid [32]

Those applications are mainly based on boric acid as starting material, which originates from the mineral sassolite and is released as well as distributed via the water cycle to the sea, plants and fruits [47]. Therefore, incorporations of boric acid into biological life is a logic consequence, starting already millions of years ago, since pink borolithochromes have been found in the jurassic algae *Solenopora jurassica* [48]. Moreover, there are plenty of

boron-containing macromolecules known, that serve as antibiotic (Fig.1.3). One famous example, is the 1967 isolated boromycin from *Streptomyces antibioticus*. It does not only show activity against gram-positive bacteria, but has also a HIV-inhibiting effect [49]. Another entity is the autoinducer 2 (AI-2), which was initially discovered in the marine bacterium *Vibrio harveyi* [50]. It is used by gram-positive and gram-negative bacteria as signal transmitter for intercellular communication in a process called *quorum sensing* and is synthesized enzymatically [51]. Although there are several functions of boron-containing compounds in nature, they all include only boron-oxygen bonds, due to boric acid as basis. There are no biomolecules known, containing a carbon-boron bond [32].

Thus, without OBs in nature, there is a lack of biocatalysts for the formation of this specific compound. Which is in fact surprising, due to the advantageous properties of OBs on the one hand and the tremendous diversity of enzymes and their catalyzed reactions on the other hand. Here, the span of biocatalysts reaches in nearly all imaginable directions. Enzymes are known to work under extreme conditions, from acidic to alkaline milieus, from temperatures below 0 °C to temperatures above the boiling point of water [52, 53]. They derive mostly from extremophile bacteria and archaea, living close to hot springs or deep in the ocean, which qualifies the organisms and the enzymes to work as well as to be stable under the found circumstances. These properties also enable microorganisms and enzymes to be applied in industrial processes [54]. Moreover, the interest in biocatalysts increases, since companies look for green and sustainable alternatives to power their plants due to the rising anthropogenic pressure on nature [55]. Enzymes can operate effectively already under mild reaction conditions, leading to a reduced energy consumption, while reaching high yields and are chemo-, regio- and enantioselective [56, 57]. Characteristics, which are not found simultaneously for hydroboration and borylation as shown before. Their expression in microorgansims from sustainable resources demonstrates the non-toxic and environmentally-friendly nature of enzymes. Concluding, the possible improvements in contrast to chemical OB synthesis methods are clearly visible. Therefore, it is only a question of time, until enzymes also have filled the gap for industrial biocatalytic OB synthesis.

1.1.2.1 Cytochrome c Driven Biocatalytic Borylation

For a enzyme-driven OB synthesis, a suitable candidate has to be identified first. Here, cytochrome c (Cytc) is an interesting applicant for this task, since this enzyme family is able to catalyze reactions with a broad substrate range [58]. Cytc belongs as oxidoreductase to enzyme class 1 and has a molecular weight of around 13.8 kDa [59, 60]. It harbours 104 amino acids, from which the hydrophilic ones are assembled on the surface, while lipophilic

amino acids are trapped inside. This distribution leads to a high solubility in water [61]. More importantly, as a heme protein, Cytc provides a porphyrin-complexed iron atom nearby its active site, which can be converted between a reduced, ferrous and an oxidized, ferric state [62]. This feature is a handy property for its main function as an electron transport protein [63]. It is located in the periplasm of mitochondria and serves as redox partner to carry electrons from cytochrome c-1 to cytochrome c oxidase for ATP generation via the electron transport chain [64, 61]. This ability seems to make Cytc as well as other heme proteins available for carbene transfer for heteroatomic bond formation [65, 66]. In particular, the heme-located iron atom is predicted to perform comparably to transition metals in chemical borylation. Thus, it was recently additionally selected for biocatalytic borylation [21].

The candidate chosen within the study of Kan *et al.* (2017), was a Cytc from the thermophilic organism *Rhodothermus marinus*. It is a halophilic and thermophilic organism from hot springs in iceland and provids its Cytc with a high temperature stability, due to its temperature optimum at 65 °C [67]. Initially, the wild-type biocatalyst itself was expressed in *Escherichia coli* BL21 DE3 and applied for the catalysis of a reaction with diazo compound (DAC) as carbene donor and a *N*-heterocyclic carbene borane (NHCB) to form the corresponding OB as illustrated in figure 1.4.

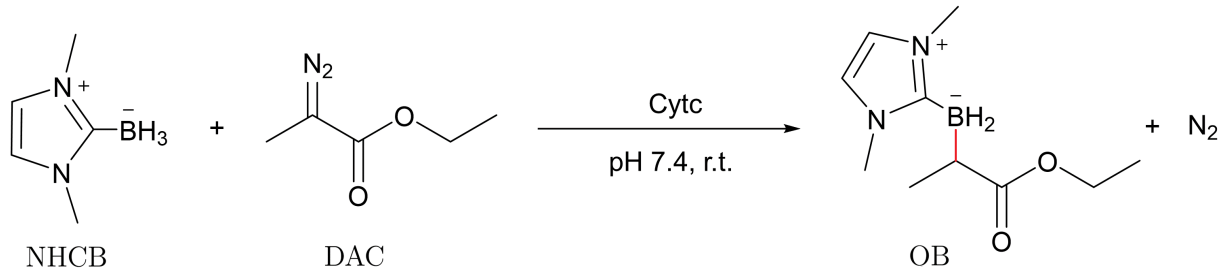

Figure 1.4: Cytc catalyzed model reaction of biocatalytic borylation for OB synthesis. NHCB and DAC are converted under anaerobic and mild reaction conditions to the corresbonding OB product and molecular nitrogen [21].

Ethyl-2-diazopropanoate delivers the organic part for the carbene insertion into the B-H bond of NHCB. It is a viscous, yellowish liquid, that has a distinctive smell. Diazo compounds in general, are organic molecules with an attached diazo group, consisting of two linearly aligned nitrogen atoms connected to one of the carbon atoms within the organic structure [68]. More importantly, diazo compounds can be decomposed by light or elevated temperatures where molecular nitrogen (N_2) is released, leaving behind a highly reactive carbon atom with two unshared valence electrons known as a carbene [69, 68]. Thus, diazo compounds are excellent carbene precursors [68].

The boron containing substrate is 1,3-dimethylimidazoyl-2-ylidene borane and is biocompatible as well as it comes along with a good stability in aqueous solutions [70]. Characteristics, that are crucial for reactions supported by enzymes or whole cells. Moreover, NHCB is a Lewis-base complex with a notable reactivity regarding carbenoid B-H insertion as proven for chemical borylation [71, 72]. Thereby, this reactant brings a valid possibility of being an appropriate starting material for biocatalyic OB synthesis on top.

The described substrates are converted already by wild-type Cytc under mild reaction conditions of 25 °C and pH 7.4 with a total turnover number (TTN) of 120, which reveals an improvement compared to the chemical counterpart [21]. This parameter is a measurement of moles product formed per mole catalyst and is determined according to equation 1.1.

$$TTN\left[\frac{mol}{mol}\right] = \frac{\Delta Product\left[\frac{mol}{L}\right]}{c_{Catalyst}\left[\frac{mol}{L}\right]} \tag{1.1}$$

$$Enantiomeric\,ratio\,(er)\left[\frac{mol}{mol}\right] = \frac{n_R[mol]}{n_S[mol]} \tag{1.2}$$

$$Enantiomeric\,excess\,(ee)\,[\%] = \frac{|n_R[mol] - n_S[mol]|}{n_R[mol] + n_S[mol]} \cdot 100[\%] \tag{1.3}$$

Nevertheless, Kan *et al.* (2017) further adapted the Cytc variant to the model reaction by means of genetic engineering, which utilizes the directed evolution of biological molecules. It is often exercised for proteins and enzymes with a stepwise artificial evolution by rounds of single amino acid exchanges via genome modification to identify critical positions for an overall development of the activity, stability or other desirable characteristics [73]. After three consecutive rounds the final Cytc variant BOR^{R1} had been evolved, being able to execute biocatalytic borylation with TTNs of up to 2490 [21]. Not only is this variant capable of converting the selected substrates above, but also numerous boranes and diazo compounds with a tremendous diversity of positions, lengths and kinds of functional groups and substituents (Fig.1.5). Despite only minor deviations in TTNs, the OB products can be obtained selectively with an enantiometric ratio of mostly above 96:4 (Eq. 1.2). However, the enantiomeric excess reveals, that there is still room for improvement especially for pharmaceutical applications requiring high enantiomeric purity (Eq. 1.3). Nevertheless, studies showed, that TTNs can be further improved to over 10,000 by a stepwise addition of the substrates, while gram-scaled syntheses are also feasible [21].

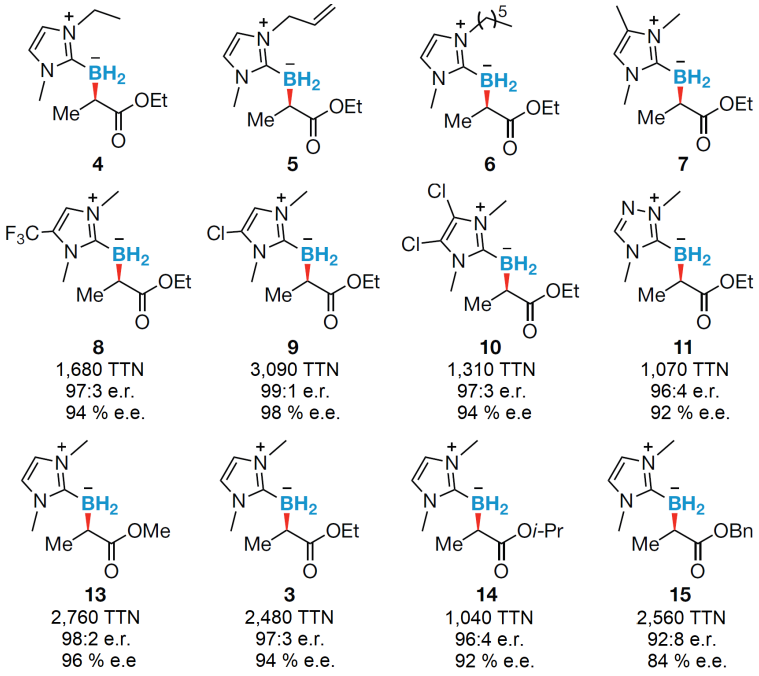

Figure 1.5: Final OB products of via enzyme-driven biocatalytic borylation with Cytc BOR^{R1} based on varying structures for NHCB (4 - 11) and DAC (13 - 15) [21].

However, although the latest results demonstrate a successful utilization of Cytc for the described model reaction, there are still some limitations known, which are inhibiting full conversions and higher yields. One major disadvantage of the reaction is the utilization of DAC as a substrate in combination with the heme-located iron atom. As demonstrated in figure 1.6, two possible irreversible deactivation pathways of DAC are imaginable, since this effect was already identified for P450 enzymes during cyclopropanation reactions with DAC as substrate [74]. After binding of the carbene to the iron, the organic residue of the former DAC can either be bound covalently to the protein backbone via a nucleophilic attack from nearby amino acids, or is directly attached to one of the porphyrine-building nitrogen atoms. In both cases the structure of the heme and the active site is irreversibly damaged, resulting in a full loss of catalytic activity. The described effect is more likely, if the concentration of DAC is higher and if DAC transport is not limited by passing cell membranes and walls. This was concluded by a severe drop of TTN for Cytc-driven OB synthesis, when lysed cells and, especially, if purified Cytc was applied instead of whole cells [21]. While Cytc in the lysate receives at least some protection by mitochondrial membranes, pure Cytc is attacked by DAC without any transport limitation.

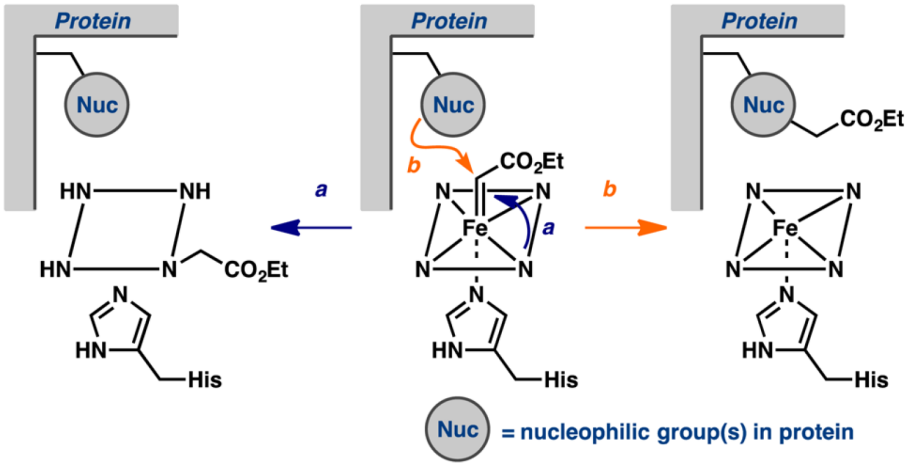

Figure 1.6: Deactivation mechanism of heme-harbouring P450 by DAC via a nucleophilic attack from the protein backbone or by covalent bond formation with the porphyrine ring. Ion charges were left away to improve discernability [74].

1.2 Kinetic Characterization

The amount of product formed in comparison to the amount of substrate consumed in a defined volume and during a defined period of time is known as reaction rate or reaction velocity, v or r respectively. This parameter is fundamental for the mathematical description of a complete reaction, which is defined as reaction kinetics [75, 76]. Every reaction, regardless of whether it is occurring naturally or is tailored and designed by scientists according to their needs, performs according to the present circumstances and has thus different reaction kinetics. Conversion, yield and reaction rate, but also the position of an equilibrium can vary widely as a consequence [77, 78]. In order to estimate the effects of different reaction conditions on these parameters, kinetic characterizations are carried out [79]. Also for the recently developed biocatalytic borylation, favourable operation ranges have to be determined, in order to identify limitations and to set optimal operation points from a kinetic point of view [80].

Temperature, pressure and reactant concentrations deliver noticeable impacts on the ongoing reaction, which was already discovered in 1888 for chemical equilibrium reactions by Henry Le Chatelier [81]. In fact, this is also the case for enzyme-driven approaches [82]. However, the broad temperature range, which is available for chemical reactions, is narrowed for enzymes, due to the nature-adapted origin of these biocatalysts. As their intracellular workplace is located predominantly in aqueous environments and since their hosting microorgansims are also based on water, suitable operation temperatures are oriented along the range of liquid water. Here, it is a rule-of-thumb, that the reaction rate doubles for an

elevation of 10 °C [82]. Obviously, this is also true for Cytc-driven OB synthesis, where Cytc itself brings already an advantage, with being adapted to operation temperatures around 65 °C [67]. However, since Cytc is expressed in *E. coli*, preferring mesophilic conditions around 37 °C, there are boundaries given by the cell around its catalytic machinery. Aside from temperature, there are further parameters influencing enzyme activity. For one, the pH-value is known to play an important role. It does not only effect the charge of reactants and thereby influences the possibilities of transport and conversion, it further impacts the charge of biocatalysts itself. In particular, surfacial amino acids are charged with respect to their isoelectric point (pI). Thereby global changes in activity and stability of the enzyme occur, why the pH is an valuable parameter to consider, when describing a reaction properly. Regarding the presented approach, Cytc provides a pI of 9.3 to 10.3, leading to a positive net charge in the periplasm with a pH around 7.5 to 6.5 [83, 84]. Fortunately, the periplasmic pH as well as the overall intercellular pH can be maintained by homeostasis of *E. coli* from pH 5.5 to 9 [85]. If reactions catalyzed by heme enzyme are observed, the ionic strength is an additional important criterion, as it modifies enzyme conformation, especially, in lower pH-ranges [86].

The three parameters mentioned are inevitable specifications for the description of a reaction. However, although being mathematical implementable for enzyme-based kinetics, they are only complements to the main enzymatic kinetic models. They focus substrate and product concentrations as central driving force for the reaction rate of an enzyme.

1.2.1 Michaelis-Menten Theory

For the mathematical characterization of enzyme kinetics, different models are established. The most applied one is the Michaelis-Menten model, which is based on several sub-steps the substrate, product and the enzyme have to pass. Here, a general reaction scheme can be derived via the Cleland notation for a unimolecular reaction 1.4.

$$\begin{array}{ccccc} & \overset{S}{\downarrow} & & \overset{P}{\uparrow} & \\ \hline E & & ES \rightleftharpoons EP & & P \end{array} \tag{1.4}$$

Initially, the substrate (S) binds to the free enzyme (E) to build the enzyme-substrate complex (ES). Then, the substrate is converted into the product within a enzyme-product complex (EP), which dissociates into the product (P) and the enzyme. Although all steps are in principle reversible, it is considered, that the back reaction from EP to ES is neglectable and the association of EP from E and P is limited by low product concentrations [87]. Thus, the reaction scheme can be transferred into the state equation 1.5.

$$E + S \rightleftharpoons ES \rightarrow E + P \tag{1.5}$$

The applied theory is only valid for steady state conditions with a constant concentration of the ES complex [82]. With some further assumptions and based on the law of mass action, an equation describing the reaction rate v, also known as activity, with respect to the substrate concentration can be derived (Eq. 1.6) [82].

$$v = \frac{v_{max} \cdot [S]}{K_m + [S]} \tag{1.6}$$

The maximal reaction rate v_{max} and the substrate concentration $[S]$ are incorporated, as well as the Michaelis-Menten constant, K_m which expresses the affinity of the substrate towards the enzyme. For the model reaction of Cytc-driven OB synthesis, equation 1.6 can be adjusted to two substrates (Eq. 1.7).

$$v = v_{max} \cdot \frac{[NHCB]}{K_{m,NHCB} + [NHCB]} \cdot \frac{[DAC]}{K_{m,DAC} + [DAC]} \tag{1.7}$$

In the same way, the Cleland notation can be tailored to our bimolecular model reaction (Eq. 1.8).

$$\begin{array}{ccccccc} & \overset{S_1}{\downarrow} & & & \overset{P_1}{\uparrow} & \overset{S_2}{\downarrow} & & & \overset{P_2}{\uparrow} & \\ \hline E & & ES_1 \rightleftharpoons FP_1 & & F & & FS_2 \rightleftharpoons EP_2 & & E \end{array} \tag{1.8}$$

This reaction can be expected to follow an ordered Ping-Pong bi-bi mechanism and is initiated by DAC (S_1) binding to Cytc (E) under formation of the enzyme-substrate complex (ES_1). The first reaction takes place, where cleavage of the diazo group leads to an activated Cytc-carbene complex with still attached N_2 (FP_1). After the diazo group is separated, N_2 (P_1) is released from Cytc with the residual carbene-enzyme complex (F). Subsequently, NHCB (S_2) binds to the carbene-enzyme complex (FS_2), and is converted with the carbene to OB while still bound to the enzyme (EP_2), before OB (P_2) dissociates from Cytc. As demonstrated with equation 1.5, the same assumptions can be applied on equation 1.8 to derive the state equation 1.9.

$$E + S_1 \rightleftharpoons ES_1 \rightarrow F + P_1 + S_2 \rightleftharpoons FS_2 \rightarrow E + P_2 \tag{1.9}$$

For a mathematical description of biocatalytic borylation, reaction kinetics can be based on equation 1.7. The equation is extendible in case of temperature- and pH-dependencies or reactant-driven effects.

1.2.2 Inhibitions

Inhibitions occur if substrates, products or other substances bind to the enzyme in a way, that the biocatalyst is thereby limited in its catalytic activity. They are distinguished in substrate or product inhibitions. Here, different binding locations for the inhibitor are possible and characterize the type of inhibition accordingly. Inhibitors can bind to the active site - competitive inhibition - or at other locations - non-competitive inhibition - of the free enzyme. It is further possible, that the inhibitor binds to the enzyme-substrate complex - un-competitive [82]. These inhibitions are all reversible and depend on the concentration and kind of the inhibitor. While the possibility to attach to the enzyme or the enzyme-substrate complex rises with the inhibitors concentration, the inhibitor can dissociate again, if its concentrations is reduced. Thus, an initially occurring substrate inhibition can decline with ongoing conversion of the substrate itself. Vice versa, a product inhibition tends to lead to incomplete conversion, as the activity decreases more and more, due to increasing product concentrations [82]. Eventually, the reaction is ceased based on severe inhibition. In both cases, the affinity between enzyme and the inhibitor is described with the inhibition constant K_i.

In comparison, irreversible inhibitions result in a complete lack of activity already at low concentrations of the inhibitor, as the dissociation of the complex is not possible. Unfortunately, the suggested deactivation of Cytc by DAC belongs to this case of interaction, resulting in a complete lack of activity and stating an important part in the kinetic characterization of biocatalytic borylation [74].

1.2.3 Kinetic Parameter Estimation

In order to predict reaction rates at specific substrate concentrations, the kinetic parameters v_{max}, $K_{m,DAC}$ and $K_{m,NHCB}$ to be determined.

At this point experimental data is required to carry out kinetic parameter determination with the mathematical model. It is either possible to execute an initial rate measurement, where the reaction rate is recorded within the first 5 % conversion in the linear region of the reaction with specific starting concentrations of NHCB and DAC [82]. The reaction rate can be directly calculated from the slope of the product formation over time and the experiments only last a few minutes[82]. In contrast, a process curve analysis can be conducted, where a complete reaction-time course is recorded [88]. This has the advantage, that the reaction rate can be determined at each point of the progress curve. This can be achieved exemplarily by calculating the slope with the first derivative at a specific time point with the respective

substrate concentrations [88]. Thus, from one experiment, it is possible to yield several reaction rates for different substrate concentrations. Nevertheless, multiple experiments are still required and this approach is more difficult to apply, when the reaction rate is additionally affected by enzyme deactivation, leading further to a time-dependent reaction rate [89]. Thus, for the model reaction of biocataltic borylation the initial rate measurement is most suitable.

After sufficient data has been collected, kinetic parameters can be determined graphically based on Michaelis-Menten plots, where v_{max} is immediately presented as highest reaction rate, while $K_{m,DAC}$ and $K_{m,NHCB}$ have to be read off the concentration at 0.5 v_{max} [90]. Another option is a numerical approach with non-linear regression, where start values for each parameters are given and are iteratively adapted until therefrom simulated reaction rates hit the experimental data with lowest standard deviation [91].

1.3 Reaction Engineering

Reaction engineering focusses on the design of a biochemical or chemical process, which can be divided into the reactor design as well as the already mentioned reaction kinetics[92]. Major aspects are the choice of a suitable reactor size and shape as well as the identification and application of reaction conditions tailored to the reaction. Moreover, the operation mode is a versatile tool to influence the reaction to the needs of the process. Overall, the main target is the establishment of an economic process, i.e. minimizing reaction time and costs of goods, as well as maximizing the conversion, yield and selectivity[92].

The reactor size and shape are important characteristics to maintain a sufficient progress of the reaction. Those parameters are applied in order to e.g. improve the flow behaviour of the reaction mixture and thereby ensures homogeneous distribution of the reactants and an accelerated heat transfer [93]. For Cytc-driven OB synthesis the distribution not only of the reactants, but also of the cells is important. Too low stirring results in sedimentation of the cells, reducing the contact area of biocatalyst and substrate [93]. Moreover, a precisely selected size can increase the production of a plant, but can also change the energy demands for heating, cooling and stirring appropriately [92]. For biocatalytic OB synthesis, with exception of a gram-scale synthesis as proof of principle, only experiments in a μL or mL-scale have been executed as of now within the literature [21]. Thus, in order to develop biocatalytic borylation, scale-up experiments are inevitable to identify limits in temperature control, mixing and agitation.

Reaction parameters are another specification used in reaction engineering, as already ex-

plained in section 1.2. After the reaction has been sufficiently characterized, the required conditions have to be applicable in the reactor as well. In addition to the characterization of the catalysts behaviour, the information about reactant parameters are here included likewise. For example, the solubilities, as well as melting and boiling points of all participating reactants can influence the operating windows for temperatures and concentrations [92]. Within biocatalytic borylation, melting as well as boiling points of the substrates and the product could not be determined. The same is true for the solubility of all reactants, where only rough estimations are present. But previous studies revealed, that an addition of 5 % (v/v) acetonitrile (MeCN) prevents the precipitation of NHCB and OB from the liquid phase, enabling a wider range of concentrations to work with [21]. Here, a temperature trade-off between solubility of reactants and Cytc activity as well as stability has to be determined. However, high temperatures can denaturate Cytc or lead to the decay of DAC by separation of the instable diazo group introducing unwanted side reactions [68]. In addition, the applied pressure also contributes to the design of the reaction process. Especially challenging is the handling of toxic or explosive substances during the reaction, where pressure changes can lead to vaporization of liquids, building up flammable gas phases [94]. Although biocatalytic borylation utilizes no flammable gases, the atmosphere is a crucial criterion. Since the reaction needs to be under anaerobic conditions. The reaction vessel has to be designed for stripping of oxygen from the gas phase and to strip remaining oxygen out the liquid phase [21]. Moreover, diazo compounds are critical substrates due to the decay under oxygen-containing atmospheres by rapid reaction with the diazo group [68].

1.3.1 Operation Modes

In addition to the reactor design and parameter choices, the selection of a suitable operation mode is a crucial element, influencing the applicability at industrial scale, as well as the economic feasibility [92]. Reaction processes can be performed in three different operation modes, which are illustrated schematically in figure 1.7.

The batch mode or discontinuous mode consists of a reaction vessel, where all substrates are added completely in the beginning, before the mixture is allowed to react until no further product formation is recorded[95]. This simple method was also employed for the first studies regarding biocatalytic borylation [21]. Although batch mode is the most simple to set up and to control, yet it is effective. It presents a trivial way to scale-up analytical and lab scales, is commonly employed on slow reactions and is thereby an appropriate mode for initial tests for novel reactions and techniques to test [96]. Furthermore, batch processes de-

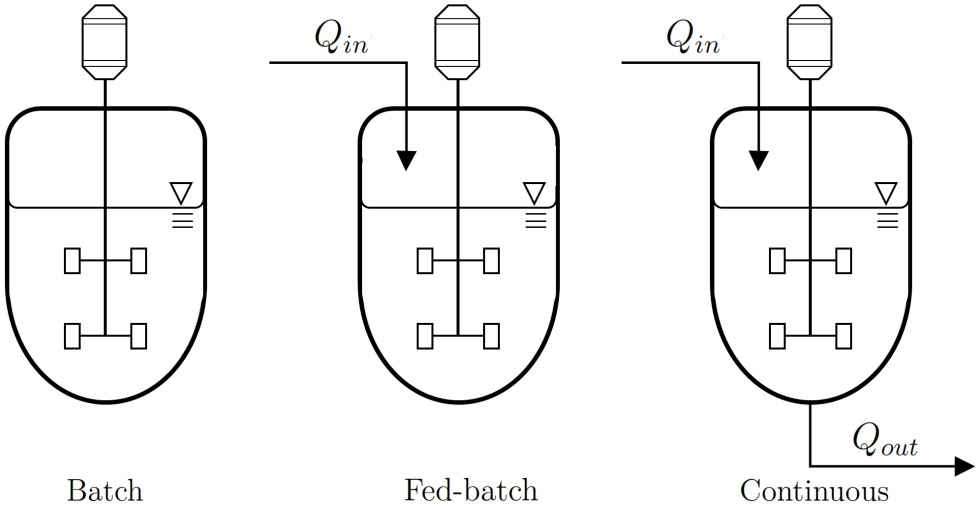

Figure 1.7: Main operation modes used in biochemical and chemical engineering shown for a stirred tank reactor.

liver advantages in pharmaceutical industry and speciality chemicals, where companies can adapt to changing markets and requirements faster [96]. Despite these advantages, there are challenges limiting further developments in biocatalytic OB synthesis. As all substrates are added in the beginning completely, also DAC is immediately present in high concentrations. At first, this leads to a rapid binding to Cytc. However, if NHCB does not associate subsequently to form OB the described deactivation mechanism is a consequence [74]. In order to reduce DAC-driven deactivation, other operation modes than batch mode are required.

In contrast to the discontinuous mode, a semi-continuous mode is an adequate alternative. The fed-batch mode consists of a reaction system, where at least one substrate is added over time to increase either cell density or product concentration [97]. After all substrate is added and converted, the reaction vessel is emptied and prepared for the following run [97]. This method is often applied, when overflow metabolisms, which convert excessive substrates, should be reduced or to suppress side reactions [98]. Here, Kan *et al.* (2017) already studied biocatalytic borylation with a stepwise addition of NHCB and DAC, resulting in 5-times higher TTN [21]. Because no deactivating effect of NHCB is known, a pure DAC feed is imaginable here as well. The complete addition of NHCB before reaction initiation, would thereby secure a higher reaction rate. Thus, the fed-batch mode provides the opportunity to improve TTN of Cytc and thereby increasing conversion, leading to a multifold OB concentration. In order to minimize unwanted effects, cell growth and reaction profile must be limited by the feed, leading to an increased process time, thus, negatively influencing the volumetric productivity [95]. Concluding, a further development of a fed-batch strategy for

our investigated system might reveal even more benefits, but has to be adapted closely to the target reaction.

In the case of the deactivating effect of DAC can be handled successfully, the third operation mode, continuous mode, can be envisioned. The continuous mode or perfusion process is characterized by not only adding substrate, but by additionally removing the reaction mixture with an equal rate [93]. This maintains a constant volume in the reactor and holds the substrate concentration at a minimum, while the product leaves the reaction in higher concentrations [93]. The reactor can either be a continuously operated stirred tank with dispersed cells or enzymes, or a plug flow reactor with immobilized catalysts [99]. The latter have gained great importance particularly in biocatalytic processes, especially in the near past [100]. If whole cells do not provide a constant expression of biocatalysts, the cells or the enzymes itself have to be restrained to maintain the reaction and preserve product formation [99]. While the processed reaction volume for batch and fed-batch applications is limited by the reactor size, continuous operated processes can theoretically handle an infinite liquid volume, due to a steady flow through the vessel. Moreover, another important advantage of the continuous mode is the reduced time for filling, draining and cleaning of the reactor, which takes up to 30 % of the process time for batch processes [99]. The technical duration of such operation however, depends on the durability of the catalyst. As an example of such application, glucose isomerase is immobilized on carriers in a packed-bed for high-fructose syrup production and is exchanged after two to four months [99]. Thus, it seems to be possible to apply a continuous mode for biocatalytic borylation, too. Therefore, the utilization of a continuously stirred tank reactor (CSTR) is beneficial, where a constantly low DAC concentration is preferably settable. As a CSTR operates under outflow conditions, this characteristic is valid for all locations in the reaction volume and thus minimizes the risk of Cytc deactivation. This can be achieved by an adjusted molar feed rate, leading to a fast conversion of DAC entering the reactor. In the ideal case, the NHCB concentration is adjusted likewise, resulting in pure OB leaving the reactor. Here, a CSTR is operating under outflow conditions within an equilibrium with stable concentrations, known a steady state [101]. After a constant and close-to-zero concentration of DAC is established by full conversion of entering DAC, a slight and stepwise increase of feed rate or concentrations are possible to further enhance the outflow concentration of the product [101]. However, it requires an non-trivial procedure to start the reactor.

Overall, each operation mode provides its own benefits. Here, several techniques and methods for the improvement of the performance also of biocatalytic borylation are available. Nevertheless, all modes have to be adapted to the process closely.

1.4 Aim of the Thesis

This thesis is carried out in corporation with the Arnold Group at the California Institute of Technology, Pasadena, USA, who provided the genetically engineered Cytc variant BOR^{R1}.

The scope of this study is the detailed development of biocatalytic borylation for OB synthesis towards an industrially applicable process. So far, OB were only produced chemically with synthesis routes, which include environmentally offensive and less-selective reactions with low TTN of the participating catalysts. In order to look for greener and more effective production processes with respect to the Sustainable Development Goals of the United Nations, a new synthesis method is required urgently [9]. Here, a novel enzyme-driven approach was developed, that converted NHCB and DAC into the corresponding OB with high enantio- and regioselectivity and presented TTNs magnitudes above their chemical counterparts. However, so far the alternative was only performed in analytical scale with conversions below 50 % and yields of 50 %, demanding for enhancements by means of reaction engineering and kinetic characterization.

Since a stable substrate is mandatory for the desired reaction mechanism, possible effects that cause changes in the molecular state have to be investigated. Here, the pKb of NHCB has to be determined via titration in order to locate the pH leading to NHCB protonation. Moreover, investigations will qunatify the decay of DAC by different temperatures from r.t. to 85 °C as well as a decomposition induced by UV-light.

The biocatalyst Cytc is the most important tool in biocatalytic borylation and demands therefore extensive analysis. Thus, the optima regarding pH and temperature have to be identified for Cytc by comparing the initial reaction rates. Initial rate measurements will determine initial reaction rates in dependence of the substrate concentration. Incubations with NHCB, DAC and OB prior to OB synthesis will determine reversible and irreversible inhibitions, where the rate of Cytc-deactivation by DAC in particular will be described mathematically. All data will lead to the build up of a mathematical model according to a double-substrate Michaelis-Menten equation to appropriatly describe the reaction kinetics. Numerical determination of kinetic parameters v_{max}, $K_{m,NHCB}$ and $K_{m,DAC}$ will be executed within MATLAB and a comparison of simulations with experimental data will evaluate the overall model.

The reaction engineering part will execute syntheses in a batch, fed-batch and continuous mode. The Cytc concentration will be changed to increase the final product concentration as well as the space-time yield. The TTN and product formation will be further optimized in fed-batch and continuous operation modes, by the adjustment of the dilution rate and

residence time, respectively. Scale-up experiments from 0.4 to 500 mL will transfer the results and to prove the effective OB synthesis at larger reaction volumes to take next steps towards and industrial relevant alternative.

2 Materials and Methods

2.1 Chemicals

The chemicals used in this thesis were of analytical grade, if not otherwise mentioned and purchased by Carl Roth GmbH + Co. KG (Karlsruhe, Germany), Sigma-Aldrich Chemie GmbH (Munich, Germany) and Tokio Chemical Industry CO., LTD. (Tokio, Japan). Ethyl-2-diazo propanoate was provided by Arch Bioscience Company (West Chester, USA), while NHCB and OB were synthesized at the Institute of Technical Biocatalysis, TUHH (Hamburg, Germany) as described later.

2.2 Buffers, Stocks and Media

2.2.1 Buffers

Buffers based on deionized (DI) water are used as liquid phase for biocatalytic OB synthesis, purifying Cytc using nickel-nitrilotriacetic acid (Ni-NTA) His-tag affinity chromatography (AC) and protein mass determination via sodium dodecyl sulfate polyacrylamide gel electrophoresis (SDS-Page). The compositions are shown below in tables 2.1, 2.2 and 2.3.

Table 2.1: Composition of the M9-N buffer for OB synthesis [21]. The pH is adjusted to 7.4 with 5 M NaOH.

Component	**Concentration [mmol·L^{-1}]**
Na_2HPO_4	47.7
KH_2PO_4	22.0
NaCl	8.6
$MgSO_4$	2.0
$CaCl_2$	0.1

Table 2.2: Composition of buffers for AC. The pH is adjusted to 8.0 with 5 M NaOH.

Buffer	Lysis	Wash	Elution
Component		**Concentration [mmol·L^{-1}]**	
Na_2HPO_4	50	50	50
NaCl	300	300	300
Imidazole	10	20	250

Table 2.3: Composition of SDS running-buffer at pH 8.3 for SDS-Page.

Component	**Concentration [mmol·L^{-1}]**
Tricine	800
Triethanolamine	1200
SDS	34.7

2.2.2 Stock Solutions

Antibiotica stocks for ampicillin (Amp) and chloramphenicol (Chl) are prepared according to table 2.4 and stored at -20 °C. The Amp stock is sterile-filtered (cellulose-acetate, 0.22 μm) prior to storage.

Table 2.4: Antibiotica stocks for Amp and Chl.

Antibiotic	**Solvent**	**Concentration [mg·mL^{-1}]**
Amp	DI water	100
Chl	Ethanol	30

Inducer stocks for isopropyl β-D-1-thiogalactopyranoside (IPTG) and 5-aminolevulinic acid (5-ALA) are prepared as described in table 2.5, sterile-filtered (cellulose-acetate, 0.22 μm) and stored at -20 °C.

Table 2.5: Inducer stocks for IPTG and 5-ALA

Inducer	**Solvent**	**Concentration [mol·L^{-1}]**
IPTG	DI water	0.1
5-ALA	DI water	2.0

Substrate stocks for NHCB and DAC are prepared according to table 2.6 and stored under argon (Ar) atmosphere at 4 °C or -20 °C, respectively.

Table 2.6: Substrate stocks for NHCB and DAC.

Substrate	**Solvent**	**Concentration [mol·L^{-1}]**
NHCB	MeCN	0.04 - 0.8
DAC	MeCN	0.04 - 0.8

2.2.3 Cultivation Media

Cultivation media used in this project were both purchased in prepared form as a powder. Lysogeny broth (LB) medium by Carl Roth GmbH + Co. KG (Karlsruhe, Germany) and hyperbroth (HB) medium by Athena Environmental Sciences, Inc. (Baltimore, USA) are dissolved in DI water according to package instructions and heat-sterilized (121 °C, 20 min). Afterwards, antibiotics are added to final concentrations of 100 mg·L^{-1} Amp and 20 mg·L^{-1} Chl. Additionally, HB medium is supplemented with an included, sterile-filtered (0.22 μm) glucose-nutrition mix.

M9-N medium is prepared as described in table 2.1 without $MgSO_4$ and $CaCl_2$, but with additional 18.7 mM NH_4Cl as N-source. The mixture (1 L) is autoclaved and aseptically supplemented with aqueous 1 M solutions of $MgSO_4$ (2 mL) and $CaCl_2$ (0.1 mL), before glucose is added to a final concentration of 4 g·L^{-1}.

2.3 Strains and Plasmids

Electro-competent *E. coli* EXPRESS BL21 DE3 from Lucigen Corp. (Middleton, USA) is used as host strain. For Cytc expression, two plasmids are transformed into the host strain. Initially, the pEC86-plasmid (plasmid card given in the supplementary information Fig. 6.1) from the Culture Collection of Switzerland (Wädenswil, Switzerland) with Cytc maturation genes ccmABCDEFGH and a Chl-resistance marker is integrated via electroporation (2.5 kV, 50 ms). Afterwards, a second electroporation cycle is executed with the pET22b(+)-plasmid, provided by the academic partner Caltech (Pasadena, USA), carrying an Amp-resistance marker and the genetic information of genetically engineered Cytc from *Rhodothermus marinus*.

The variant was designed from wild-type Cytc by three amino acid exchanges M100D, V75R and M103T to receive the variant Rma cytc BOR^{R1}, which is investigated within this study[21].

2.4 Cultivation

The expression strain *E. coli* BOR^{R1} is cultivated via two consecutive cultures, originating from a cryo stock (-80 °C).

The cryo stock inoculates a pre-culture, containing 10 mL of antibiotics-supplemented LB medium in a baffled 100 mL shaking flask, which is incubated for 16 h at 37 °C with 150 rpm to gain sufficient biomass.

Then, 3 mL of pre-culture are transferred to a non-baffled 300 mL shaking flask, containing 100 mL of antibiotics-supplemented HB medium. This main-culture is incubated at 37 °C with 125 rpm. When the OD_{600} reaches 0.6, cells are cooled on ice for 30 min and 5-ALA and ITPG are added to final concentrations of 200 μM and 20 μM, respectively. Afterwards, the main-culture is incubated for 22 h at 18 °C with 100 rpm.

2.5 Cytochrome c Purification

Cytc is purified by His-Tag AC prior to OB synthesis if not stated differently. Therefore, *E. coli* BOR^{R1} cells are harvested from the main-culture by centrifugation (20 min, 4 °C, 5000 xg) and resuspended in lysis buffer, lysed mechanically with the French Pressure Cell Press (FPCP) FA-078A (SLM Aminco, Illinois, USA), centrifuged (20 min, 4 °C, 5000 xg) and sterile-filtered (cellulose-acetate, 0.22 μm) to yield the cell free extract (CFE). An appropriate amount of CFE is loaded onto 3 mL of ROTI®Garose-His/Ni-NTA beads (Carl Roth GmbH + Co. KG, Karlsruhe, Germany) in a 50 mL column, which has been washed with 50 mL DI water and equilibrated with 50 mL of lysis buffer and is incubated for 1 h at 4 °C in a rotary shaker. Afterwards, the residual liquid is removed and the resin is rinsed with 50 mL wash buffer, before Cytc is eluted with elution buffer in 1 mL steps and collected in micro reaction tubes. The Cytc-containing fractions are pooled and the buffer is exchanged immediately with M9-N buffer using a PD10 Sephadex G-25 M desalting column (GE Healthcare, Chalfont St. Giles, United Kingdom) to avoid imidazole-affected denaturation.

2.6 Cytochrome c Immobilization

Immobilization of Cytc is executed on different carriers. HisPur^{TM} Ni-NTA magnetic beads (Thermo Fisher Scientific, Rockford, USA) are purchased as slurry, of which 30 mg are rinsed twice with 300 μL lysis buffer. 1 mL CFE is added and incubated using a rotary shaker (1 h, 4 °C) and the beads are rinsed twice with 200 μL lysis buffer, before being stored in M9-N

buffer at 4 °C.

For EziG carriers (EnginZyme AB, Solna, Sweden), 1 mL CFE is added to 10 mg beads and is incubated (1 h, 4 °C), centrifuged (30 s, r.t., 10000 xg), rinsed twice with 200 μL lysis buffer, before being stored in M9-N buffer at 4 °C.

Immobilization on silica beads (TRISOPOR, 36 - 80 μm, VitraBio GmbH, Sonneberg, Germany) is carried out by undirected covalent binding with a 10 % (w/v) mixture of beads (1 mL), which are rinsed initially with 3 x 1 mL M9-N buffer and centrifuged (30 s, r.t., 10000 xg). A 8 % (v/v) solution of glutaraldehyde (GA) in M9-N buffer is added and the beads are incubated with a rotary shaker overnight (4 °C). Subsequently, beads are separated form the liquid phase and washed with M9-N buffer. 1 mL purified Cytc in M9-N buffer is added and the mixture is incubated overnight on a rotary shaker (4 °C). The beads are separated again from the liquid phase by centrifugation, washed with M9-N buffer (3 x 1 mL) and stored at 4 °C.

2.7 *N*-Heterocyclic Carbene Borane Synthesis

NHCB is synthesized from 1,3-dimethyl-1H-imidazol-3-ium iodide by chemical borylation according to a well established procedure[102]. Therefore, a 250 mL three-necked flask is equipped with a reflux condenser with a hose, leading away produced hydrogen (H_2) gas. One neck is connected to a Schlenk-line for N_2 supply, while a rubber septum seales the last neck. 60 mmol 1,3-dimethyl-1H-imidazol-3-ium iodide and 60 mmol sodium borohydride are added and mixed with 50 mL anhydrous toluene. The solution is heated to 125 °C under a N_2 atmosphere and stirred at 400 rpm. After the mixture reaches reflux, the reaction is carried on for 20 h. Afterwards, the upper NHCB-containing clear toluene phase is separated, before the white viscous lower phase is charged with additional 25 mL toluene to extract residual NHCB (15 min, 125 °C). The extraction step is repeated one additional time, all decanted clear fractions are pooled and toluene is removed by rotary evaporation (40 mmHg, 40 °C) in the Rotavapor R-200 (BÜCHI Labortechnik AG, Essen, Germany). The crude NHCB is redissolved inside a 300 mL round-bottomed flask with a reflux condenser (100 °C) via stepwise addition of DI water. NHCB is allowed to recrystalize from this solution, the crystals are washed via vacuum filtration with ice-cold DI water and dried overnight (60 °C).

2.8 Chemical Organoborane Synthesis

Chemical synthesis of OB is executed according to a recently published and up-scaled protocol[71]. A 20 mL thermostated glass reactor vessel with two ports is loaded with 5 mmol NHCB and 2.5 mol% $Rh_2(OAC)_4$, sealed with rubber septa, heated to 38 °C and the atmosphere is exchanged with Ar via a Schlenk-line connection with the head port. Then, 10 mL anhydrous CH_2Cl_2 are added, stirring is initiated and 5 mL of 5 mmol DAC in anhydrous CH_2Cl_2 are added dropwise over 4 h via a syringe through the head port. The reaction is carried on for additional 16 h, before the solvent is removed by rotary evaporation (40 mmHg, 40 °C). OB is purified by reversed phase chromatography by applying a *n*-hexane : ethylacetate gradient from 4:6 to 1:9 (v/v). Fractions are checked via thin layer chromatography for OB and pure fractions are pooled and the solvent is removed by rotary evaporation (40 mmHg, 40 °C) and drying at 40 °C for 24 h.

2.9 Biocatalytic Organoborane Synthesis

Cytc-driven OB synthesis in whole cells is investigated in three different operation modes. However, cells are harvested identically from the main-culture by centrifugation (20 min, 4 °C, 5000 x*g*) and resuspension in M9-N buffer to a desired OD_{600}. The cell suspension is stored on ice until further use.

Temperature is controlled via a RS6 thermostate with a RC6 water bath (LAUDA GmbH & Co. KG, Lauda-Königshofen, Germany) while anaerobic conditions are maintained with a Schlenk-line connected via three-way cock to a vacuum pump PK8D (ILMVAC GmbH, Ilmenau, Germany), N_2 supply and the reaction vessel itself as illustrated schematically in figure 2.1. A homogeneous distribution of all reactants is maintained with a magnetic stirrer RCT basic (IKA, Staufen, Germany).

2.9.1 Batch Mode

Batch mode experiments for initial rate measurements and long-time experiments are carried out in a 10 mL thermostated glass reactor vessel with two ports (fig. 2.1). A magnetic stirr bar is added and 4.75 mL of cell suspension in M9-N buffer are added before both ports are sealed with rubber septa. Stirring is started (1100 rpm) and the gas phase is evacuated via a hose from the schlenk-line, which is connected to a syringe with a canula penetrating the rubber septum on top. When the cell suspension starts to boil, the valve is immediately

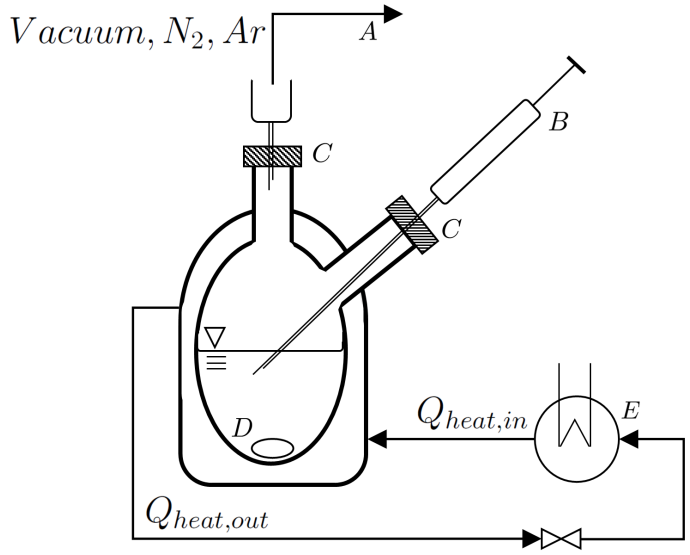

Figure 2.1: Schematic drawing of the experimental setup for biocatalytic OB synthesis in a 5 mL scale. A: Schlenk-line connection, B: sampling syringe, C: septa, D: magnetic stir bar, E: temperature control.

switched to enable N_2 to flush inside the reactor. This procedure is repeated two additional times. Moreover, the gas phase of the reactor is evacuated again and backfilled with Ar via a latex balloon, that is connected to a syringe with a canula. The reactor is flushed with Ar two additional times, before the balloon is left on top to ensure anaerobic conditions during the whole experiment. To initiate the reaction, 0.125 mL of each substrate stock are transferred to a 1.5 mL micro reaction tube and added to the reactor by an Ar-flushed 1 mL syringe through the side port. For initial rate measurements, samples are taken every minute over 7 minutes, while samples for long-time experiments are taken over a range of 2 h with increasing time intervals.

2.9.2 Fed-Batch Mode

Fed-batch mode experiments are executed in either the same vessels as the batch mode experiments, or in 500 mL and 1000 mL DASGIP reactors (Eppendorf AG, Hamburg, Germany) for scale-up tests (Supplementary information, Fig. 6.2).

For small-scale approaches, the cell suspension is added and anaerobic conditions are applied as mentioned above. In contrast to the batch mode, only 0.125 mL of NHCB stock are added by syringe directly into the reactor, while 0.125 mL of DAC stock are loaded into a 5 mL syringe, which is connected to the reaction vessel by a Teflon tube (0.1 mm $\oslash_i$). An Aladdin-1000 syringe piston pump (WPI, Sarasota, USA) is used to add DAC to the reaction

mixture with different flow rates (Fig. 2.2). After the addition is completed, the reaction is allowed to continue for further 2 h to convert accumulated DAC.

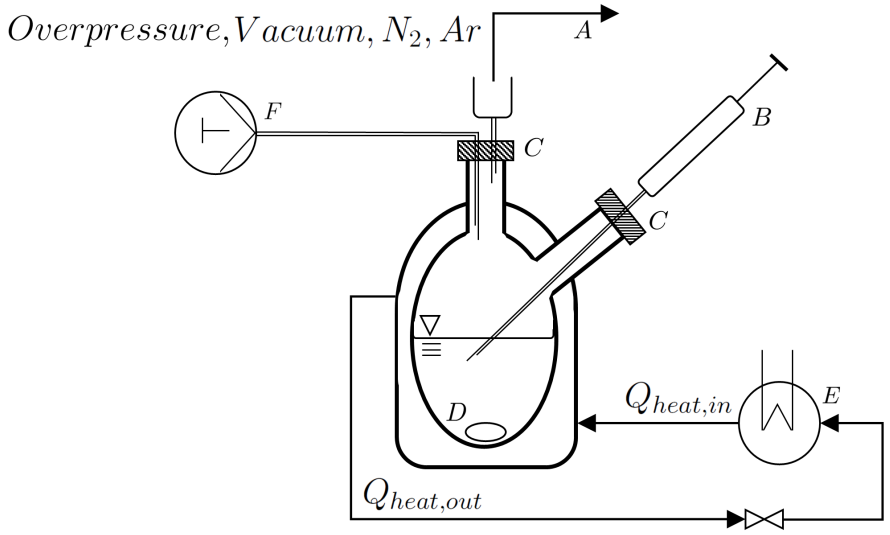

Figure 2.2: Schematic drawing of the experimental setup for biocatalytic OB synthesis in a 5 mL scale in fed-batch mode. A: schlenk-line connection, B: sampling syringe, C: Septa, D: magnetic stir bar, E: temperature control, F: Syringe piston pump.

Scale-up tests with 150 mL reaction volume are carried out with 112.5 mL cell suspension, 30 mL glucose (250 mM) as well as 3.75 mL NHCB stock and 3.75 mL DAC stock. The 500 mL tests are executed with 375 mL cell suspension, 100 mL glucose (250 mM) as well as 12.5 mL NHCB stock and 12.5 mL DAC stock. Reactors are controlled with the DASGIP control software to maintain 40 °C and anaerobic conditions. Cell suspension, glucose and NHCB stock are added into the reactors, which are closed afterwards and axial stirring is initiated. Ar (500 mL scale) or N_2 (150 mL scale) are bubbled trough a aeration pipe. DAC stock is added as described above with syringe pumps and samples are taken via a separate syringe.

2.9.3 Continuous Mode

OB synthesis in a continuous mode is carried out in a cylindrically shaped 3 mL acrylic glass reaction vessel containing a magnetic stir bar (Fig. 2.3). 2.9 mL of the cell suspension are added to the reactor where a hydrophilic Biomax polyethersulfone ultrafiltration membrane (Merck KGaA, Darmstadt, Germany) with 5 kDA MWCO and a support disk are placed on top and are sealed with two o-ring ruber seals. The reactor is capped, placed in a 40 °C water bath and N_2-gassed M9-N buffer is injected by a syringe via a Teflon tube (0.1 mm $\oslash_i$). The

reactor is drained with anaerobic M9-N buffer, until the OD_{600} is below 0.01 to minimize post-membrane OB synthesis. Subsequently, a second syringe is filled with anaerobic M9-N buffer, that is supplemented with the substrates to final concentrations of 6 mM NHCB and 12.5 mM DAC and is gassed with N_2 for 5 min to reach anaerobic conditions. The reaction is initiated by pumping the substrate-containing buffer into the reaction vessel via a syringe piston pump and aqueous samples are taken at the outlet.

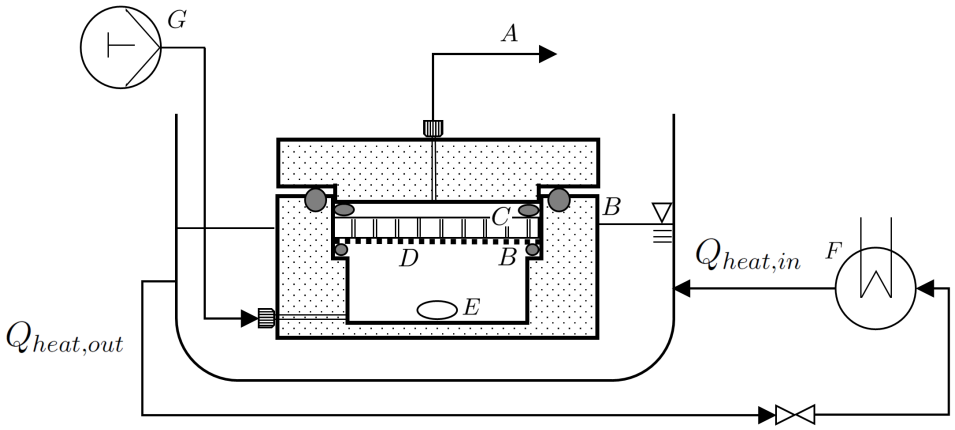

Figure 2.3: Schematic drawing of the experimental setup for biocatalytic OB synthesis in a 3.4 mL scale in continuous mode. A: sampling outlet, B: rubber o-rings, C: support disk, D: membrane, E: magnetic stir bar, F: temperature control, G: Syringe piston pump.

2.10 Analytics

2.10.1 Cell Concentration

For the control of cell growth and to adjust the cell concentration before each OB synthesis, optical density measurements at 600 nm are applied by using UV-Vis spectrophotometry with a Libra S12 spectrophotometer (Biochrom Ltd.,Cambridge, United Kingdom).

2.10.2 Cytochrome c Concentration

Cytc is quantified via the reported hemochrome assay in a slightly modified version[21]. Therefore, the used cell suspension is lysed mechanically with the FPCP, centrifuged (20 min, 4 °C, 5000 xg) and sterile-filtered (cellulose-acetate, 0.22 μm), to receive the CFE. A solution of sodium dithionite (10 mg·mL^{-1}) is prepared in M9-N buffer, pH 7.4. Separately, 1 M NaOH and pyridine are mixed 4:10 (v/v), vortexed 30 s, centrifuged (30 s, r.t., 10000 xg) before the

organic NaOH-pyridine phase is separated for the assay. A cuvette is filled with 700 μL CFE and 250 μL of the NaOH-pyridine phase and 50 μL of the sodium dithionite solution are added. The cuvette is sealed with parafilm immediately and the UV-Vis spectrum is recorded (300 - 600 nm) in 1 nm intervals, immediately. The Cytc concentration can be calculated by Lambert-Beer's law using $\varepsilon_{550-535} = 22.1\,\mathrm{mM^{-1}cm^{-1}}$.

2.10.3 Protein Concentration

The protein content is determined according to Bradford[103]. A calibration curve of bovine serum albumin (BSA) is prepared (20 - 100 μg·mL^{-1}) in M9-N buffer and 50 μL of each calibration standard and sample are transferred to a 96-well plate in triplicates. 200 μL of the diluted ROTI® Quant (Carl Roth GmbH + Co. KG, Karlsruhe, Germany) staining solution is added to each standard or sample containing well and the plate is shaken, incubated (5 min, r.t.) before OD_{595} is recorded with a Infinite 200 Pro plate reader (Tecan Group AG, Männedorf, Switzerland).

2.10.4 Protein Mass

The mass of expressed Cytc and contaminating proteins is quantitatively checked via SDS-PAGE. 15 μL of sample are mixed with 5 μL of RunBlue™ LDS sample buffer (Expedeon AG, Heidelberg, Germany) and incubated (5 min, 80 °C, 600 rpm) in a thermoshaker TS1 (Analytik Jena Taiwan Co., Ltd, New Taipei City, Taiwan). Pre-fabricated RunBlue™ SDS-Page gels (Expedeon AG, Heidelberg, Germany) are placed in a rack, rinsed with running buffer and loaded with the incubated samples and a prestained protein standard Kaleidoscope™ (Bio-Rad Laboratories GmbH, Feldkirchen, Germany) as marker. Electrophoresis is executed with a Phero-Stab 500 powersupply (Biotec-Fischer, Reiskirchen, Germany) for 60 min at <110 mA with 200 V and the gel is stained with Coomassie Instant Blue™ (Expedeon AG, Heidelberg, Germany) for 15 min.

2.10.5 Substrate and Product Concentration

The concentrations of NHCB and OB are quantified from 100 μL of aqueous sample, which are quenched with 150 μL of a 4:6 (v/v) mixture of n-hexane and ethyl acetate containing 6.45 mM 1,2,3-trimethoxybenzene (TMB) as internal standard. The mixture is vortexted 3 x 10 s, centrifuged (3 min, r.t., 10000 xG) and the upper organic phase is transferred to a 2 mL screw-top vial equipped with a 250 μL glass insert. The samples are analyzed by chiral gas

chromatography (GC) using the GC system 7890B and the automatic liquid sampler 7693 (Agilent Technologies Inc., Santa Clara, USA) equipped with a flame ionization detector (FID) and a 25 m x 0.25 mm chiral Lipodex E γ-cyclodextrin column (Machery-Nagel, Düren, Germany) with 5 μL sample and a split ratio of 10:1 at 1.5 mL H_2 carrier gas flow. Calibration curves for NHCB and OB are given in figure 2.4 A and B. The temperature profile is shown in figure 2.4 C with typical retention times of TMB, NHCB and OB.

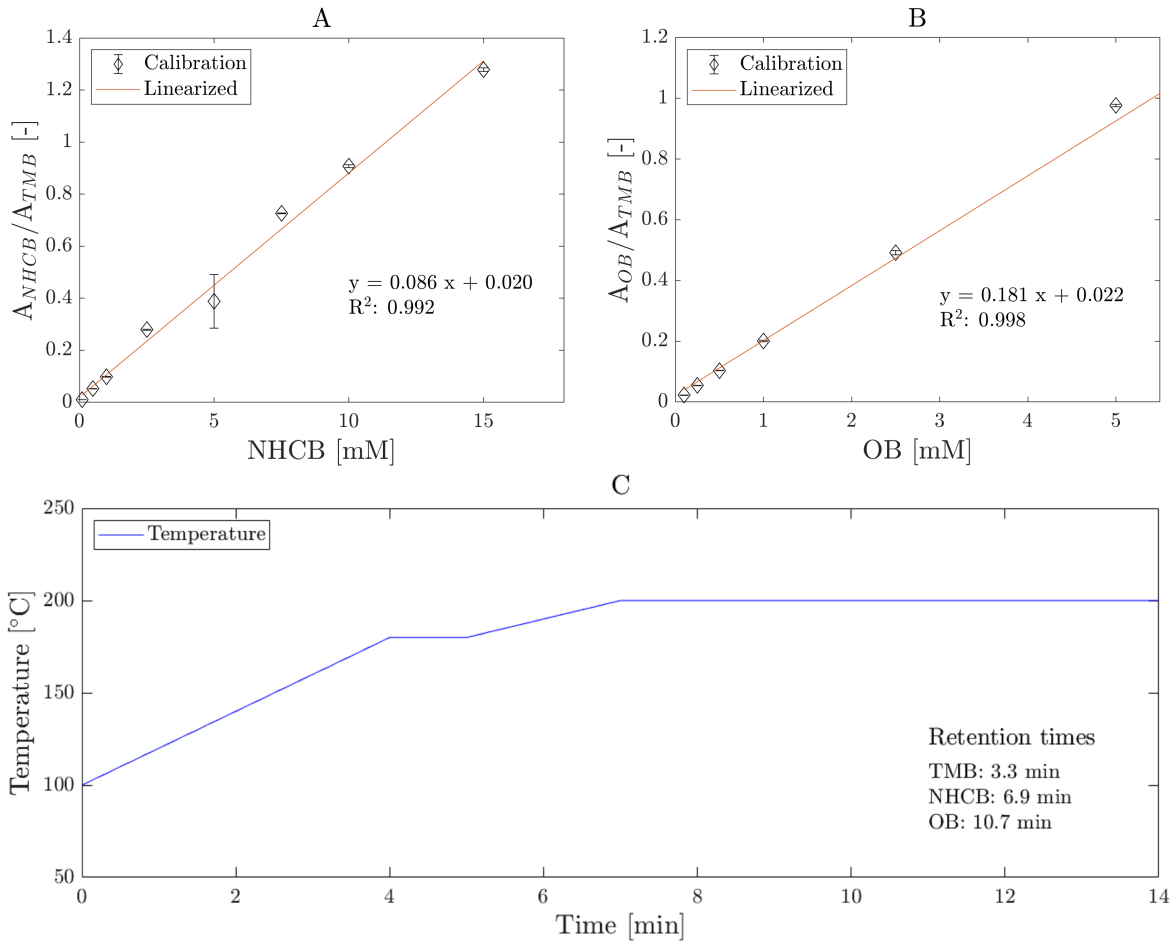

Figure 2.4: Calibration curves of NHCB (A) and OB (B) for GC analysis and the applied temperature profile with typical retention times of TMB (3.3 min), NHCB (6.9 min) and OB (10.7 min) (C).

2.11 Calculations

$$Activity\left[\frac{U}{mg_{Cytc}}\right] = \left[\frac{\mu mol}{min \cdot mg_{Cytc}}\right] = \frac{\frac{\Delta OB}{\Delta t}\left[\frac{mmol}{L \cdot min}\right] \cdot 1000\left[\frac{\mu mol}{mmol}\right] \cdot 1000000\left[\frac{\mu mol}{mol}\right]}{c_{Cytc}\left[\frac{\mu mol}{L}\right] \cdot M_{Cytc}\left[\frac{g}{mol}\right] \cdot 1000\left[\frac{mg}{g}\right]} \tag{2.1}$$

$$STY\left[\frac{mg}{L \cdot h}\right] = \frac{\Delta OB\left[\frac{mmol}{L}\right] \cdot M_{OB}\left[\frac{g}{mol}\right] \cdot 1000\left[\frac{mg}{g}\right]}{\Delta t_{React}\left[h\right] \cdot 1000\left[\frac{mmol}{mol}\right]} \tag{2.2}$$

$$Molar\,OB\,production\,rate\left[\frac{mmol}{min}\right] = \frac{\Delta OB}{\Delta t_{React}}\left[\frac{mmol}{L \cdot min}\right] \cdot V_{Reaction}\left[L\right] \tag{2.3}$$

$$Molar\,OB\,feed\,rate\left[\frac{mmol}{min}\right] = \frac{c_{DAC,Stock}\left[\frac{mmol}{L}\right] \cdot V_{Feed}\left[L\right]}{t_{Feed}\left[min\right]} \tag{2.4}$$

$$D\left[\frac{1}{h}\right] = \frac{Q\left[\frac{L}{h}\right]}{V_{Reactor}\left[L\right]} \tag{2.5}$$

$$\tau\left[h\right] = \frac{V_{Reactor}\left[L\right]}{Q\left[\frac{L}{h}\right]} \tag{2.6}$$

3 Results

This thesis investigates the biocatalytic organoborane synthesis in different fields. Here, substrate properties as well as their stability are explored. Furthermore, the reaction is described kinetically by establishing a mathematical model to simulate the reaction process. Finally, different operation modes were tested finally in order to enhance the space-time yield (STY), final OB concentration (OB_{final}) as well as the TTN of Cytc. In summary, the obtained results shall give an overview of possible opportunities and limitations of enzyme-driven borylation for OB synthesis.

3.1 Starting Material Investigation

A reaction is mostly characterized by focusing on the catalytic activity or process parameters like conversion, yield and selectivity. However, equally important is the investigation of the starting material, where chemical properties of the substrates can be impacted by the reaction conditions. Here, NHCB was investigated with respect to a possible protonation-deprotonation mechanism based on the pH. Furthermore, studies targeted DAC decomposition to examine the impact by water, heat and UV-light.

3.1.1 *N*-Heterocyclic Carbene Borane

Borane Lewis base complexes such as NHCB can be protonated (NHC-B_2^+) or deprotonated (NHCB) according to a solutions pH and thereby influence catalytic reactions [104]. Thus, the pK_b value was determined to identify the pH value, where NHBC and NHC-B_2^+ are in equilibrium.

Experiments were carried out in quintuples via autotitration of 10 and 20 mM NHCB solutions in DI water with 10 mM HCl. The pH was recorded over the added volume of titrant, where a good reproducibility was achieved for all runs (Fig. 3.1).

The equivalence point was determined to 5.44 ± 0.17, leading to a half-equivalence point pK_a of 6.12 ± 0.05. Via equation 3.1 the pK_b value was calculated to 7.88 ± 0.05.

$$pK_b = 14 - pK_a \tag{3.1}$$

Although the determined standard deviation fits to the recorded titration curves a higher error can be assumed due to calibrating titrations of NaOH with HCl with a deviation of 0.8. Thus, the pK_b value of NHCB can be corrected to 7.88 ± 0.8. Independently from this correction, its pK_b classifies NHCB as semi-strong to weak base [105]. The corresponding

conjugated acid is NHC-BH_2^+ with a pK_a of 6.12 ± 0.8 which indicates NHC-BH_2^+ as weak acid [106]. With respect to the Henderson-Hasselbalch equation 3.2, it can be followed, that for a pH value below 6.12 NHC-BH_2^+ is more present, while above pH 6.12 deprotonated NHCB is more common.

$$pH = pK_a - log_{10}\frac{(NHC - BH_2^+)}{(NHCB)} \tag{3.2}$$

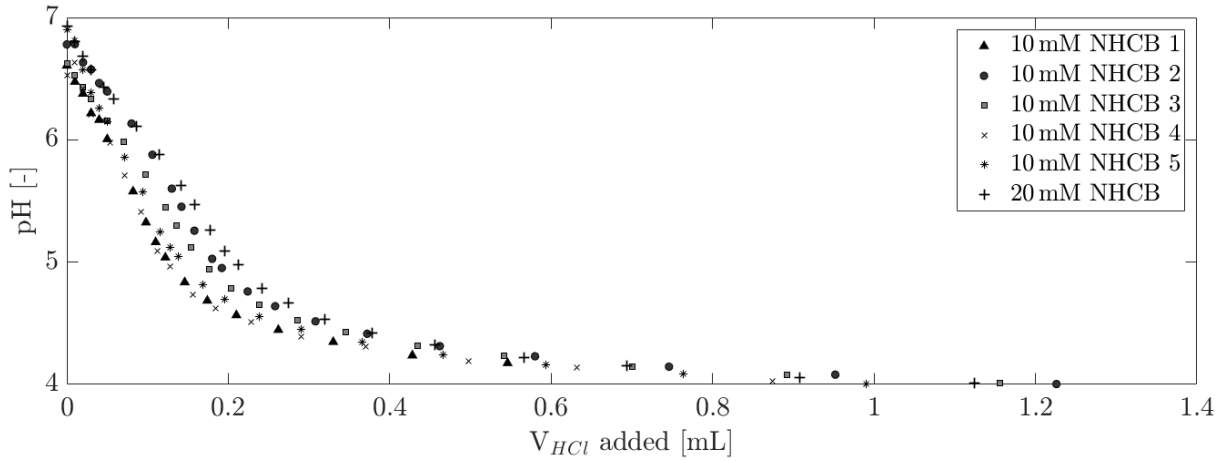

Figure 3.1: Titration of NHCB (10 and 20 mM) with HCl (10 mM) at r.t. and 200 rpm. The pH is displayed over the volume of added HCL. NHCBs equivalence point is determined to 5.44 indication NHCB as semi-strong to weak base.

Since biocatalytic borylation is carried out at pH 7.4, NHCB is prevalently available in its deprotonated form during OB synthesis. This states an important information, as intracellular transport can be strongly influenced by the charge of molecules. Especially, due to the location of Cytc in the mitochondrial intermembrane space, the transport over membranes might be additionally impacted by the protonation state of the borane substrate. Moreover, a direct effect on the reaction rate of Cytc is also imaginable, because DAC associates with Cytc first in form of an electron-deficient carbene. Here, a positively charged NHC-BH_2^+ can be assumed to be more electromagnetically repelled than deprotonated NHCB. However, even though living cells are able to maintain and control a pH gradient, the intracellular or mitochondrial pH is more effecting on the charge of NHCB than the extracellular pH.

Concluding, the titration of NHCB demonstrated, that NHCB is a semi-strong base. Moreover, NHCB is deprotonated under reaction conditions at pH 7.4 but protonates to NHC-BH_2^+ below pH 6.12. As the protonation state is assumed to influence the activity of Cytc, this aspect is additionally worth studying.

3.1.2 Ethyl 2-Diazopropanoate

In order to be able to calculate correct process parameters like conversion and yield based on substrate concentrations, possible side reactions and decompositions of DAC were investigated. Here, the hydrolysis in water was studied as well as the effect of water, increased temperatures and UV-light exposure on diazo group cleavage.

3.1.2.1 Hydrolysis

The utilized DAC ethyl 2-diazopropanoate is an ester, which is known to take part in hydrolysis in water under formation of an alcohol and an acid. Thus, the hydrolysis of DAC would result in a decrease of pH. Therefore, the pH for an aqueous system was recorded over time before and after DAC addition as well as for pure MeCN addition as co-solvent (Fig. 3.2).

The data show a step-wise rise of pH by supplementing 10 mM phosphate buffer with MeCN after 14.6 min (Fig. 3.2A). Since MeCN as organic solvent does not have free protons unlike water, the observed effect is probably caused by a diluted concentration of H^+ ions and leads thereby to an increase in pH. No significant change in pH was recognized afterwards, which marks the equilibrium in the system. In contrast, when MeCN was added with DAC to a final concentration of 12.5 mM DAC, the step-wise pH-increase was recorded again, but was followed by an exponential-shaped decrease, annealing to an equilibrium pH of 7.96 after 83 min (Fig. 3.2B). The drop of pH can be allocated with the hydrolysis of DAC under acid formation, since this effect was not observed without DAC. Although the pH-drop is roughly the scale of MeCN-caused increase, the actual influence of DAC hydrolysis on the availability of undecayed DAC for OB synthesis might be negligible. However, to quantify the amount of hydrolyzed DAC, a comparison experiment with HCl is required. To receive more precise statements with an increasing pH-drop, additional experiments contained 5 mM phosphate buffer in order to evaluate the influence of buffer concentration on the pH-drop during DAC hydrolysis. With 5 mM phosphate buffer the decrease in pH was higher (0.10 ± 0.02) than with 10 mM phosphate buffer (0.04) (Fig. 3.2 C). In addition, the hydrolysis was not completely finished, as the pH did not reach a stable value to indicate an equilibrium. Nevertheless, it has been demonstrated that the pH drops further when applying lower concentrations of buffer.

Within this investigation the hydrolysis of DAC in water was shown. The amount of hydrolyzed DAC is only minor and thus might be negligible when calculating yield or conversion of biocatalytic OB synthesis. In contrast, the cleavage of the diazo group is a severely

topic and, therefore, needs to be investigated intensively.

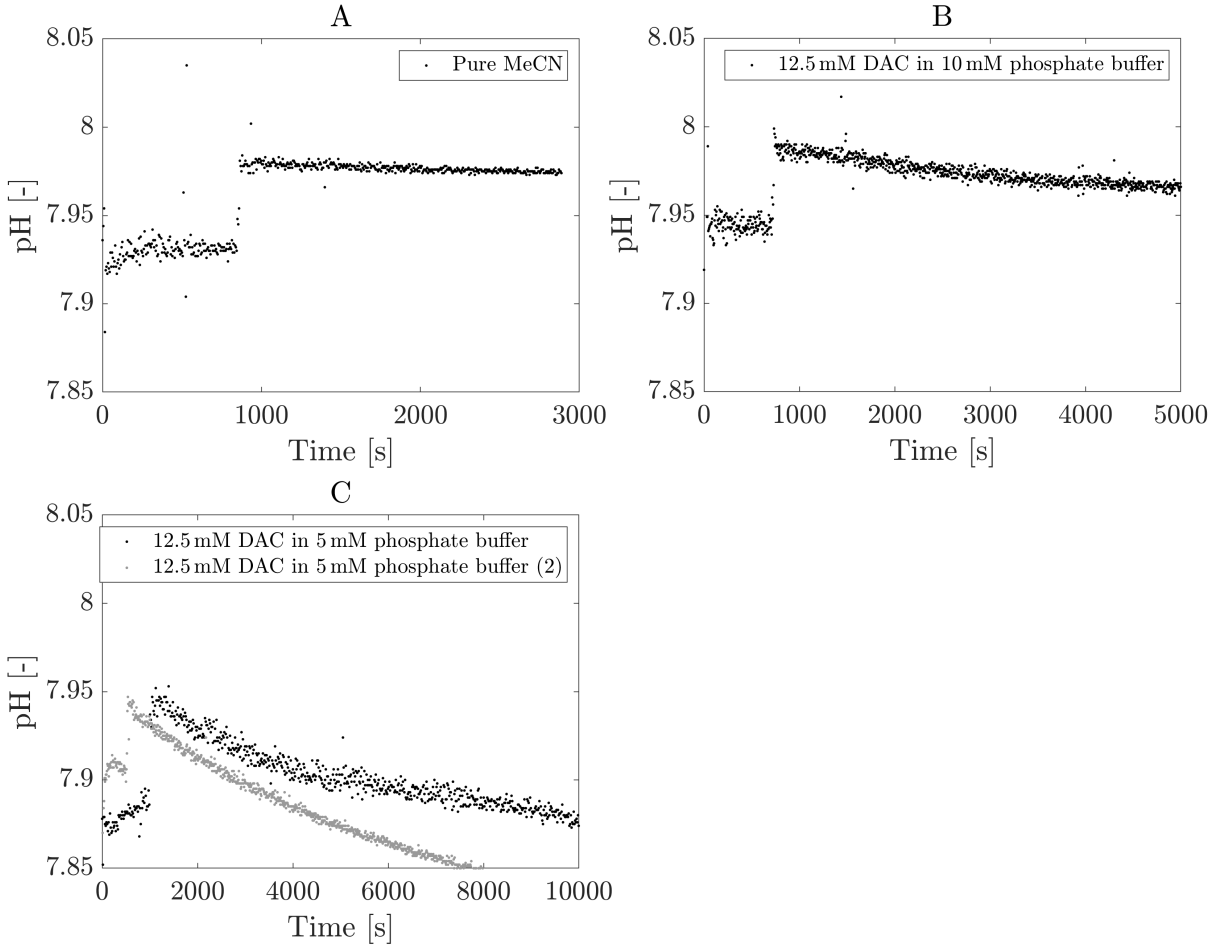

Figure 3.2: PH change due to addition of 5 %(v/v) pure MeCN (A) or MeCN with 12.5 mM DAC in 5 mM (C) and 10 mM (B) phosphate buffer at r.t. and 200 rpm. The pH was allowed to stabilize and reach equilibrium with CO_2 in the air before DAC and MeCN were added. pH was recorded over time before and after DAC addition. Slight decrease of pH after addition due to hydrolysis, which does not effect biocatalytic OB synthesis measurable range.

3.1.2.2 Water-Induced Decay

Aside from the hydrolysis of DAC the cleavage of the diazo moiety into N_2 is a second crucial aspect when considering its stability. A side reaction in water was hypothesized, where DAC would give up its diazo group under the formation of ethyl lactate (EL) and N_2 with converting water into H_2. Therefore, DAC was added into 10 mM phosphate buffer to 12.5 mM and incubated under anaerobic conditions for 24 h. Samples analyzed by GC were compared with commercially purchased EL.

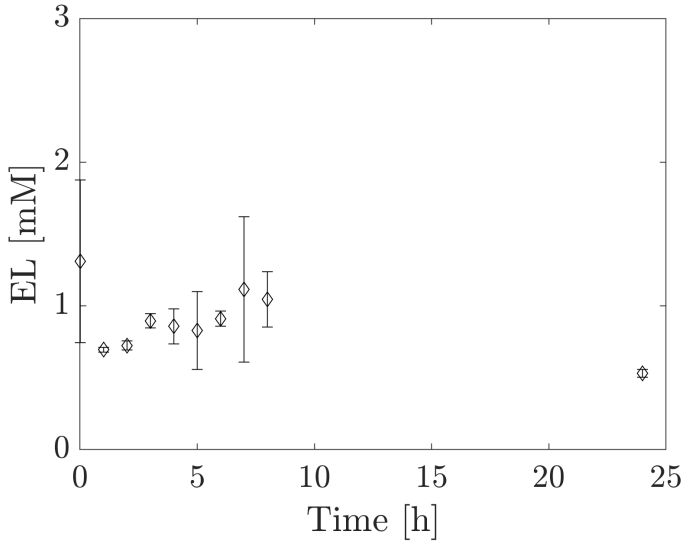

Figure 3.3: EL concentration over time in 10 mM phosphate buffer under anaerobic conditions in a 5 mL thermostated reactor vessel at 40 °C and 1100 rpm. EL was formed immediately to final 1 mM.

EL was found in the samples and its concentration was determined with respect to a calibration curve given in supplementary information (Fig. 6.3). Figure 3.2 shows the EL content over time. Already after 30 s 1.3 ± 0.5 mM EL were present, but declined afterwards before started to increase again up to 1.1 ± 0.5 mM after 7 h. After 24 h the concentration was at 0.5 mM EL. Overall, the EL content seemed to fluctuate only within a range up to 1 mM and with respect to the starting concentration of 12.5 mM DAC the loss of DAC can be considered as minor issue. Nevertheless, the decay into EL is assumed to be an unidirectional reaction, since the rebuilding of the diazo moiety is unlikely due to escaping N_2 and H_2. Thus, an equilibrium is not likely a reason for the fluctuations, which might also not only be caused by deviations in the measurement. Rather a secondary following hydrolysis of EL into lactic acid (LA) and ethanol (EtOH) is imaginable. However, no additional peaks were found to be identified with either EtOH or LA concluding only minor hydrolysis and cleavage rates. As already mentioned, the maximum content of EL reached roughly 10 % of the applied DAC, while the final EL concentration was even lower. If this side reaction would have led to accumulated EL at higher concentrations, this effect would be crucial. Thus, 10 % in the worst case are acceptable, since a fast conversion of DAC by Cytc can minimize the observed loss.

Concluding, DAC can lose its diazo moiety in water to form EL but only to a low percentage of up to 10 %. A secondary hydrolysis of EL into LA can be expected, but only in an even lower ratio and is thereby negligible. However, aside from water-induced losses of DAC

other parameters are known to have enhanced impacts especially on diazo group cleavage.

3.1.2.3 Temperature-Induced Decay

DAC looses its diazo moiety not only due to side reactions with water, but also because of its thermal instability. In order to estimate the margin of DAC loss by elevated temperatures, DAC was exposed to different temperatures for 2 h representing the duration to reach a constant OB concentration during biocatalytic borylation. However, since DAC can not be quantified like OB and NHCB via GC, another analysis method has to be derived.

As DAC and other compounds possessing a diazo moiety absorb UV-light with respect to its molecular conformation, a fingerprint-like absorption spectra can be assumed [68]. Thus, UV-Vis spectrophotometry was applied to quantify and identify DAC. The overall concentration was quantified by using the yellowish colour of DAC resulting from an absorption between 350 and 500 nm with the absorption maximum at λ_{max} of 425 nm. The spectra were recorded for concentrations of 5 to 200 mM and were correlated with the peak height for calibration (Fig. 3.4 A).

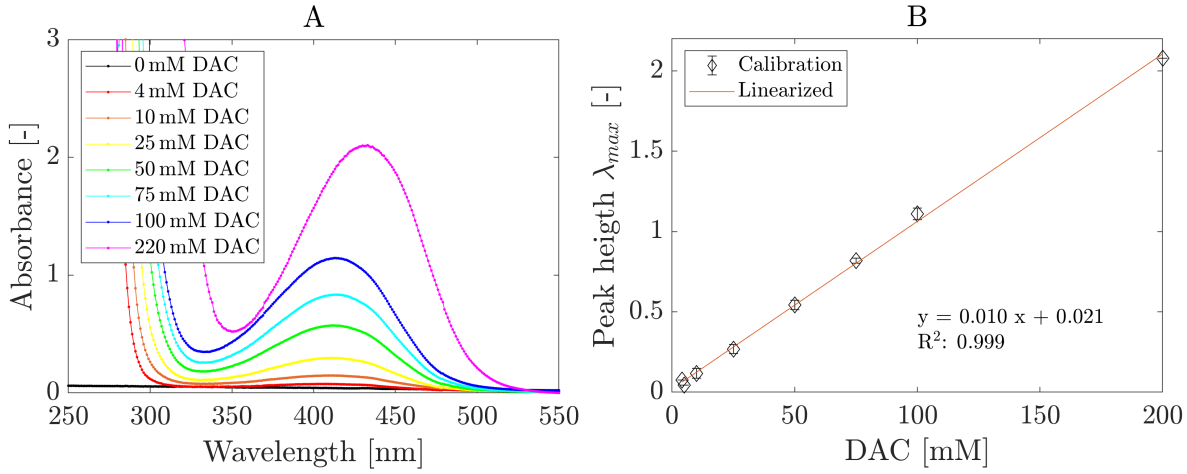

Figure 3.4: Absorption spectra of 0 to 200 mM DAC in MeCN recorded with UV-Vis spectrophotometry (A) and the calibration based on the correlation between concentration and peak height at λ_{max} (B). A reliable quantification of DAC in MeCN according to the recorded peak height is visible.

The data show an increase of peak area and height with rising DAC concentration. When correlating the peak height at λ_{max} to the concentration a linear trend was noticeable and was from this point on used for DAC quantification (Fig. 3.4 B). However, the absorption peaks within the fingerprint-region in the UV range was not visible and seemed to be overloaded. As a result, the concentration was reduced below 3 mM leading to two separated peaks at 220 and 270 nm, which were in the range of fingerprint peaks of other diazo compounds (Fig.

3.5) [68]. The first peak at $\lambda_{DAC,1}$ at 220 nm was flat and narrow, while the second peak $\lambda_{DAC,2}$ at 270 nm was higher and wider.

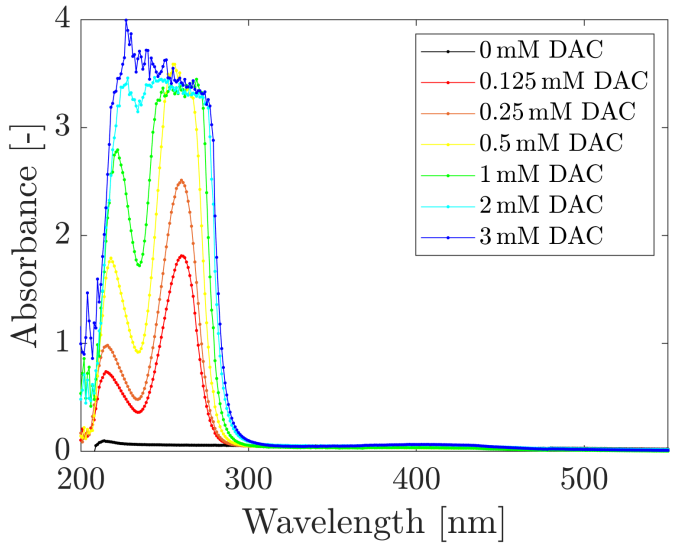

Figure 3.5: Absorption spectra of DAC in MeCN recorded with UV-Vis spectrophotometry to identify diazo group specific absorption peaks in the UV range. Fingerprint-peaks were found at $\lambda_{DAC,1}$ of 220 nm and $\lambda_{DAC,2}$ of 270 nm.

With a fingerprint region in hand, the temperature-induced decay of DAC was targeted. Several samples of 0.25 mM DAC in MeCN were incubated with a thermoshaker at temperatures from 20 to 85 °C for determined time intervals, before being cooled on ice and measured afterwards via UV-Vis spectrophotometry. The procedure was repeated for different temperatures. Figure 3.6 displays the UV-spectra of DAC after incubation at 20, 55, 60, 65, 75 and 85 °C for up to 120 min.

The recorded spectra revealed a visible influence due to temperature on both peaks in the UV-range. Most prominently, the peak height at $\lambda_{DAC,1}$ began to increase at 60 °C after 15 min. Same was observed at 65 °C with a higher increase after 15 min. A higher temperature and longer incubation time correlated with an increased peak at $\lambda_{DAC,1}$ increased. At 85 °C the peak at $\lambda_{DAC,1}$ after 120 min was even higher than at $\lambda_{DAC,2}$. In contrast, $\lambda_{DAC,2}$ stayed within its height and area and seemed to be unaffected by incubation with elevated temperatures. Thus it can be assumed, that the separation of the diazo moiety, which is the main decomposition step, is visualized by the increase of the peak height at $\lambda_{DAC,1}$. Since the peak at $\lambda_{DAC,2}$ stayed unchanged, it could be utilized as reference value to estimate the degree of decomposition. Here, a ratio of the peak heights of the peaks at $\lambda_{DAC,1}$ to $\lambda_{DAC,1}$ was calculated for each temperature after 120 min (supplementary information tab.

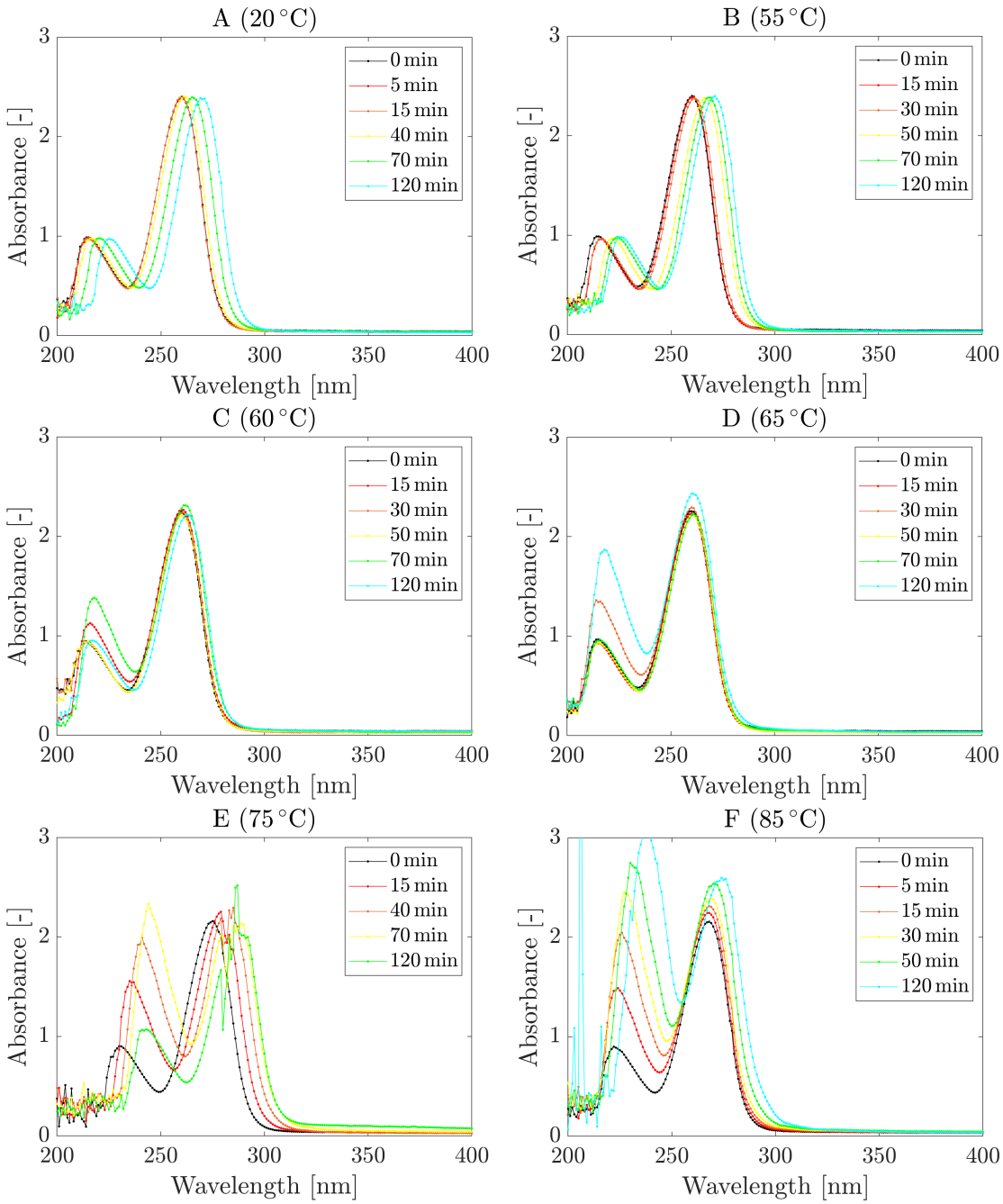

Figure 3.6: Change of absorption spectra of 0.25 mM DAC in MeCN recorded with UV-Vis spectrophotometry in the fingerprint-region due to decomposition caused by incubation at elevated temperatures between 20 and 85 °C at 600 rpm. Fingerprint-peak at $\lambda_{DAC,1}$ grew with increasing incubation time $t_{Incubation}$ and T, while peak height at $\lambda_{DAC,2}$ stayed constant. Peak $\lambda_{DAC,1}$ was assumed to correspond to degree of thermal decomposition of DAC.

6.1). While at 20 and 55 °C the ratio stayed at 0.4, indicating undecayed DAC, the ratio increased over 0.89 at 65 °C to 1.19 at 85 °C. This demonstrates a clear trend of increasing

ratio and thereby an increasing decomposition with rising temperatures.

In summary, the results demonstrate, that it is possible to quantify DAC in pure MeCN using UV-Vis spectrophotometry. Moreover, a change of diazo moiety-related peak heights was observed in the UV-range of the recorded spectra during elongated incubation at elevated temperatures starting at 60 °C. Thus, a ratio of the heights between two peak was introduced to estimate the decomposition of DAC. However, since no end point of the decay was known, the determined ratio can only be used to compare the samples with each other. Nevertheless, the change of the molecular structure of DAC by temperature is supported.

3.1.2.4 UV-Light-Induced Decay

In addition to water and temperature, UV-light is known to cause the separation of N_2 from DAC. To investigate the dimension of the UV-light-induced decay, quartz glass vials were supplemented with DAC to 0.25 mM, flushed with Ar, sealed and incubated at r.t. for up to 30 d to naturally daylight at a window. The degree of decomposition was evaluated via UV-Vis spectrophotometry with respect to the fingerprint-peaks of DAC in the UV-range (Fig.3.7).

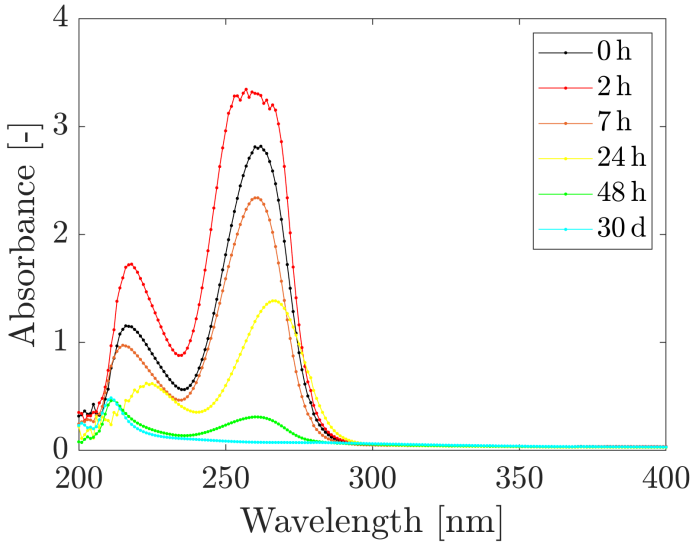

Figure 3.7: Change of absorption spectra of 0.25 mM DAC in MeCN recorded with UV-Vis spectrophotometry in fingerprint-region due to decomposition caused by incubation under UV-light at r.t. for 30 d. Fingerprint-peaks at $\lambda_{DAC,1}$ and $\lambda_{DAC,2}$ decreased with increasing incubation time. Peak height ratio increased over time until peak at $\lambda_{DAC,2}$ was no longer detectable, probably indicating full decomposition of DAC.

The results show initial fingerprint-peaks of the unexposed sample at $\lambda_{DAC,1}$ and $\lambda_{DAC,2}$ as expected, while the peak height ratio is also comparable to the ratio of undecayed DAC

as already determined during temperature studies. The same behaviour was observed after 2 h exposure to daylight. With ongoing exposure to UV-light both peak heights changed significantly. Since the peak at $\lambda_{DAC,2}$ was not to be expected to change due to decomposition, another effect has to be considered here. As evaporation of the solvent MeCN would lead to a rise of DAC content, the peak at $\lambda_{DAC,2}$ would rather increase than decrease. Hence, a side reaction or decay followed by a further reaction of the created carbene are two possible explanations. Since no further sample analysis via GC-MS or NMR was executed, no exact statement can be made here. Nevertheless, the peak ratio of $\lambda_{DAC,1}$ to $\lambda_{DAC,2}$ rose from 0.4 to 1.4, which states an advanced decay. After 30 d the peak at $\lambda_{DAC,1}$ was fully flattened resulting in a complete decomposition, which could have also be the case shortly after 48 h due to lack of data.

Concluding, although the decomposition by UV-light takes at maximum one month to complete and is thereby much slower compared to temperature-induced decay, this demonstrated, that UV-light has a significant effect on the chemical stability of DAC. However, since unconverted DAC is only present for minutes to a few hours in the reaction medium and since the reactors in industry are usually light-proof, the effect on biocatalytic borylation can be considered as low. Even for the examined tests within this study using glass-reactors, the influence of UV-Light can be neglected. Instead, the determined behaviour under UV-light is more important on storage conditions of DAC. However, analytics should be performed under the exclusion of light to enhance the accuracy.

3.2 Kinetic Characterization

A kinetic characterization is executed for Cytc-driven OB synthesis. Therefore, the temperature and the pH-value are screened for suitable ranges for the measurement of initial reaction rates depending on NHCB and DAC concentrations. Further kinetic studies are carried out in order to identify inhibitions and deactivations by the substrates or the product. The collected data is utilized to feed a model for the determination of kinetic parameters (codes given in supplementary information 6.2). Those fitted values are required for the simulation of OB synthesis based on the determined parameters to evaluate the overall kinetic model.

3.2.1 Temperature Screening

The enzymatic reaction rate v depends on the temperature. Thus, a temperature screening was executed to locate suitable temperatures for the subsequent Michaelis-Menten studies.

Cytc as a biocatalyst from a hyperthermophilic organism delivers catalytic activity over a widened temperature range leading to investigated temperatures from 15 to 85 °C. The initial reaction rate (Eq. 2.1) was measured via initial rate measurements normalized to the Cytc content in 5 mL thermostated glass reactors in a batch mode with *E. coli* BOR^{R1} whole cells at OD 5 resuspended in pH 7.4 M9-N buffer with 12.5 mM DAC and 6 mM NHCB with 5 % (v/v) MeCN as co-solvent under anaerobic conditions. Samples were taken for the first seven minutes every minute and the initial reaction rate was calculated using the slope of product formation over time in the linear range. Figure 3.8 gives an overview on the initial reaction rate of Cytc depending on different temperatures.

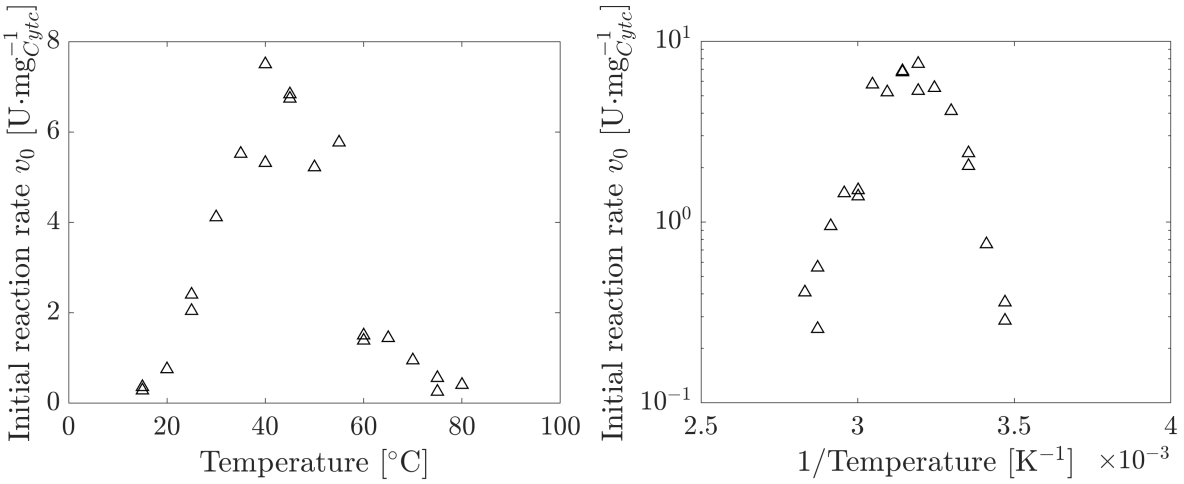

Figure 3.8: Temperature screening for Cytc BOR^{R1} hosted in *E. coli* BL21 DE3 at OD 5 resuspended in M9-N buffer at pH 7.4 catalyzing biocatalytic borylation. Initial reaction rates were measured during the first 7 min of synthesis with substrate concentrations of 6 mM NHCB and 12.5 mM DAC at temperatures from 15 to 85 °C and normalized to the Cytc concentration. Results are plotted in linear proportion (A) as well as in logarithmic reciprocal dependence for an Arrhenius plot (B). A temperature increase to 40 °C improved the initial reaction rate significantly.

Within the temperature range from 15 to 25 °C an exponential increase of the initial reaction rate to 2 U·mg^{-1} is visible. This is additionally proved with a linear increase shown in the Arrhenius plot. With further elevation of the temperature the initial reaction rate rises linearly to 5.8 U·mg^{-1} at 35 °C, before reaching its maximum at 40 °C with 7.5 U·mg^{-1}. This was expected due to the rule of thumb derived from van't Hoffs equation [82]. At temperatures above 40 °C the initial reaction rate fades slowly to 6 U·mg^{-1} at 55 °C, because the deactivation starts to dominate, before dropping significantly to below 2 U·mg^{-1} at 60°C. At 80 °C the initial reaction rate is at 0.4 U·mg^{-1}, which resolves in a completely denaturated Cytc. According to the Arrhenius plot, the deactivation follows an exponential decrease. However, temperatures up to 40 °C revealed impressing improvements in the initial reaction

rate, where 35 and particularly 40 °C reach reaction rates of more than twice the value the reference temperature of the study of Kan *et al.* (2017) at 25 °C [21]. Moreover, cells stayed intact during the tests for at least 30 min demonstrating stability due to favourable temperatures of the mesophilic host *E. coli* at around 37 °C. Here, temperatures *E. coli* above 42 °C lead to extended stress and a reduced protein expression. This could be a reason for the lowered initial reaction rate at 45 °C as mass transfer of substrates and product might be connected to protein arrangement in different cell compartments and along membranes. Further elevated temperatures of 46 °C and above lead to a significantly increased cell death rate where an extended cells lysis releases Cytc to substrates, co-solvent and other hazards [107]. Especially the liberation of Cytc to DAC at elevated concentrations is surely one of the most crucial effects on the initial reaction rate of Cytc, as the described deactivation mechanism immediately interferes with the biocatalyst. Since intense foaming was observed at temperatures above 45 °C, being associable with protein release during cell lysis, these effects are highly likely here [108]. If temperatures rise even higher, they do not only damage the host cell, but also interfere negatively with Cytc itself. The origin of Cytc, hyperthermophilic *R. marinus*, favours 65 °C, giving Cytc the ability to maintain the initial reaction rate at elevated temperature. But due to the missing protection of several cell membranes, Cytc possibly forfeits most of its catalytic activity already at 60 °C by partial denaturation.

Concluding the temperature screening, Cytc was found to be active over a wide temperature range. However, a compromise of reaction initial rate and cell stability needs to be found to protect Cytc from exposure to extracellular hazards. Thus, 35 and 40 °C were selected with 25 °C as reference temperature for kinetic studies for Michaelis-Menten parameter determination. The same needs to be examined for the pH as second influential parameter.

3.2.2 pH Screening

As a change in temperature revealed a tremendous improvement on initial reaction rate of Cytc, a second screening is examined to locate a pH optimum yielding for comparable effects. Here, the stability of the host cell is as important as the initial reaction rate of Cytc.

E. coli can manage intracellular pH control via homeostasis from pH 5.5 to 9, which is mandatory to maintain an functional Cytc. Thus, the screening investigated pH values from acidic 5 to basic 9 to determine the activity as initial reaction rate normalized to the Cytc concentration. Experiments took place in 5 mL thermostated glass reactors in a batch mode with *E. coli* BOR^{R1} whole cells resuspended to OD 5 with initial substrate concentrations

of 12.5 mM DAC and 6 mM NHCB with 5 % (v/v) MeCN as co-solvent under anaerobic conditions in M9-N buffer, which was set to the respective pH. Temperature was set to 40 °C, because Cytc showed the highest initial reaction rate in temperature investigations. pH-depending reaction rates are displayed in figure 3.9.

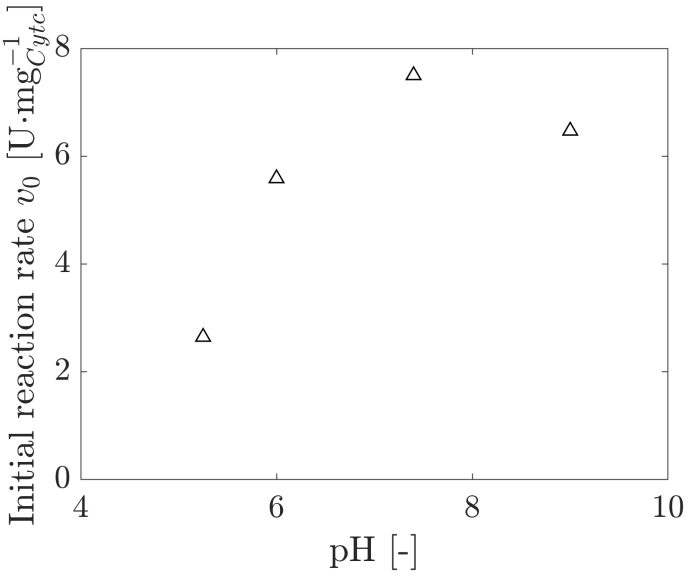

Figure 3.9: Temperature screening for Cytc BOR^{R1} hosted in *E. coli* BL21 DE3 at OD 5 resuspended in M9-N buffer catalyzing biocatalytic borylation. Initial reaction rates were measured during the first 7 min of synthesis with substrate concentrations of 6 mM NHCB and 12.5 mM DAC at pH 5 to 9 and 40 °C and normalized to the Cytc concentration. pH 7.4 lead to the highest initial reaction rate, while even a slightly acidic or basic pH reduced the enzyme performance.

The recorded reaction rates proved the expectation, that a neutral pH would be beneficial for the catalytic performance of Cytc. Here, pH 7.4 reached the highest initial reaction rate of 7.5 U·mg^{-1}. For more acidic pH values a lowered initial reaction rate was observed, where in particular pH 5 yielded less than 40 % of the initial reaction rate at pH 7.4. An alkaline milieu at pH 9 leads to a reduction of the initial reaction rate as well. The loss is about 15 % and is thereby slightly less significant as the lack of initial reaction rate at pH 6. However, it is questionable, if the determined optimum at pH 7.4 is also the global optimum. With narrower intervals enhanced reaction rates could have been found inbetween the studied pH values. Aside from the activity aspect, the stability of the host cell was additionally evaluated visually. Here, especially at pH 5 the cell suspension started to foam already before the reaction was initialized. The suspension of cells in particular led to an intense foaming, which was partly reduced by instant cooling on ice before OB synthesis. After supplementing the reactors with the suspension and elevating the temperature to 40 °C, cells started to foam again. Although not having a microscopic proof, cell lysis can

be expected as foaming can indicate a rising protein content, which was also observed at elevated temperatures [108]. Thus a connection between foaming and the decline of the initial reaction rate can be drawn. Foaming was also visible at pH 6 and 9 but less pronounced and at a later state of the experiment. Nevertheless, the foaming increased with ongoing duration of the experiment up to 20 min. Since a synthesis of OB would take longer than 20 min up to hours to complete, the application of acidic and alkaline milieus is more than challenging. Only pH-neutral milieus seem to maintain cell stability over an elongated time. Without a pH-controlling host, Cytc would be released to the hazards described above and is additionally changed in its charge by the pH according to its pI. Here, a pH below the pI leads to a positive charge of the proteins surface, while a more alkaline pH has a negatively charged Cytc as consequence. Within the fluctuations in charge, structural adjustments are also happening due to electromagnetic molecular attraction and repulsion of the amino acid residues. This might lead to additional losses in initial reaction rate by changing the conformation and blocking the way to the active side for the substrates.

Overall a pH screening demonstrated that a neutral milieu brings the highest initial reaction rate of Cytc for biocatalytic borylation. An acidic as well as an alkaline pH results in a drop of initial reaction rate although *E. coli* can control its intercellular pH. This might be caused by structural changes achieved by charging of Cytcs surface according to its pI. Moreover, an extended test duration at pH 5, 6 and 9 pH stressed the cells since foaming was observed later. Thus pH 7.4 was selected for the study of Michaelis-Menten kinetics for biocatalytic borylation.

3.2.3 Determination of Kinetic Parameters

The estimation of kinetic parameter requires experimental data, which feeds the mathematical model. Thus, the initial reaction rate depending on the substrate concentration is measured and plotted as Michaelis-Menten plot. Moreover, inhibition studies give view on activity-reducing interactions between OB, NHCB and DAC with Cytc.

3.2.3.1 Michaelis-Menten Kinetics

Michaelis-Menten plots contain important knowledge on a kinetic behaviour of an enzyme-catalyzed reaction. Therefore, with selecting suitable reaction conditions based on the previous screening, initial reaction rates depending on NHCB and DAC concentration were determined.

The Michaelis-Menten plots were generated by changing the concentration of one sub-

strate, while keeping the second substrate constant and measuring the initial reaction rate. Experiments were carried out in 5 mL thermostated glass reactors at 25, 35 and 40 °C under anaerobic conditions in a batch mode with *E. coli* BOR^{R1} whole cells at OD 5 resuspended in M9-N buffer at pH 7.4. For NHCB studies, the substrate concentration varied from 1 to 18 mM, while DAC stayed at 12.5 mM. Here, pre-study experiments showed (data not shown), that this concentration is sufficient to reach the maximum initial reaction rate v_{max}. For DAC studies, concentrations varied between 1 and 12.5 mM DAC, while NHCB stayed at 6 mM. Figure 3.10 shows the Michaelis-Menten plots for DAC and NHCB at the investigated temperatures. The initial reaction rate is normalized to the Cytc content and plotted against the concentration of the varying substrate.

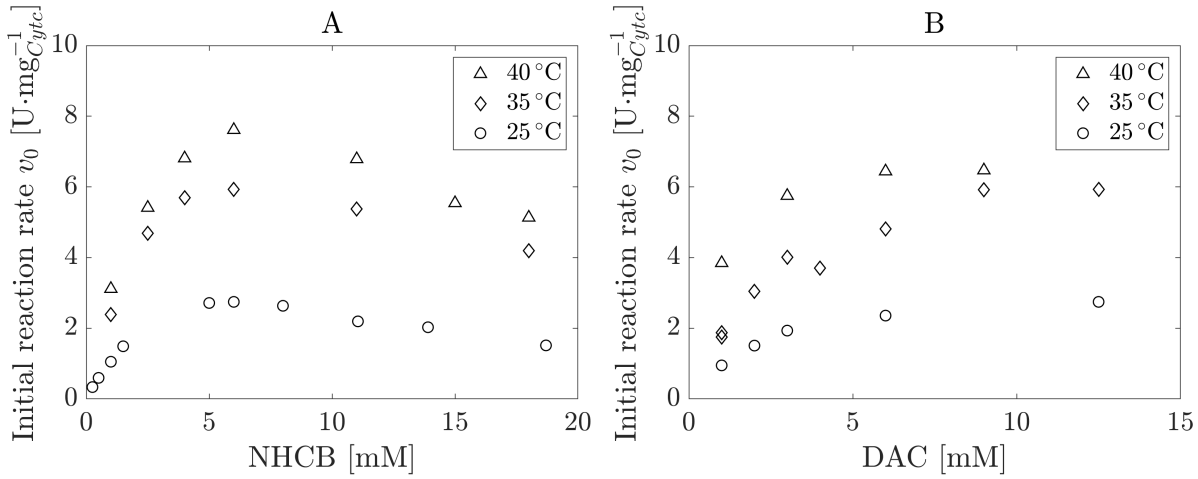

Figure 3.10: Michaelis-Menten plots for biocatalytic borylation for NHCB (A) and DAC (B), catalyzed by Cytc BOR^{R1} harboured in *E. coli* BL21 DE3 at OD 5 resuspended in M9-N buffer at pH 7.4. Reaction rates were measured during the first 7 minutes of synthesis with substrate concentrations of 1 – 18 mM NHCB, while DAC stayed constant at 12.5 mM and 1 – 12.5 mM DAC, while NHCB stayed constant at 6 mM. Temperatures of 25, 35 and 40 °C were tested. DAC kinetics did not show any hint for a reversible substrate inhibition up to 12.5 mM. NHCB inhibited Cytc above 6 mM. An increase of the initial reaction rate with elevated temperatures was detected for all substrate concentrations.

The Michaelis-Menten plots for NHCB show an increase of the initial reaction rate from 25 over 35 to a maximum of 7.5 U·mg^{-1} at 40 °C for all investigated NHCB concentrations. This was expected due to the results from the temperature screening. Nevertheless, these insights were now widened to a broad substrate concentration. In addition, a clear gap was observed between the plots of 25 and 35 °C, which leaves space for the plot at 30 °C fitting to the linear increasing initial reaction rate found in the temperature screening. Aside from the temperature influence, a substrate surplus inhibition was observed, which leads to reduced reaction rates above 6 mM NHCB and causes a decline of the initial reaction rate of

almost 25 % at 18 mM. Thus, the initial reaction rate measurements depending on DAC were examined at 6 mM NHCB. In contrast to NHCB, DAC does not show any case of substrate surplus inhibition up to 12.5 mM. The progress of the curves for 25 and 40 °C are shaped comparable and only factorized. But at higher DAC concentrations at 35 °C the increase of the initial reaction rate is steeper and longer until curve saturation. This might be caused by some data points at 3 and 6 mM DAC, which show in combination with each other an unsteady and slightly fluctuating progress within the Michaelis-Menten plot.

The sufficient collection of experimental data allowed the determination of kinetic parameters via numerical fitting using the non-linear regression function *nlinfit* in MATLAB according to Michaelis-Menten kinetics. For DAC a correlation without correlation was assumed, while the term for NHCB was based on a substrate-surplus inhibition type, which in summary leads to the adapted equation 3.3.

$$v = v_{max} \cdot \frac{[NHCB]}{K_{m,NHCB} + [NHCB](1 + \frac{[NHCB]}{K_{i,NHCB}})} \cdot \frac{[DAC]}{K_{m,DAC} + [DAC]} \tag{3.3}$$

With the kinetic parameters v_{max}, $K_{m,NHCB}$, $K_{m,DAC}$ and $K_{i,NHCB}$ fitted to the measured data, the Michaelis-Menten plots were simulated based on these results with respect to the obtained experimental data (Fig 3.11).

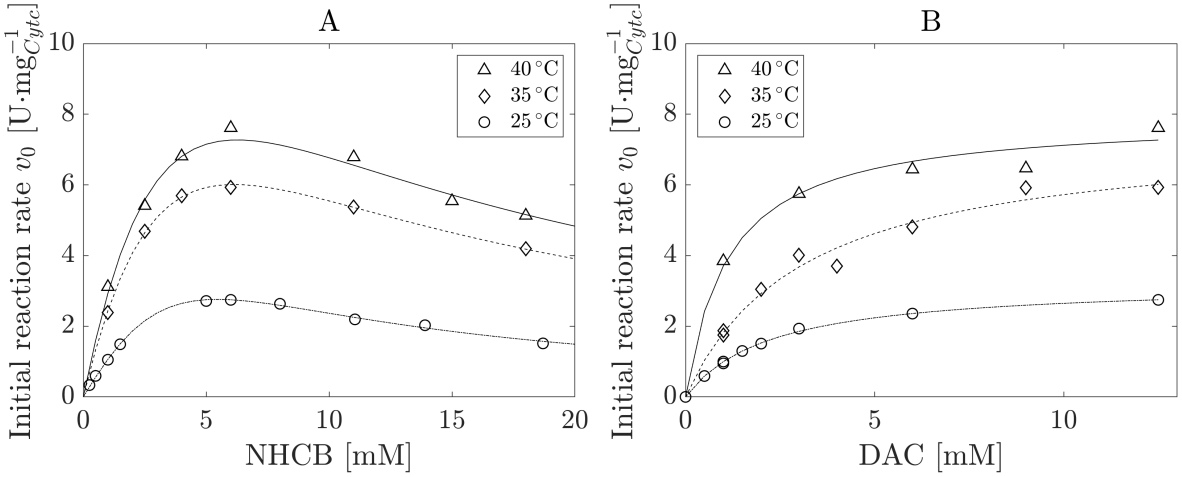

Figure 3.11: Numerically fitted Michaelis-Menten plots for biocatalytic borylation catalyzed by Cytc BOR^{R1} harboured in *E. coli* BL21 DE3 for NHCB and DAC, based on experimental data to determine kinetic parameters v_{max}, $K_{m,NHCB}$, $K_{m,DAC}$ and $K_{i,NHCB}$. Simulated Michaelis-Menten curves (shown as lines) anneal closely to the experimental data.

It can be shown, that the simulated Michaelis-Menten curves anneal closely to the experimental data, leading to realistic values for the fitted kinetic parameters, which are shown in table 3.1.

Table 3.1: Numerically estimated kinetic parameters for Cytc-driven biocatalytic borylation. The parameters were calculated via non-linear regression in MATLAB. 95 % confidence intervals are given in addition.

Parameter	25 °C	35 °C	40 °C
v_{max} [U·mg^{-1}]	26.4 ± 20.0	23.8 ± 15.4	24.1 ± 15.6
$K_{m,NHCB}$ [mM]	19.4 ± 16.2	6.6 ± 5.8	6.4 ± 5.8
$K_{m,DAC}$ [mM]	2.2 ± 0.3	3.1 ± 0.8	1.1 ± 0.5
$K_{i,NHCB}$ [mM]	1.5 ± 1.3	5.7 ± 5.1	6.2 ± 5.6

The obtained kinetic parameter support the collected experimental data. In particular, v_{max} was estimated to increase with rising temperature from 35 to 40 °C. Additionally, $K_{m,NHCB}$ and $K_{i,NHCB}$ were approximated to concentrations within a close range. This behaviour is typical for a substrate surplus inhibited Michaelis-Menten kinetic with an initial reaction rate-concentration course similar to the course shown in figure 3.10 [109]. $K_{m,NHCB}$ decreases at elevated temperatures, which is connected to a stronger bond between NHCB and Cytc at higher temperatures. Additionally, as $K_{i,NHCB}$ is increasing at elevated temperatures, the substrate surplus inhibition seems to be less impacting. Moreover, $K_{m,NHCB}$ and $K_{i,NHCB}$ anneal with a rise in temperature, which further supports the assumption above. Thus, it might be possible, that even higher temperatures could thereby lead to a reaction, that is way less inhibited by NHCB. Nevertheless, the 95 % confidence intervals for most approximated parameters are in the scale of the values itself, usually indicating error-prone and less trust-worth values [110]. Moreover, v_{max} at 25 °C do not fit to expectations, as the fitted value is higher than for 35 and 40 °C. In contrast, only the confidence intervals of $K_{m,DAC}$ are less than 50 % of the estimated value for the parameter. Although the confidence intervals were calculated to relatively high values compared to the kinetic parameters, the fit of the simulated and the experimental Michaelis-Menten plots is more than precise. This demonstrates, that the relationship between substrate concentration and the initial reaction rate was closely reproduced. Thus, the confidence intervals should not be overinterpreted.

Additionally, the correlation between $K_{i,NHC}$ and $K_{m,NHC}$ was determined, since this ratio gives information on expectable conversions (Fig. 3.11A). While an advantageous conversion can be expected at $K_{i,NHC}/K_{m,NHC}$ above 1, the reaction is severely inhibited at ratios below 1 [111]. Moreover, K_{cat} was further determined from v_{max} to get further statements of the effect of temperature on Cytc performance (Fig. 3.12B).

The ratio $K_{i,NHC}/K_{m,NHC}$ correlates the effects of initial reaction rate reduction by inhibition to initial reaction rate elevation according to Michaelis-Menten kinetics. Thus, a

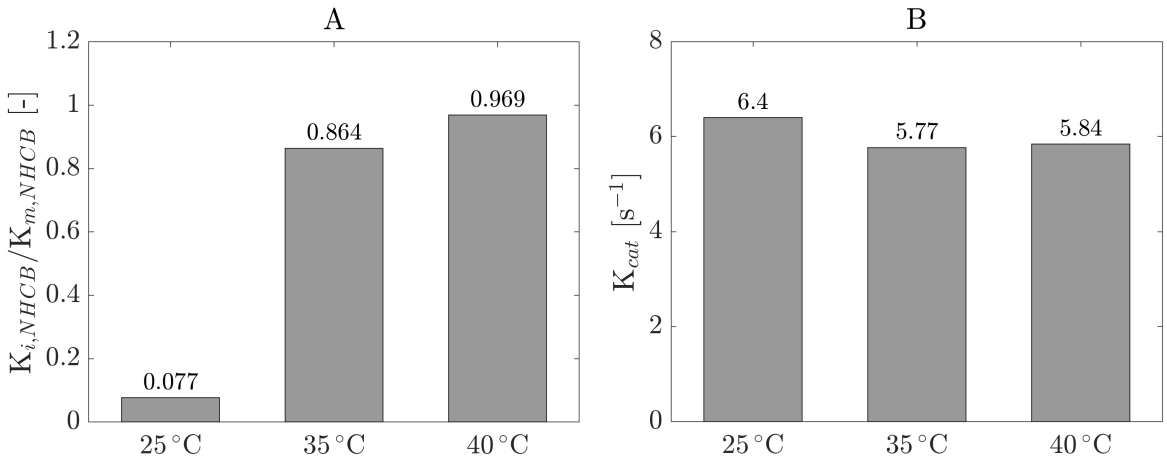

Figure 3.12: Ratio of numerically fitted $K_{i,NHC}$ and $K_{m,NHC}$ (A) as wells as K_{cat} (B) for biocatalytic borylation catalyzed by Cytc BOR^{R1} harboured in *E. coli* BL21 DE3

.

rising ratio is beneficial since activity limiting conditions occur at elevated substrate concentrations at a high $K_{i,NHC}$. At this point, the obtained data show this behaviour, as the $K_{i,NHC}/K_{m,NHC}$ increased with rising temperature. Especially, between 25 and 35 °C the ratio multiplies by more than a magnitude, which is mainly caused by an increase of $K_{i,NHC}$ from 1.5 to 5.7 mM. Above 35 °C the ratio only rose slightly to 0.97 mM·mM^{-1}. Despite this improvement, the $K_{i,NHC}/K_{m,NHC}$ stays below 1 mM·mM^{-1}, which states a boundary for good conversions [111]. This value needs therefore to be surpassed to gain an effective process. In contrast to $K_{i,NHC}/K_{m,NHC}$, K_{cat} does not increase with rising temperature, but drops slightly from 6.4 to 5.77 s^{-1}. This was expected due to a direct correlation to the estimated v_{max}. K_{cat} values above 100 s^{-1} state a reaction rate, which is sufficiently fast for industrial applications [112]. Since the calculated K_{cat} values are two magnitudes below this threshold, either additional reaction engineering or genetic engineering of the investigated Cytc is required.

In summary, the dependency of the initial reaction rate on the concentration of DAC and NHCB, respectively, were determined for 25, 35 and 40 °C. The data show a substrate-surplus inhibition by NHCB, but no reversible inhibition by DAC. The highest initial reaction rate of 7.5 U·mg^{-1} was achieved at 12.5 mM DAC and 6 mM NHCB. The Michaelis-Menten equation was adjusted to the observed behaviour and kinetic parameters were approximated numerically to fit the experimental data. The simulation reproduces the experimental data precisely and the determined kinetic parameters give important insights about the strength of inhibition, but yield a low accuracy. Overall, the obtained parameters can be utilized to

simulate the reaction process of biocatalytic OB synthesis. Nevertheless, additional knowledge about a product inhibition as well as irreversible deactivations is required to complete the kinetic model.

3.2.3.2 Inhibition and Deactivation Studies

Aside from reversible inhibitions, which reduces the initial reaction rate for a specific range of concentration, irreversible inhibitions or deactivations lead to a permanent change in protein conformation and are thereby a more severe aspect in reaction kinetics. Here, the deactivating effect of DAC on Cytc has to be described quantitatively in order to simulate the reaction process realistically [74, 21]. For NHCB such behaviour is not yet described in literature, but should be checked, additionally. Thus, deactivation studies are carried out to investigate both substrates towards deactivation of Cytc.

As the deactivation of enzymes by possible inhibitors increases with expanding duration of substrate-to-enzyme contact, the initial reaction rate was determined with respect to the incubation time with one of the substrates. Experiments were examined in 5 mL thermostated glass reactors at 40 °C under anaerobic conditions in a batch mode with *E. coli* BOR^{R1} whole cells at OD 5 resuspended in M9-N buffer at pH 7.4. Only the substrate to be investigated was added in the beginning of the experiment and incubated for changing durations, before the addition of the second substrate initiated the reaction process and the sampling in 1-minute intervals over 7 min. Substrate concentrations were at 6 mM NHCB and 12.5 mM DAC and substrates were incubated up to 60 min and 90 min, respectively. Figure 3.13 pictures the results of the collected experimental data for the deactivation studies.

The results prove the expectations due to a described denaturation effect of DAC on P450 [74]. An incubation with DAC prior to reaction initiation leads to a reduction of the initial reaction rate. This effect is severe, as the drop of the initial reaction rate is exponential and results in a complete lack of activity after 60 min. Although it could be shown, that DAC deactivated Cytc irreversibly, it is questionable, if the deactivation follows the same mechanism as described in literature. Since Cytc is build up by a different sequence of amino acids compared to the investigated P450, the active side of Cytc is probably surrounded by other amino acid residues. Therefore, the explained nucleophilic attack of the protein backbone can not be transferred equally. In contrast, the formation of a covalent bond between the connected carbene and the porphyrin ring assemble is rather likely. Although P450s provide a heme *b* instead of a heme *c*, the nitrogen atoms as bonding partner can be found in the same conformation, while only the other organic moieties of the heme differ. In contrast to the deactivation by DAC, NHCB does not deactivate or reduce the activity

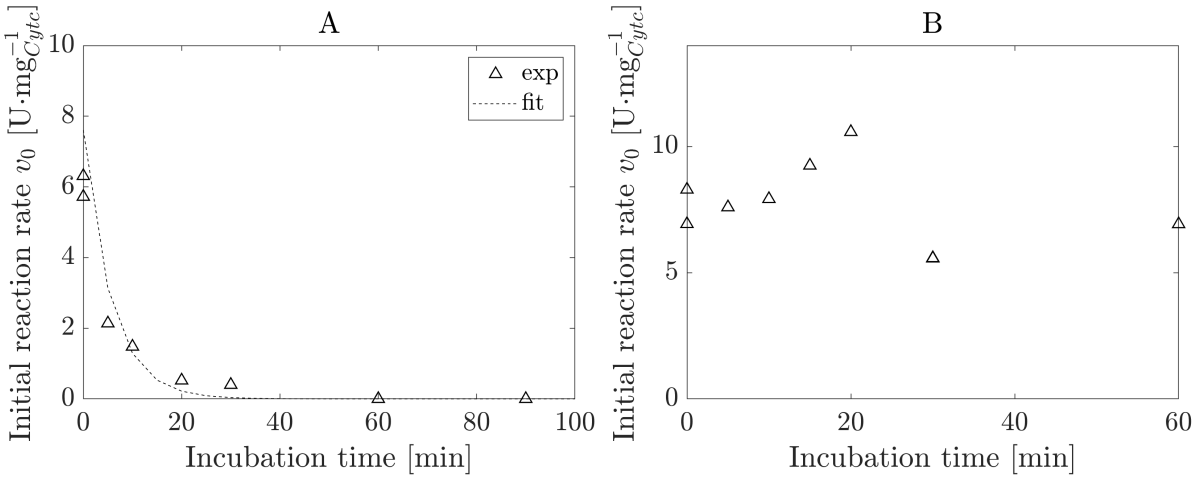

Figure 3.13: Influence of pre-incubation with DAC (A) and NHCB (B) on the initial reaction rate of biocatalytic borylation catalyzed by Cytc BOR^{R1} harboured in *E. coli* BL21 DE3 at OD 5 resuspended in M9-N buffer at pH 7.4. Initial reaction rates were measured during the first 7 min of synthesis with substrate concentrations of 6 mM NHCB and 12.5 mM DAC at 40 °C and normalized to the Cytc concentration. The initial reaction rate is plotted against the incubation time of one of the substrates. DAC shows to deactivated Cytc within 60 min completely when not converted, while NHCB does not show a deactivating effect on Cytc. Additionally, the loss of activity by DAC is simulated numerically following a first order decline.

of Cytc. Instead a slight increase of the initial reaction rate to over 10 mM can be observed within an incubation time of 20 min. Afterwards, initial reaction rates vary, but do not show a full loss and stay in the region of non-incubated Cytc.

Since the observed deactivation by DAC incorporated a serious effect on the initial reaction rate over time, the deactivation was additionally described mathematically to be implementable into the overall kinetic model. Due to the exponential decrease of the initial reaction rate, a first order decline was assumed and used as basis with a deactivation constant that incorporates the velocity of initial reaction rate reduction as shown in equation 3.4.

$$v = v_0 \cdot exp^{-K_{dea} \cdot t} \tag{3.4}$$

Here, K_{dea} was fitted numerically with the non-linear regression function *nlinfit* in MATLAB. The estimation resulted in a K_{dea} of $0.165 \pm 0.056\,\text{min}^{-1}$. As seen in figure 3.13, the fitted constant was used to simulate the decline of the initial reaction rate with elongating substrate-to-enzyme contact duration and compared to the experimental data. In contrast to previous simulations, where the simulations of Michaelis-Menten plots hit the experimental data precisely, the simulation does not fully anneal to the experimental data of the deac-

tivation tests over the whole time range. Although the first data points are approximated sufficiently, data from 20 to 90 min are undershot. This results in a faster decrease and a complete lack of initial reaction rate already after 30 min. This is twice as fast as conclusive from the experimental data and might result in errors during the simulation of OB synthesis.

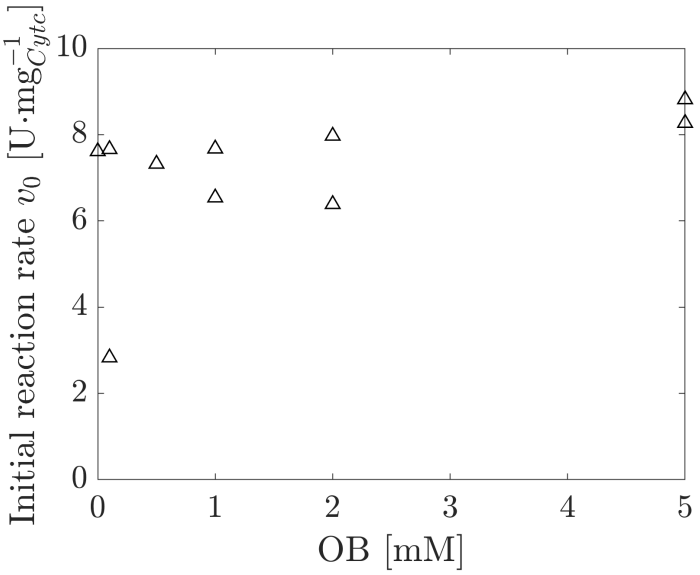

Figure 3.14: Influence of different OB contents on the initial reaction rate of biocatalytic borylation catalyzed by Cytc BOR^{R1} harboured in *E. coli* BL21 DE3 at OD 5 resuspended in M9-N buffer at pH 7.4. Initial reaction rates were measured during the first 7 min of synthesis with substrate concentrations of 6 mM NHCB and 12.5 mM DAC at 40 °C and normalized to the Cytc concentration. The initial reaction rate is plotted against the OB concentration. No change of the initial reaction rate up to 5 mM DAC is observable.

Additionally, the effect of the product itself on the catalytic performance of Cytc was investigated. As NHCB leads to a reversible inhibition, a comparable effect was hypothesized for OB due to structural agreements. Therefore, a product inhibition study was executed to search for possible product concentration-dependent influence on the initial reaction rate. The experiments were carried out in 5 mL thermostated glass reactors at 40 °C under anaerobic conditions in a batch mode with *E. coli* BOR^{R1} whole cells at OD 5 resuspended in M9-N buffer at pH 7.4 with initial substrate concentrations of 12.5 mM DAC and 6 mM NHCB with 5 % (v/v) MeCN as co-solvent. Additionally, OB was added prior to substrate addition in concentrations of 0.5 to 5 mM. Afterwards, the reaction was initiated and the samples were taken in 1-minute intervals over 7 min. Initial reaction rates were determined and normalized to the enzyme concentration. The collected experimental data is shown in figure 3.14, where the initial reaction rate is plotted against the initial OB concentration.

The experimental data provides no indication for a product inhibition up to a concentration of 5 mM OB. Nevertheless, it is possible, that inhibiting effects occur at higher concentrations. Moreover, a time-dependent deactivation as observed for DAC, even if less likely, can not be excluded. However, the advantageous characteristics of an absence of a product inhibition up to 5 mM OB paves the way to elevated OB_{final}.

In summary, within this study NHCB and DAC were investigated for irreversible inhibitions of Cytc. Here, only DAC shows a deactivation of Cytc leading to a full loss of initial reaction rate after pre-incubation of 60 min. The experimental data was fitted numerically to determine the deactivation constant to $0.165 \pm 0.056\,\mathrm{min}^{-1}$. Despite a small confidence interval, the deactivation was over-interpreted. NHCB does not show a negative influence on Cytc towards a possible deactivation and no product inhibition is present up to 5 mM OB. Since all kinetic information was collected, an evaluation of the obtained kinetic parameters is required.

3.2.3.3 Reaction Simulation for Parameter Evaluation

The obtained kinetic model for biocatalytic borylation simulated the reaction progress of OB synthesis to qualitatively evaluated the kinetic parameter estimation. The simulation was executed in MATLAB via the function *ode45*. This model was utilized to calculate the reaction rate at a specific set of substrate concentration according to equation 3.3.

$$v = v_{max} \cdot \frac{[NHCB]}{K_{m,NHCB} + [NHCB](1 + \frac{[NHCB]}{K_{i,NHCB}})} \cdot \frac{[DAC]}{K_{m,DAC} + [DAC]} \tag{3.3}$$

The product formation as well as the substrate conversion were calculated via ordinary differential equations 3.5, 3.6 and 3.7. Each equation contains the reaction rate calculated by equation 3.3, the Cytc concentration and is further extended with equation 3.4 for the DAC-driven deactivation.

$$\frac{\partial[NHCB]}{\partial t} = -v \cdot c_{Cytc} \cdot exp^{-k_{dea} \cdot t} \tag{3.5}$$

$$\frac{\partial[DAC]}{\partial t} = -v \cdot c_{Cytc} \cdot exp^{-k_{dea} \cdot t} \tag{3.6}$$

$$\frac{\partial[OB]}{\partial t} = v \cdot c_{Cytc} \cdot exp^{-k_{dea} \cdot t} \tag{3.7}$$

The simulated progress curves for DAC, NHCB and OB during biocatalytic borylation

is visualized in figure 3.15. As a reference, experimental data from time experiments of OB synthesis is shown. The experiments were examined as triplicates in 5 mL thermostated glass reactors at 40 °C under anaerobic conditions in a batch mode with *E. coli* BOR^{R1} whole cells at OD 5 resuspended in M9-N buffer at pH 7.4 with initial substrate concentrations of 12.5 mM DAC and 6 mM NHCB with 5 % (v/v) MeCN as co-solvent. Samples were taken in varying intervals for 2 h.

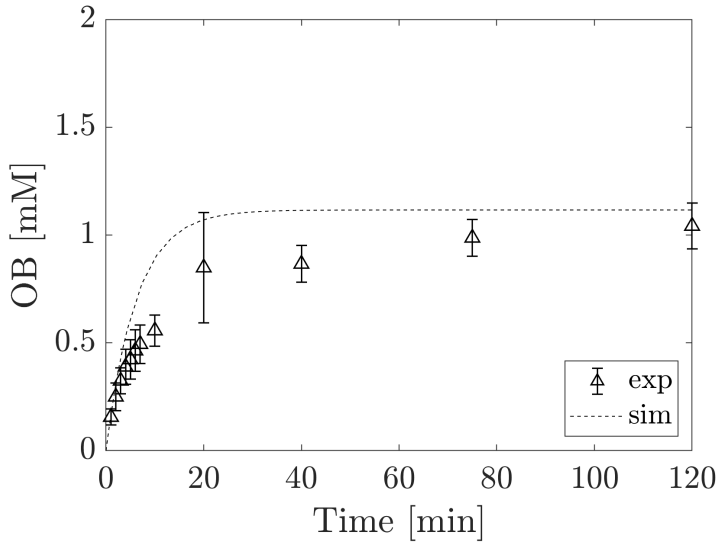

Figure 3.15: Simulation of biocatalytic OB synthesis catalyzed by Cytc BOR^{R1} harboured in *E. coli* BL21 DE3 according to numerically estimated kinetic parameters for starting concentrations of 6 mM NHCB and 12.5 mM DAC at 40 °C. The reactant concentrations were calculated according to a set of ordinary differential equations and the OB content are plotted with experimental data from OB synthesis in whole cells at OD 5 (1.7 μM Cytc) as reference against the reaction time. The simulation fits the experimental data only during the initial part of the reaction and for OB_{final}.

The simulation starts accurately during the initial 5 min of the synthesis. Afterwards, the experimental OB concentration does not increase as fast as predicted by the simulation. Nevertheless, the experimental data shows product formation for longer than 60 min. In contrast, the simulated OB concentration does not rise further after 30 min, since the deactivation of Cytc is expected to be completed at that point. The experimentally determined OB concentration after 2 h as well as the simulated OB_{final} anneals closely. Although the reaction progress between 10 and 100 min have deviations, the simulation overall approximates OB formation in a reasonable scale with the given parameters.

However, as the simulation does not describe the synthesis during broken-order kinetics correctly, the enzyme concentration and the deactivation constant were fitted manually in order to look for possible errors and to reduced the deviation. Figure 3.16 gives the simulation

adjusted to the experimental data with manually changed parameters v_{max} of 11.1 U·mg^{-1} and K_{dea} of 0.08 min^{-1}, which was executed in MATLAB via function *ode45*.

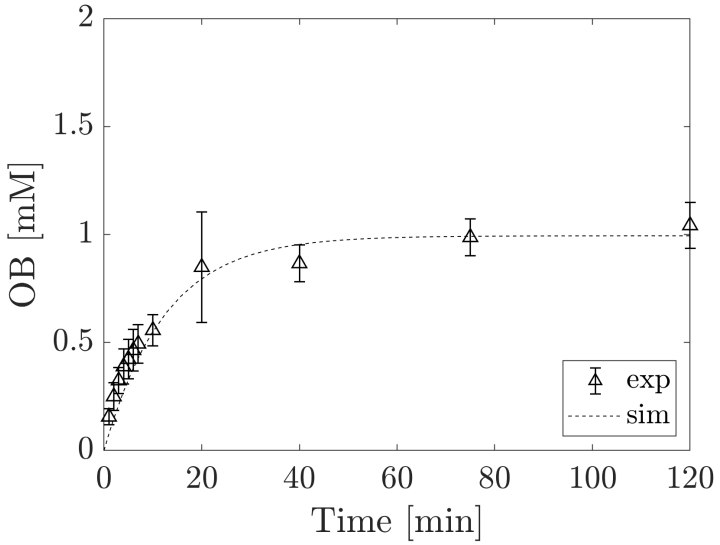

Figure 3.16: Simulation of biocatalytic OB synthesis catalyzed by Cytc BOR^{R1} harboured in *E. coli* BL21 DE3 according to numerically fitted kinetic parameters for starting concentrations of 6 mM NHCB and 12.5 mM DAC at 40 °C and adapted values for c_{Cytc} and K_{dea}. The reactant concentrations were calculated according to a set of ordinary differential equations and the OB content is plotted with experimental data from OB synthesis in whole cells at OD 5 (1.7 μM Cytc) as reference against the reaction time. The simulation fits the experimental data closer due to the adapted parameters v_{max} and K_{dea}.

Due to the adaptation of v_{max} and K_{dea}, the simulation stays longer in a close range of the experimental data. In particular, the reduction of K_{dea} results in a delayed decline of activity and a flattened curve with longer OB synthesis instead, leading to a higher final OB concentration. A reduction of the overall OB synthesis rate counteracts this effect, depending on v_{max} as well as c_{Cytc} according to equation 3.7. Since the error of the quantification of Cytc via the hemochrome assay is a magnitude smaller at roughly 5 %, v_{max} was manually adjusted. The fitted v_{max} provides a comparably wide confidence interval of over 60 % of the actual value. Thus, the manual adjustment to less than 50 % of its former value does not required to leave the borders of the confidence interval, stating a reaction simulation with valid kinetic constants. This compresses the progress curve along the y-axis to overall match the experimental data. In contrast, this adjustment would not have been valid for c_{Cytc}, since the error of its quantification via the hemochrome assay is a magnitude smaller at roughly 5 %. Regarding K_{dea}, the performed reduction of this parameter explains the observed activity loss more suitable, since activity is present over a longer time range. Although the confidence interval of the numerically estimated K_{dea} is comparably narrow, the

elongated activity represents the delayed activity loss similarly, even if the absolute fit of the experimental data would decrease. All in all, the changes can be justified, as the adjusted parameters stays within confidence intervals were.

Concluding the results of the model based simulation of OB synthesis, the designed double substrate Michaelis-Menten model predicts biocatalytic OB formation reasonable. The initial product formation as well as the final OB concentration are approximated closely. In between, simulated and measured OB concentrations deviate. A manual adjustment of v_{max} and K_{dea} results in a better fit to the experimental data over an expanded conversion range. The examined changes are within a range that can be justified with the confidence intervals of the determined kinetic parameter as well as explanation of experimental data. Overall, the established substrate-surplus inhibited double-substrate Michaelis-Menten model with the determined kinetic parameters v_{max}, $K_{m,NHCB}$, $K_{m,DAC}$, $K_{i,NHCB}$ and K_{dea} can be considered as useful for the prediction and simulation of OB synthesis.

3.3 Reaction Engineering

Since the reactant properties are explored and the reaction is described kinetically, the next logical step includes the reaction engineering characterization of biocatalytic OB synthesis. Here, the investigation of different operation modes aims for the improvement of the process parameters TTN, OB_{final} and STY.

3.3.1 Batch Mode

Batch mode experiments already delivered primary results for the desired process parameters of OB synthesis and gave reference values for subsequent tests using other operation modes. At this point, Cytc content and the form of Cytc application in the reaction are investigated as main specifications.

3.3.1.1 Application of Cytc

Before the variation of a biocatalysts concentration can be investigated, its application in different forms has to be carried out. Here, enzymes can not only be applied in whole cells, but also in purified form as free enzyme or immobilized, which are both characterized in initial tests.

The batch experiments investigated the effect of purified enzymes catalyzing the reaction in a free form or immobilized on different carriers. For the free enzyme, Cytc was purified

and resolved in the desired concentration, whereas immobilized Cytc was added on varying carrier amounts to match an equal final Cytc content overall. Experiments were carried out in 5 mL thermostated glass reactors at 40 °C under anaerobic conditions in either immobilized form on different carriers or purified and resolved Cytc in M9-N buffer at pH 7.4 with initial substrate concentrations of 12.5 mM DAC and 6 mM NHCB with 5 % (v/v) MeCN as co-solvent. Samples were taken in varying time intervals for 2 h. The OB concentration was compared to the amount of product formed at OD 5 (fig. 3.17).

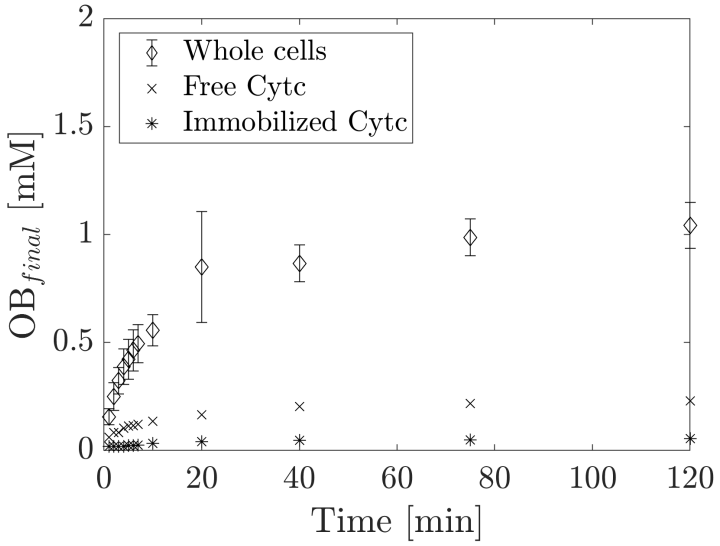

Figure 3.17: Product formation of biocatalytic OB synthesis in batch mode catalyzed by Cytc BOR^{R1} as free enzyme (4.4 μM Cytc) or immobilized via GA on silica beads (0.5 μM Cytc) in M9-N buffer at pH 7.4. Starting substrate concentrations were at 6 mM NHCB and 12.5 mM DAC. Immobilized and free enzyme achieve way lower OB$_{final}$ compared to Cytc in whole cells (1.7 μM Cytc).

The results show, that immobilized Cytc achieves an OB$_{final}$ of 0.09 mM OB in average, while purified Cytc yieldes a maximum of 0.45 mM OB after 2 h reaction time. This is a tremendous drop of OB$_{final}$ compared to whole cell catalysis where over 1 mM OB could be formed. To get a normalized view on the catalytic performance, TTNs were calculated (Eq. 1.1, which describe the amount of formed molecules of OB per molecule Cytc. Here, whole cell catalysis delivers a higher TTN with 624 mol·mol^{-1} compared to 76 mol·mol^{-1} for free Cytc and 180 mol·mol^{-1} for immobilized Cytc. This effect is probably caused by an accelerated deactivation due to a direct enzyme-to-substrate contact without the protecting membranes of the periplasm [113]. As a result, higher concentrations of DAC could increase the rate of deactivation, which seems to be reduced in contrast with an intact cell. However, an improvement of TTN for immobilized Cytc compared to free Cytc can still be found. This effect can indeed be a result of the immobilization and the binding to the carriers, since

immobilization is known to drop the reaction rate, but to increase stability instead, leading to an elongated OB formation.

All in all, the examined tests demonstrate a severe reduction of TTN towards a cell-free OB synthesis, which can mainly be referred to DAC-induced deactivation of Cytc. Despite slight improvements regarding TTN for immobilized Cytc compared to free Cytc, the activity loss without a protecting cell is too serious to follow these variants of Cytc application further during this project. Thus, other parameters has to be varied to improve TTN and OB_{final}.

3.3.1.2 Varying Cytc Concentration

Due to the conclusion, that free and immobilized Cytc do not perform OB formation efficiently due to fast and severe deactivation, additional whole cell tests focused on the Cytc concentration by changing the OD. This was done in comparison to the long time tests carried out for the evaluation of kinetic parameters at OD 5.

Experiments were carried out at OD 15 in triplicates in 5 mL thermostated glass reactors at 40 °C under anaerobic conditions with *E. coli* BOR^{R1} whole cells resuspended in M9-N buffer at pH 7.4 with initial substrate concentrations of 12.5 mM DAC and 6 mM NHCB with 5 % (v/v) MeCN as co-solvent. Samples were taken in varying intervals for 2 h. The OB concentration was compared to the amount of product formed at OD 5 (fig. 3.18).

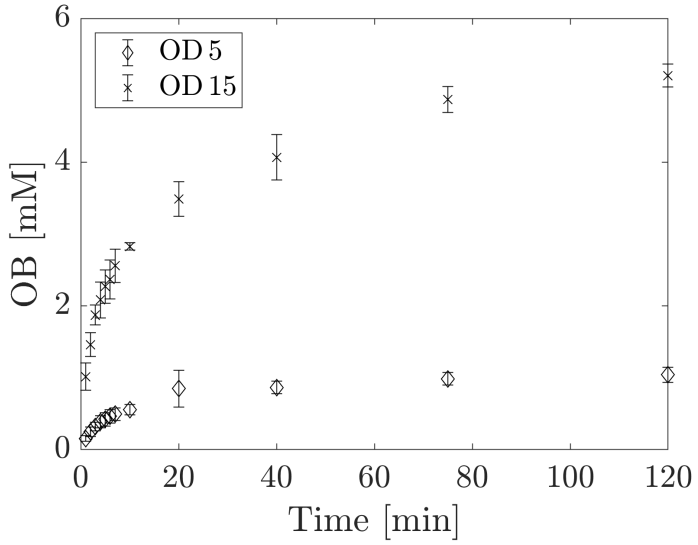

Figure 3.18: Product formation of biocatalytic OB synthesis in batch mode catalyzed by Cytc BOR^{R1} harboured in *E. coli* BL21 DE3 at OD 5 (1.7 μM Cytc) and OD 15 (4.4 μM Cytc), resuspended in M9-N buffer at pH 7.4. Starting substrate concentrations were at 6 mM NHCB and 12.5 mM DAC. An increase of Cytc concentration by 150 % leads to 5-fold higher final OB content.

After the first minute, more than 1 mM OB are synthesized with a initial reaction rate of 7.2 U·mg^{-1}, being in close range of the reaction rates reached under equal conditions during kinetic characterization studies. The final OB concentration rises to over 5 mM, due to a 3-fold higher cell density, which is an improvement of 400 %. Since the Cytc concentration at OD 15 was only 2.5 times higher, the synthesis was even more effective in terms of TTN. Moreover, noticeable OB formation is still observed after 80 min with OD 15 reactors, while OB formation in OD 5 reactors is comparably lower already after 40 min. This gives a reason to suspect a lowered deactivation by DAC being connected with the apparent DAC concentration. Since 4 mM DAC are already converted after 40 min, this is a clear reduction of DAC concentration, which may already reduce the rate of deactivation. As a consequence, a higher amount of intact Cytc is still available after an expanded reaction time. So, the faster DAC can be converted, the longer Cytc stays intact and is, therefore, available for ongoing OB synthesis, which is obviously the case for higher ODs providing more Cytc.

In order to pay more attention on this aspect, the Cytc concentration was further increased with cell suspensions of OD 30 during additional experiments to reach even higher conversions of DAC. More importantly, the ratio of Cytc content to OD varied in the examined tests, which was prevented in the following experiments with the preparation of all cell suspensions from one *E. coli* BOR^{R1} culture. Thus, the investigations were extended with repeated tests at OD 5 and OD 15 to have the same Cytc to OD ratio for all cell suspensions. OB_{final} as well as the TTN were targeted as main parameters in dependence of Cytc content to evaluate the catalytic performance of Cytc in batch mode (fig. 3.19).

As the Cytc concentration increases, OB_{final} is boosted likewise, proving the expectations. At OD 30 OB_{final} is additional 25 % higher than at OD 15 reaching the highest OB_{final} until this point of 9.4 mM. However, a sampling or measuring error probably had occurred, since only 6 mM NHCB should be added to all reactors. If there was no mistake in NHCB supplementation, then the calibration may not be accurate at regions around 9 mM OB. But since all samples were evaluated according to the same calibration all determined concentrations are in a correct ratio with each other. Thus, there is definitely more OB formed at OD 30 than at OD 15. In contrast, the TTN declines at OD 30 to 960 mol·mol^{-1} compared to 1180 mol·mol^{-1} at OD 15. Because the Cytc concentration doubles between OD 15 and OD 30, same is assumed for OB_{final}, if TTN should stay constant. But due to a conversion of 83 % NHCB in OD 15 reactors, OD 30 reactors reach a full conversion and are thereby limited in achieving higher TTNs. Thus, additional test with 12.5 mM NHCB were executed and reached a TTN of 1400 mol·mol^{-1}. This embodies an improvement of TTN as well as OB_{final} to 12.5 mM. Although the calibration might be inaccurate at these concentrations, the im-

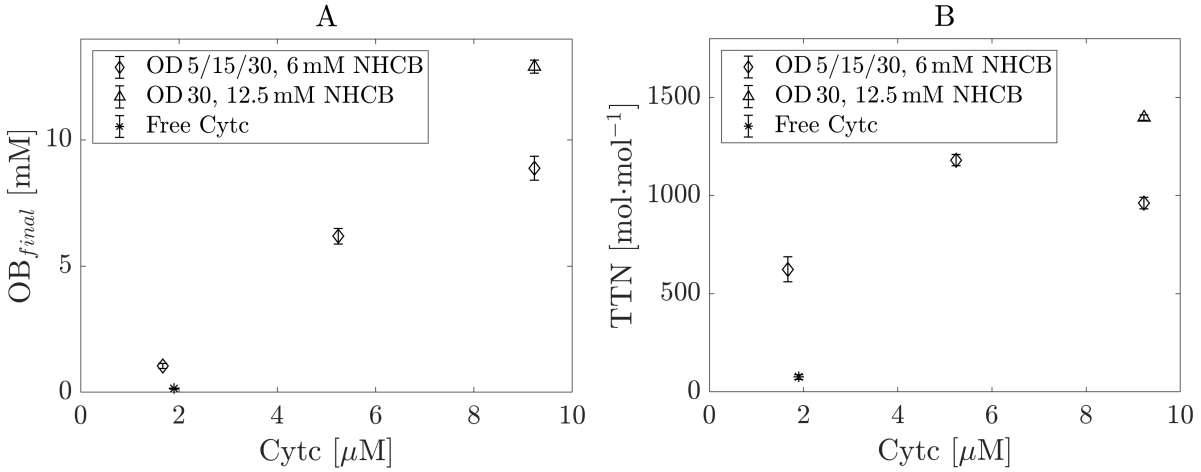

Figure 3.19: Process parameters OB_{final} (A) and TTN (B) in dependence of Cytc concentration of biocatalytic OB synthesis catalyzed by Cytc BOR^{R1} harboured in *E. coli* BL21 DE3 at OD 5 (1.7 μM Cytc), 15 (5.2 μM Cytc) and 30 (9.2 μM Cytc) in batch mode. Synthesis was executed at starting substrate concentrations of 6 mM NHCB and 12.5 mM DAC at 40 °C and pH 7.4 in M9-N buffer. An increase of Cytc content increases OB_{final} and leads to higher TTNs, if DAC is almost converted completely.

provement is clearly noticeable and a full conversion was probably missed closely. Therefore, DAC needs to decrease significantly within a short time frame, reaching concentration ranges which deactivate Cytc way less compared to experiments at lower ODs, where DAC is converted slower. Thus, more Cytc can stay native due to a fast and nearly full conversion of DAC within a short time, which itself enables an ongoing OB formation. Overall and aside from having more substrate available, this effect can be assumed as one major factor for the additional boost in TTN at OD 30 experiments.

Summarizing the results, the elevation of Cytc content by adjusting the OD yields a faster conversion of substrates. Here, especially the significant reduction of DAC concentration gains an elongated period of OB formation, due to a minimized effect of deactivation. Thus, a lower available DAC concentration over the whole reaction process would be advantageous to maintain Cytc activity during a longer time. Therefore, a limited addition of DAC would be beneficial here, which brings the fed-batch as possible operation mode into view.

3.3.2 Fed-Batch Mode

According to the previous findings, a fast conversion of DAC, to minimize the present concentration, helps noticeably to reduce Cytc deactivation. Thus, an application of a fed-batch mode was targeted with an adjusted supplementation of DAC. This was considered to hold the present DAC content at a minimum or close to zero due an immediate and fast con-

version of added DAC. Here, the low $K_{m,DAC}$, calculated to 1.1 mM, demonstrates the high activity of Cytc already at minor DAC concentrations. Different Cytc concentrations as well as dilution rates should give hints about possible enhancements in TTN and OB_{final}. In the case of a successful optimization of OB synthesis, scale-up tests should make first steps towards an industrially relevant process.

3.3.2.1 Varying Cytc Concentration

The dilution rate D is a crucial value for a fed-batch process. D describes how much volume is added per time through the feed with respect to the reaction volume $V_{Reactor}$ of the reactor (Eq. 2.5). Low dilution rates were investigated at first, to hold the available DAC concentration inside the reactor close to zero. Dilution rates increased to find suitable dilution rates to maximize TTN and OB_{final}.

The fed-batch experiments took place in 5 mL thermostated glass reaction vessels with *E. coli* BOR^{R1} whole cells resuspended to OD 5 in M9-N buffer at pH 7.4 with 6 mM NHCB with initial 2.5 % (v/v) MeCN as co-solvent under anaerobic conditions in M9-N buffer 40 °C. DAC was added via syringe pump to a final concentration of 12.5 mM without conversion as in batch mode. Dilution rates varied between 0.012, 0.036, 0.36 and 0.96 h^{-1}, resulting in feed durations of 125, 41, 4.2 and 1.8 min, respectively. Samples were taken after feed termination and after additional 2 h. Figure 3.20 shows OB_{final} in dependence of D.

The obtained data show a clear trend of increasing OB_{final} with decreasing D. This behaviour is observable for the OB concentration directly after feed termination, as well as after additional 2 h. The highest product concentration of 2.8 mM is reached at 0.012 h^{-1}, while a dilution rate of 0.96 h^{-1} only leads to 1.9 mM OB. The elongation of the reaction time by 2 h causes only minor elevations of product concentrations for dilution rates 0.012 and 0.036 h^{-1} of 5 and 25 %, respectively. In contrast for faster DAC addition at 0.36 and 0.96 h^{-1}, OB_{final} increases by over 90 and 175 %. This significant improvement can be explained with an overfeeding with DAC and relatively short feed durations. Especially at 0.96 h^{-1} the feed ends already after 2 min, which is obviously not sufficient for a fast conversion of all added DAC. Thus, the elongation of reaction time makes a huge impact on further OB formation. In opposite, the supplementation of small amounts of DAC over a longer time frame causes more OB to be formed already within the feed time of 125 min. Here, additional 2 h have less influence compared to the feed time and have thereby only a low benefit towards product formation. Nevertheless, all reactions were terminated after the additional 2 h. As hypothesized in early batch syntheses, a slower addition of DAC increases the OB_{final} in summary. However, since no samples could be taken during the feed no clear

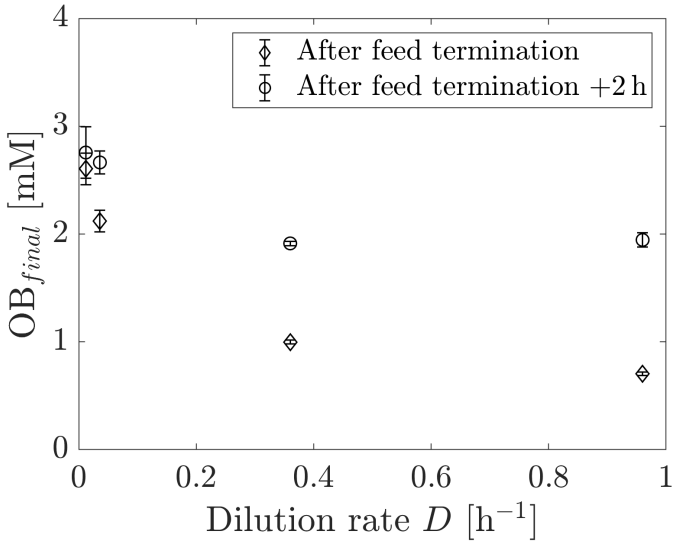

Figure 3.20: OB_{final} in dependence of the dilution rate for biocatalytic OB synthesis catalyzed by Cytc BOR^{R1} harboured in *E. coli* BL21 DE3 at OD 5 (1.7 μM Cytc) in fed-batch mode after feed termination ($\Diamond$) and additional 2 h (O). Synthesis was executed at 6 mM NHCB at 40 °C and pH 7.4 in M9-N buffer and DAC was added with dilution rates of 0.012, 0.036, 0.36 and 0.96 h^{-1} to final 12.5 mM without conversion. OB_{final} rises with decreasing D.

statement towards an instant complete conversion of DAC could be made. Following, to aim for even higher OB_{final}, the enzyme content was increased in subsequent tests to OD 15.

With an elevation of the Cytc concentration, OB_{final} rise as well. Maximum OB_{final} with 7.1 mM are reached at 0.012 and 0.036 h^{-1}, whereas the lowest final concentration is at 6.4 mM at a dilution rate of 0.96 h^{-1}. Overall, the same trends as with 1.7 μM Cytc at OD 5 can be drawn, where OB_{final} increases with decreasing D and further OB synthesis after feed termination especially at higher D. Nevertheless, although the OB concentration differs widely after the feed, the advancements towards higher product concentrations after further 2 h for different dilution rates are not as promoted as at OD 5. As described above, OB_{final} varies only by 0.7 mM, being about 10 % of the maximum concentration reached at 0.012 h^{-1}. It seems, that the advantageous effect of a limited DAC availability is highlighted especially at lower Cytc concentrations. Since less Cytc needs longer to convert the added DAC, a present DAC content as of close to zero is easier to establish during DAC feeding with more biocatalyst. Thus, accumulations might be less likely at higher Cytc contents, resulting in a reduced Cytc deactivation by DAC, leading to a declined impact of the dilution rate. To strengthen this idea, more fed-batch experiments were carried out at OD 30 with 10.2 μM Cytc (fig 3.22). Since even higher product concentrations were expected, tests with 12.5 mM NHCB were carried out as well.

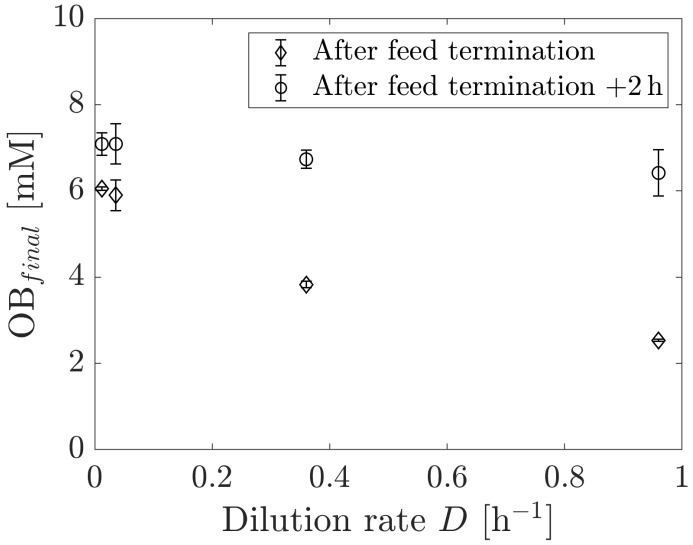

Figure 3.21: OB_{final} in dependence of the dilution rate for biocatalytic OB synthesis catalyzed by Cytc BOR^{R1} harboured in *E. coli* BL21 DE3 at OD 15 (4.2 μM Cytc) in fed-batch mode after feed termination ($\Diamond$) and additional 2 h (O). Synthesis was executed at 6 mM NHCB at 40 °C and pH 7.4 in M9-N buffer and DAC was added with dilution rates of 0.012, 0.036, 0.36 and 0.96 h^{-1} to final 12.5 mM without conversion. OB_{final} rises with decreasing D.

Syntheses at OD 30 and 10.2 μM Cytc results in a further increase of OB_{final}. Independently from the dilution rate, OB is synthesized up to 10 mM at 2 h after feed termination. For 12.5 mM NHCB, OB_{final} exceeds 12.5 mM, which would mean a full conversion of both substrates. Although unrealistic high product concentrations are reached for syntheses with initial 6 mM NHCB, the ratio of OB_{final} at different ODs proves the unmistakable effect, that more Cytc forms more OB. Once again, the effect of the dilution rate is less pronounced compared to OD 15 and in particular to OD 5. This supports the stated hypothesis, of less accumulated DAC at higher biocatalyst contests, leading to a reduced deactivation. Thus, the more Cytc is provided, the less impacting is the dilution rate, since also faster additions of DAC can be compensated. To be able to better compare the results from experiments with different ODs, TTNs were calculated for all experiments to get further information of how Cytcs performance is influenced by the dilution rate.

The calculations extends the conclusions made above for OB_{final} towards the TTN. Namely, for limited Cytc availability e.g. at OD 5, a reduction of the present DAC concentration with low dilution rates improves the catalytic performance of Cytc resulting in boosted TTNs. Thus, TTNs of close to 2000 are reached at OD 5 and 0.012 h^{-1}. However, if the applied catalytic activity is increased with OD 15 and OD 30, more DAC at higher dilution rates can also be converted fast enough to maintain low DAC concentrations, suppressing or at least

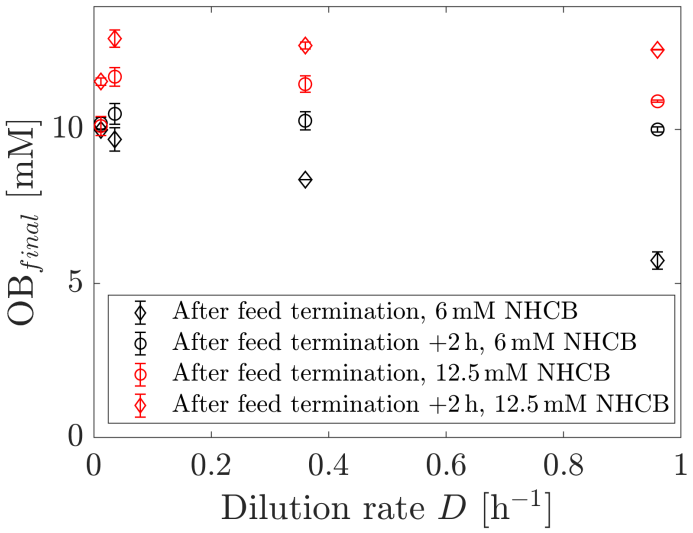

Figure 3.22: OB$_{final}$ in dependence of the dilution rate for biocatalytic OB synthesis catalyzed by Cytc BOR^{R1} harboured in *E. coli* BL21 DE3 at OD 30 (10.2 μM Cytc) in fed-batch mode after feed termination ($\Diamond$) and additional 2 h (O). Synthesis was executed at 6 (black) or 12.5 mM (red) NHCB at 40 °C and pH 7.4 in M9-N buffer and DAC was added with dilution rates of 0.012, 0.036, 0.36 and 0.96 h^{-1} to final 12.5 mM without conversion. OB$_{final}$ rises with decreasing D.

minimizing Cytc deactivation as seen in batch modes. But as more Cytc converts NHCB faster, the reaction rate is also dropping faster as more substrate is converted. This leads to less OB formed per Cytc before the reaction is ended by deactivation of Cytc, why TTNs declined with rising OD. Moreover, OD 30 reaches probably a full conversion of one of the substrates which limits further product formation and leads to even minor TTNs.

In summary, the obtained results for the OB synthesis in fed-batch mode show improvements for the TTN as well as for OB$_{final}$. The reduction of DAC supplementation via a feed boosts OB$_{final}$, particularly, if the Cytc content is not sufficient to convert DAC fast enough to maintain a low concentration that minimizes Cytc deactivation. If Cytc contents increase to OD 15 and 30, the effect is less impacting in the tested range. Moreover, TTNs are also promoted by a reduced DAC feeding, if Cytc is limited. Overall, it is possible to increase the TTN from 600 mol·mol^{-1} in the batch mode to 2000 mol·mol^{-1} in the fed-batch mode at OD 5. Furthermore, the highest OB$_{final}$ of 12.5 mM is reached at OD 30 indicating a full conversion. Since the presented experiments lead to a clear improvement of OB synthesis, additional parameters should be investigated to further enhance product formation in the fed-batch mode.

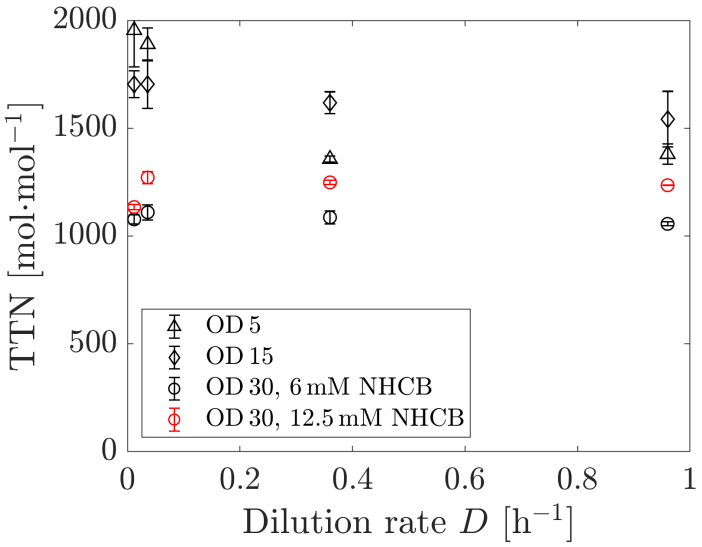

Figure 3.23: TTN in dependence of the dilution rate for biocatalytic OB synthesis catalyzed by Cytc BOR^{R1} harboured in *E. coli* BL21 DE3 at OD 5(1.4 μM Cytc), 15(4.2 μM Cytc) and 30(10.2 μM Cytc) in fed-batch mode. Synthesis was executed at 6 (black) or 12.5 mM (red) NHCB at 40 °C and pH 7.4 in M9-N buffer and DAC was added with dilution rates of 0.012, 0.036, 0.36 and 0.96 h^{-1} to final 12.5 mM without conversion. TTN declines at higher Cytc content and is only impacted by D if Cytc is limited.

3.3.2.2 Supplementation With Glucose

In contrast to the used experimental fed-batch set-up in this study, the reaction medium in literature contained glucose [21]. Thus, additional tests targeted the influence of this carbon-source on OB formation.

The fed-batch experiments took place in 5 mL thermostated glass reaction vessels with *E. coli* BOR^{R1} whole cells resuspended to OD 5 in M9-N buffer at pH 7.4 with 6 mM NHCB with initial 2.5 % (v/v) MeCN as co-solvent supplemented with 50 mM glucose under anaerobic conditions in M9-N buffer 40 °C. DAC was added via syringe pump to a final concentration of 12.5 mM without conversion as in batch mode. Dilution rates varied between 0.012, 0.036, 0.36 and 0.96 h^{-1}. The study focused on the dependence of OB$_{final}$ on the dilution rate and results were compared with the OB synthesis in fed-batch mode without glucose supplementation (fig. 3.24).

OB$_{final}$ increases with decreasing D as it has been already observed for the OB synthesis in fed-batch mode without glucose. The maximum OB$_{final}$ is at 3.4 mM at 0.012 h^{-1}. Furthermore, OB synthesis proceeds after feed termination for all dilution rates during 2 h extension of reaction time. This achieves elevated OB$_{final}$ particularly at high D. In comparison to the fed-batch syntheses without glucose, the TTN increases from 2000 to 2250 mol·mol^{-1}. The

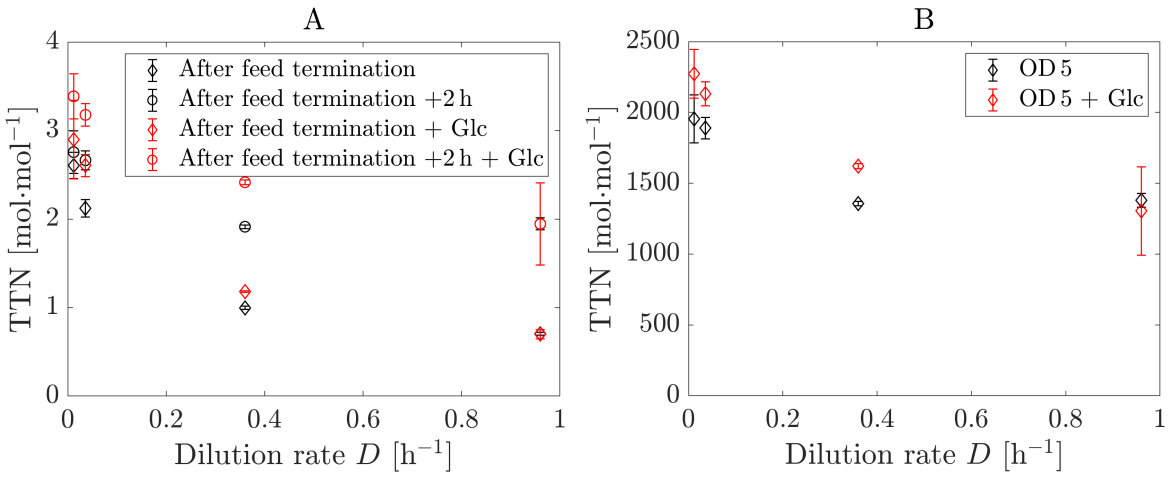

Figure 3.24: OB_{final} in dependence of the dilution rate for biocatalytic OB synthesis catalyzed by Cytc BOR^{R1} harboured in *E. coli* BL21 DE3 at OD 5 (1.4 μM Cytc) in fed-batch mode after feed termination ($\Diamond$) and additional 2 h (O)(A). Synthesis was executed with additional 50 mM glucose at 6 mM NHCB at 40 °C and pH 7.4 in M9-N buffer and DAC was added with dilution rates of 0.012, 0.036, 0.36 and 0.96 h^{-1} to final 12.5 mM without conversion. TTNs were compared with TTNs of tests without glucose (B). Additional glucose improves the OB formation especially at low dilution rates.

effect is visible for 0.012, 0.036 and 0.36 h^{-1}, whereas TTNs at 0.96 h^{-1} does not improve with additional glucose.

Concluding the results, glucose leads to higher OB_{final} and TTN and was thereby supplemented in all further fed-batch studies.

3.3.2.3 Scale-Up to 150 mL

The fed-batch mode was successfully applied in 5 mL-scaled reactors. However, since this scale is not relevant for industrially applied processes, consecutive studies investigated OB synthesis in magnified scales.

First tests were carried out in 150 mL reaction volume in 500 mL DASGIP reactors (supplementary information fig.), bringing an enlargement factor of 30, with *E. coli* BOR^{R1} whole cells resuspended to OD 5 in M9-N buffer at pH 7.4 with 6 mM NHCB with initial 2.5 % (v/v) MeCN as co-solvent supplemented with 50 mM glucose under anaerobic conditions in M9-N buffer 40 °C. DAC was added via syringe pump to a final concentration of 12.5 mM without conversion. The dilution rate stayed at 0.012 h^{-1}, because 5 mL-syntheses were most efficient under these conditions for OD 5. OB formation was recorded during the feed phase and after additional 2 h (fig. 3.25).

The OB synthesis in 150 mL reaction volume yields improved results as OB_{final} is at

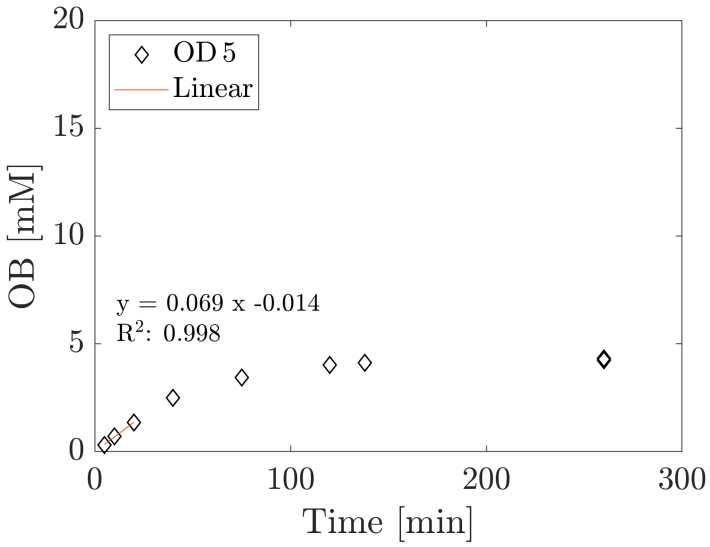

Figure 3.25: OB formation over time in biocatalytic borylation catalyzed by Cytc BOR^{R1} harboured in *E. coli* BL21 DE3 at OD 5 (1.5 μM Cytc) in fed-batch mode with 2 h reaction time extension after feed termination at 128 min. Synthesis was executed with additional 50 mM glucose at 6 mM NHCB at 40 °C and pH 7.4 in M9-N buffer. DAC was added with a dilution rate of 0.012 h^{-1} to final 12.5 mM without conversion. OB_{final} reaches at 4.28 mM, being the highest product concentration with OD 5.

4.3 mM. With a Cytc content of 1.5 μM, the TTN reaches 2850 mol·mol^{-1} compared to 2273 mol·mol^{-1} in the 5 mL scale. The pure enlargement of the reaction volume itself can not be considered as direct factor for the improvement of Cytc TTN. Anaerobic conditions are observed with probes measuring the dissolved oxygen (DO) in real time and contained with Argon bubbling through the reaction mixture. Mixing time tests proved, that all substances are equally distributed within 1.4 s by stirring at 400 rpm and thus no difference to the 5 mL scale is made here (Supplementary information, Fig. 6.4). However, the addition of DAC by syringe pump is assumed as a possible influencing candidate. Since the syringe does not penetrate the liquid surface of the reaction mixture, DAC joins the liquid in droplets instead of a continuous flow. Since the droplet size is relatively small to the reaction volume of 150 mL, this might not lead to severely high local DAC concentrations. But the same application in a 5 mL scale could cause local deactivations of Cytc, accumulating to a negative impact, which can be recognized with a lower OB_{final}. The deactivation of Cytc can thereby be delayed in upscaled processes, where the droplet to reaction volume ratio is smaller. Nevertheless, deactivation of Cytc still occurs, since no further OB is formed after feed termination and without reaching a full conversion at 6 mM OB. Here, OB synthesis is not limited by DAC addition, as OB is formed linearly only during the first 20 min of feed phase.

Afterwards, DAC accumulates and causes Cytc to deactivate. Still, the examined tests in a 150 mL scale were successful and led to improvements of OB_{final} and TTN.

Since OD 5 suspensions did not provide enough Cytc to prevent DAC from accumulating, the Cytc concentration was increased at following experiments with OD 15 while staying at a dilution rate of $0.012\,h^{-1}$. Moreover, the NHCB content was increased to 12.5 mM to prevent a limitation by a lack of the borane substrate, which was observed at 5 mL-scaled syntheses. OB synthesis was carried out in duplicates and mean values were calculated for product formation during the feed phase and after additional 2 h (fig. 3.26).

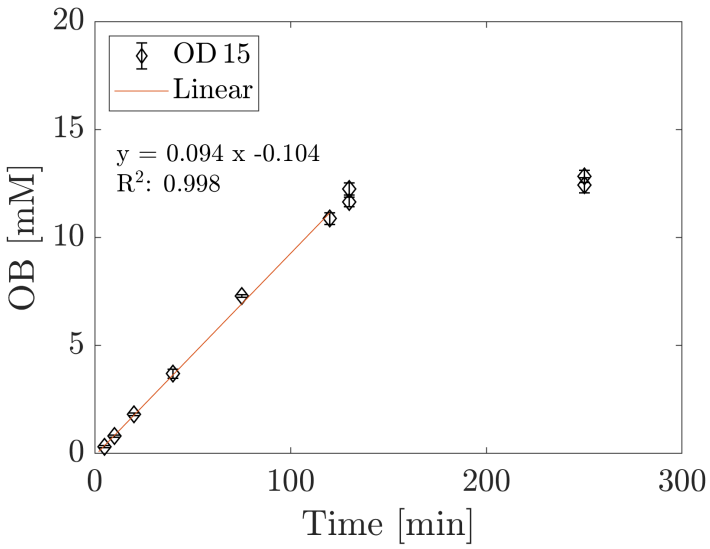

Figure 3.26: OB formation over time in biocatalytic borylation catalyzed by Cytc BOR^{R1} harboured in *E. coli* BL21 DE3 at OD 15 (4.1 μM Cytc) in fed-batch mode with 2 h reaction time extension after feed termination. Synthesis was executed with additional 50 mM glucose at 12.5 mM NHCB at 40 °C and pH 7.4 in M9-N buffer. DAC was added with a dilution rate of $0.012\,h^{-1}$ to final 12.5 mM without conversion. OB_{final} was at 12.5 mM, labelling a full conversion.

The increase of Cytc concentration to 4.1 μM causes an OB_{final} of 12.5 mM. Thus, Cytc converts DAC completely to OB. Moreover, the OB content rises linearly with a rate of $0.093\,mM{\cdot}min^{-1}$. A recalculation via equation 2.3 into a molar rate of $0.014\,mmol{\cdot}min^{-1}$ covers nearly the molar feed rate (Eq. 2.4) of $0.015\,mmol{\cdot}min^{-1}$. The slight difference in feeding and reaction rates causes only minor accumulations, which are converted without residues after additional 2 h after feed termination. This demonstrates, that all added DAC is nearly instantaneously converted holding DAC at a present concentration close to 0 mM. As a further result, TTN expands to $3130\,mol{\cdot}mol^{-1}$, being even higher than for OB synthesis at OD 5 with the same dilution rate. At this point, the product formation can not be further improved except by enhancing the overall production rate of OB. For a fed-batch

process, where the fed substrate is directly converted, the dilution rate is, therefore, a good opportunity to improve this production rate.

For the increase of the production rate, the dilution rate was doubled to 0.024 h^{-1}. To ensure a complete conversion of the added DAC, the OD was also doubled to OD 30 causing a Cytc content of 12.1 μM. The tests were carried out in duplicates and mean values were calculated for product formation during the feed phase and after additional 2 h (fig. 3.27)

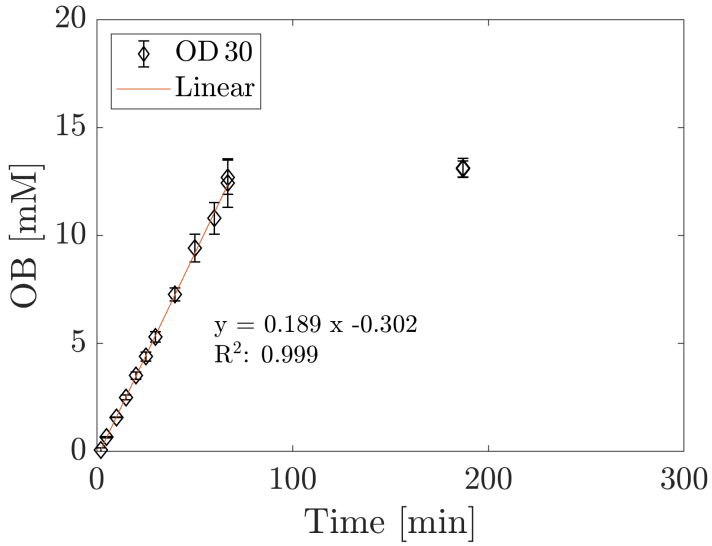

Figure 3.27: OB formation over time in biocatalytic borylation catalyzed by Cytc BOR^{R1} harboured in *E. coli* BL21 DE3 at OD 30 (12.1 μM Cytc) in fed-batch mode with 2 h reaction time extension after feed termination. Synthesis was executed with additional 50 mM glucose at 12.5 mM NHCB at 40 °C and pH 7.4 in M9-N buffer. DAC was added with a dilution rate of 0.024 h^{-1} to final 12.5 mM without conversion. OB_{final} is at 12.5 mM, labelling a full conversion after 67 min.

The data demonstrate, that a OD 30 suspension leads to a full conversion of DAC at a dilution rate of 0.024 h^{-1}. Again, the syntheses achieve a full conversion with an OB_{final} of 12.5 mM. This is possibly a result of the increase of the Cytc concentration by a factor of 3, while the dilution rate only doubles. Thus, more enzyme is available as needed to convert the twice as fast fed DAC. TTNs drop with respect to the OD 15 tests to 1081 mol·mol^{-1}. Here, OB is synthesized at a molar rate of 0.029 mmol·min^{-1}, while DAC is supplemented at 0.030 mmol·min^{-1}. The difference can be explained with deviations of the desired and the actual feed rate of the syringe pump. Overall, an accumulation of DAC throughout the feeding time can be excluded for a dilution rate of 0.024 h^{-1}, since no significant amount of OB is formed after feed termination. To identify limitations and to use the full potential of OD 30 suspensions, the substrate concentrations has to be increased.

As additional tests within the 150 mL scale, OB synthesis at OD 30 was executed with

substrate concentrations of NHCB and DAC elevated to 20 mM. The dilution rate stayed at 0.024 h^{-1}, the tests were carried out in duplicates and mean values were calculated for product formation during the feed phase and after additional 2 h (fig. 3.27).

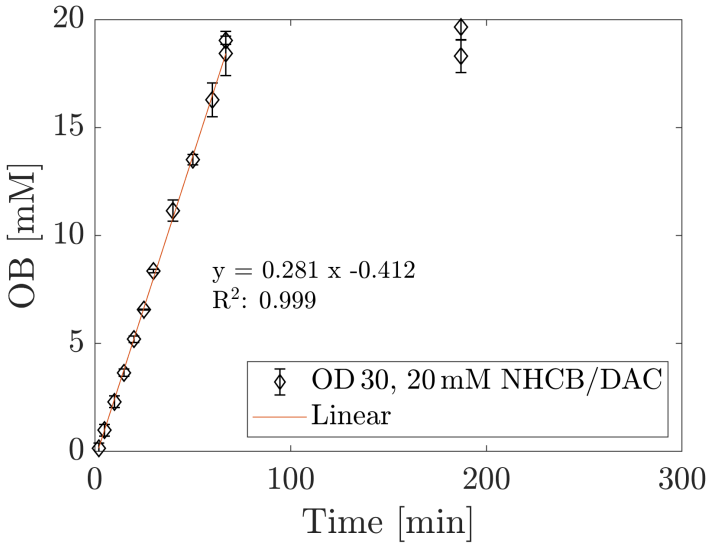

Figure 3.28: OB formation over time in biocatalytic borylation catalyzed by Cytc BOR^{R1} harboured in *E. coli* BL21 DE3 at OD 30 (10.0 μM Cytc) in fed-batch mode with 2 h reaction time extension after feed termination. Synthesis was executed with additional 50 mM glucose at 20 mM NHCB at 40 °C and pH 7.4 in M9-N buffer. DAC was added with a dilution rate of 0.024 h^{-1} to final 20 mM without conversion. OB_{final} reaches 19 mM, labelling a nearly full conversion of 20 mM substrates after 67 min.

Even with more NHCB present and more DAC being fed per time, the OB concentration increases linearly according to the applied feed. A final concentration of 19 mM iss achieved after 67 min, which is not further increased during additional 2 h after feed termination. Thus, it can be assumed, that less DAC was added than it was required for a final concentration of 20 mM OB. The molar synthesis rate is at 0.042 mmol·min^{-1} during the feeding of DAC at a theoretical molar rate of 0.048 mmol·min^{-1}. The deviations can be caused by errors in the applied feed rate of the pump as well as by a lower concentration of DAC in the stock solution. Nevertheless, the TTN rises to 1900 mol·mol^{-1} due to an increase of the substrate stock concentration to 20 mM. Since higher TTNs were already achieved, further increases in substrate concentration or dilution rate are imaginable. However, with increasing substrate concentration the substrate surplus inhibition of NHCB gets more and more severe. Also, since product inhibitions were only tested until 5 mM.

Summarizing the results of OB synthesis in a 150 mL scale in fed-batch mode, precise recordings of OB formation show further information about DAC conversion during the

feed phase. Here, an increase of the Cytc concentration causes an OB synthesis limited to the dilution rate. This enables a minimized risk of Cytc deactivation, since DAC is immediately converted. The effect is proved for dilution rates up to $0.024\,h^{-1}$ and substrate concentrations of 20 mM at OD 30 cell suspensions. OB_{final} is boosted to 19 mM and a TTN of $3130\,mol{\cdot}mol^{-1}$ shows opportunities for improvements in Cytc performance. All in all, the successful OB synthesis in the fed-batch mode in a 150 mL scale means a further development towards an industrially relevant process. In order to meet industrial expectations the scale was enlarged further.

3.3.2.4 Scale-Up to 500 mL

Since the scale up to a 150 mL scale yielded valuable improvements for OB_{final} and TTN, the scale was consequently increased to 500 mL reaction volume to transfer the previous results.

First experiments were executed in 500 mL reaction volume in 1 L DASGIP reactors, bringing a further enlargement factor of 3.33, with *E. coli* BOR^{R1} whole cells resuspended to OD 5 in M9-N buffer at pH 7.4 with 6 mM NHCB with initial 2.5 % (v/v) MeCN as co-solvent supplemented with 50 mM glucose under anaerobic conditions in M9-N buffer at 40 °C. DAC was added via a syringe pump to a final concentration of 12.5 mM without conversion. The dilution rate was at $0.012\,h^{-1}$ since syntheses were most efficient under these conditions for OD 5 cultures. OB formation was executed in duplicates and the mean values were calculated for product formation during the feed phase and after additional 2 h (fig. 3.29).

For OD 5 reactors, the molar OB formation rate of $0.0501\,mmol{\cdot}min^{-1}$ during the initial 15 min hits the molar feed rate of 0.05 precisely, stating a direct conversion of all fed DAC within this period. However, the product formation drops between 15 and 75 min by nearly 50 % to $0.0278\,mmol{\cdot}min^{-1}$ allowing DAC to accumulate in the same rate, as OB is formed. As a consequence, DAC-induced Cytc deactivation leads to even lower OB formation rates and no further substrates are converted after the feed is terminated at 126 min. Finally, the reactors reached an OB_{final} of 4.7 mM, which was an improvement to the 150 mL scaled syntheses yielding 4.3 mM. Furthermore, the TTN rise slightly to $2860\,mol{\cdot}mol^{-1}$. Despite the improvements, no full conversion is achieved, since NHCB was added to 6 mM. However, a positive trend towards TTN and OB_{final} compared to the 150 mL is visible, although Cytc deactivation is repeatedly observed in the 500 mL scale. Here, the lowered ratio between droplet volume of the DAC feed and the reaction volume can still have an influence as explained before. Since this ratio rises as well by a theoretical factor of 3.33 according to the scale enlargement, elevated local DAC contents are even lower. Thus, local Cytc deactivation can be assumed to be less likely.

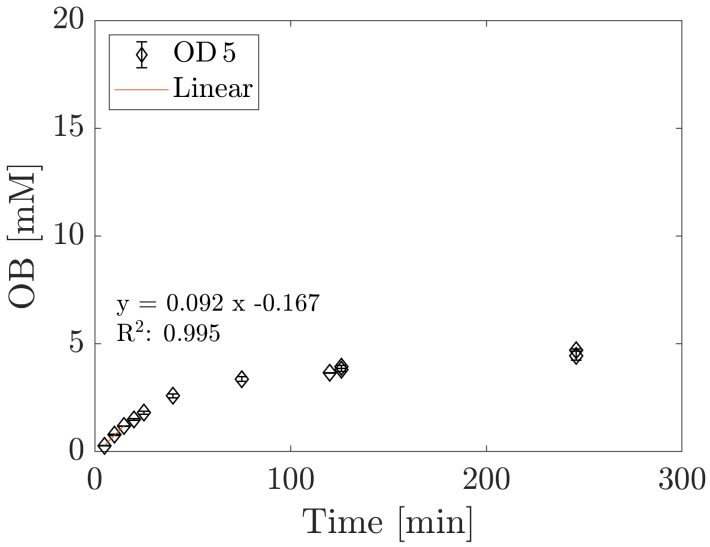

Figure 3.29: OB formation over time in biocatalytic borylation catalyzed by Cytc BOR^{R1} harboured in *E. coli* BL21 DE3 at OD 5 (1.5 μM Cytc) in fed-batch mode with 2 h reaction time extension after feed termination. Synthesis was executed with additional 100 mM glucose at 6 mM NHCB at 40 °C and pH 7.4 in M9-N buffer. DAC was added with a dilution rate of 0.012 h^{-1} to final 12.5 mM without conversion. OB_{final} was at 4.7 mM, yielding the highest OB concentration in with a OD 5 suspension.

The comparison between the 150 mL- and the 500 mL-scaled tests at OD 5 revealed further benefits. Thus, a complete conversions of NHCB and DAC was targeted with OD 30 suspensions. Thereby, the dilution rates increased to 0.024 h^{-1} as well as the substrate contents to 20 mM. The syntheses were examined in duplicates and mean values were calculated for product formation during the feed phase and after additional 2 h (fig. 3.30).

For the first time within this project, OB synthesis reaches an OB_{final} of 20 mM. This states a full conversion of NHCB as well as DAC and an increase of TTN to 2110 mol·mol^{-1} compared to the synthesis under equal conditions in the 150 mL scale. Since the Cytc content was over 6-fold higher and DAC was added 3.2-fold faster, a DAC content close to 0 mM was assumed. Thus, deactivation is not an issue during the feed phase, where OB is linearly synthesized with a rate of 0.1534 mmol·min^{-1} while DAC is added at 0.16 mmol·min^{-1}. Due to no further product formation after feed termination, the immediate full conversion DAC is proved once again. The difference in the rates of product formation and substrate addition can therefore be explained with deviations in the desired and the actual feed rate of the syringe pump. Overall, both syntheses at OD 30 successfully reach 20 mM OB and no full deactivation of Cytc after feed termination is visible. In particular, TTNs do not reach 3000 mol·mol^{-1}, which is in the repertoire of Cytc under good conditions as OD 15 reactors

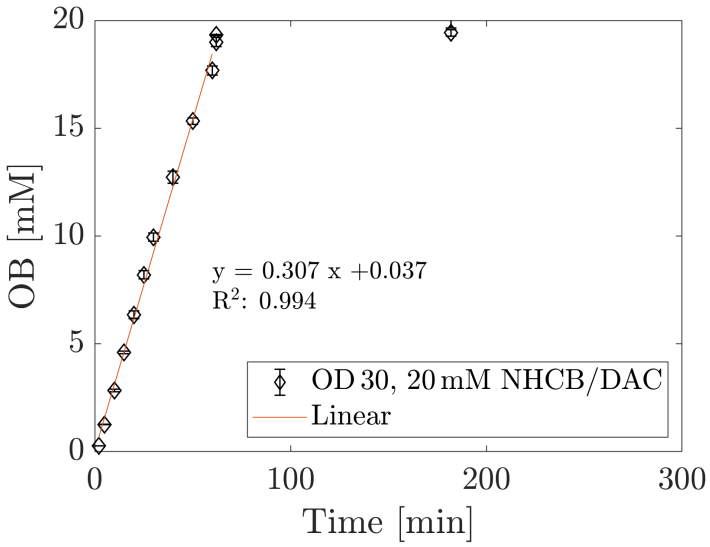

Figure 3.30: OB formation over time in biocatalytic borylation catalyzed by Cytc BOR^{R1} harboured in *E. coli* BL21 DE3 at OD 30 (9.45 μM Cytc) in fed-batch mode with 2 h reaction time extension after feed termination. Synthesis was executed with additional 50 mM glucose at 20 mM NHCB at 40 °C and pH 7.4 in M9-N buffer. DAC was added with a dilution rate of 0.024 h^{-1} to final 20 mM without conversion. OB_{final} reaches 20 mM, indicating a full conversion of 20 mM substrates after 62 min.

in the 150 mL scale proved. This leaves space for more substrate being converted within the same reaction.

Therefore, an additional experiment was executed in the 500 mL scale at OD 30, where the substrate concentration of 20 mM and a dilution rate of 0.024 h^{-1} should initially deliver a replicate of the previous tests. But in addition, substrate supply increased by a second supplementation with NHCB to 20 mM after the termination of the first feed. Subsequently, a repeated addition of DAC via a second feed with the same feed rate was executed. Thus, twice the amount of substrate was added to the reactor. Moreover, a change of the dilution rate should give hints about the response time of the system and a fast elevation of DAC supplementation could be handled without problems. The OB formation was recorded during the whole process time (fig. 3.31)

The OB synthesis at OD 30 with a stepwise increased feed rate yields 33.4 mM as OB_{final}. This embodies the highest OB content achieved in this project. TTN increases as a result, compared to the 500 mL scale synthesis with a single feed, to 2760 mol·mol^{-1}. During the first feed phase at a dilution rate of 0.0072 h^{-1}, OB is synthesized with a linear increase at a rate of 0.0478 mmol·min^{-1}. The feed adds DAC at 0.0480 mmol·min^{-1}, giving a ratio of 99.4 % between both rates, leaving only less doubt about possible accumulated DAC,

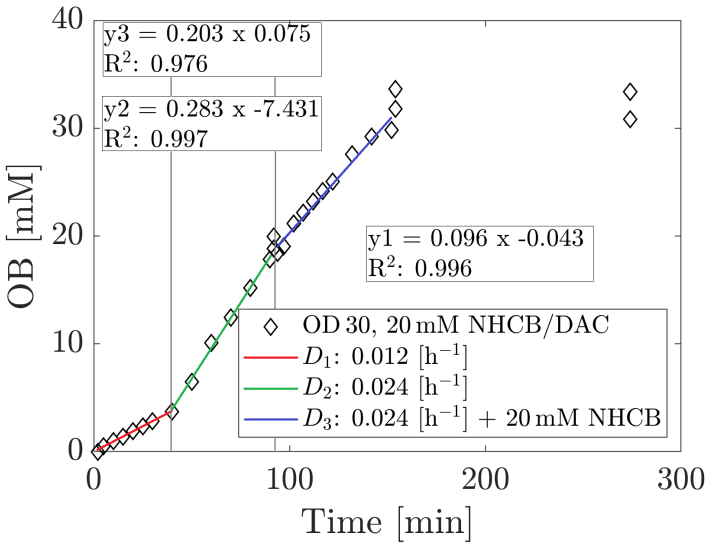

Figure 3.31: OB formation over time in biocatalytic borylation catalyzed by Cytc BOR^{R1} harboured in *E. coli* BL21 DE3 at OD 30 (12.2 μM Cytc) in fed-batch mode with 2 h reaction time extension after feed termination. Synthesis was executed with initial 100 mM glucose at 2 times 20 mM NHCB at 40 °C and pH 7.4 in M9-N buffer. DAC was added twice with a dilution rate of 0.0072 h^{-1} for the first 40 min and 0.024 h^{-1} afterwards to final 40 mM without conversion. OB_{final} reaches 33.4 mM, which is the highest product concentration ever within this project.

as Cytc is present in too high concentrations. After 40 min the dilution rate is increased to 0.024 h^{-1}, from where on product is formed at 0.1426 mmol·min^{-1}, while DAC is added at 0.16 mmol·min^{-1}. If no technical issue influenced the feed rate, DAC might possibly has accumulated as the OB formation rate is only about 88 % of the feed rate. However, after termination of the first feed at around 100 min, the OB content does not increase further than 19.9 mM. This demonstrates a nearly complete conversion until here. A slightly negative deviation in the DAC content in the stock can have also occurred, explaining the small discrepancy. After the interim supplementation with NHCB to 20 mM, the second feed at a rate of 0.024 h^{-1} was initiated. Although the dilution rate is the same, the OB formation stays at low 0.1016 mmol·min^{-1}. This is only 63 % of the feed rate of DAC, which enables DAC to accumulate and to deactivate Cytc. The deviation might be caused by either deactivated Cytc, or by a varied feed rate due to a change of the syringe pump. After termination of the second feed a product content of 33.4 mM is achieved. This would usually mean, that Cytc was severely deactivated, as a full conversion of 40 mM DAC can not be achieved. In this case, the course of OB formation should saturate towards OB_{final} instead of being linear until feed termination. Since no further OB was synthesize afterwards, one of the substrates is likely to be converted completely. Thus, also the second feed can be

concluded as successfully converted without a rise in the present DAC content. Hence, this extensive OB synthesis in fed-batch mode was successful in applying changing dilution rates rates, adding more substrate and boosting OB_{final} to new heights. This experiment supports, that the adaptation of the dilution rates to the applied activity is mandatory. This aspect is responsible, whether a fed-batch OB synthesis is limited by DAC supplementation to maintain Cytc activity or the reaction suffers by Cytc deactivation due to overfeeding with DAC. Here, the molar OB synthesis rate during the feed phase can be used as reference point. Figure 3.32 shows the specific molar OB synthesis rate in dependence on the activity loading for the carried out reactions in 150 mL and 500 mL scale.

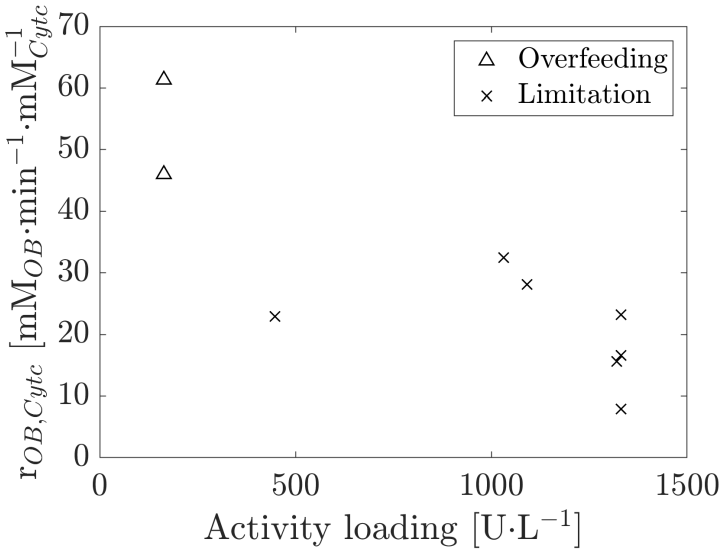

Figure 3.32: Specific molar OB synthesis depending on different activity loadings for biocatalytic borylation catalyzed by Cytc BOR^{R1} harboured in *E. coli* BL21 DE3. DAC limitations during the feed lead to a reduced but ongoing OB synthesis, while an overfeeding causes DAC accumulation and Cytc deactivation. Deactivations occur, if the specific molar OB synthesis rate is above 40 $mM_{OB} \cdot min^{-1} \cdot mM_{Cytc}^{-1}$, particularly at low activity loadings.

Studies in the 150 mL and 500 mL scale with OD 15 and OD 30 suspensions contained 447 $U \cdot L^{-1}$ and between 1100 and 1330 $U \cdot L^{-1}$, respectively. In contrast, OD 5 reactors provided an activity loading of 163 $U \cdot L^{-1}$. For these experiments, molar OB formation rates above 40 $mM_{OB} \cdot min^{-1} \cdot mM_{Cytc}^{-1}$ are achieved but run into DAC accumulation. As a result, Cytc deactivated and activity declined. Despite higher molar OB synthesis rates, the molar feed rate is above the capacity of the activity loadings. In contrast, for experiments with activity loadings above 400 $U \cdot L^{-1}$, DAC supplementation is low enough to keep OB increasing linearly, proving a DAC limitation to maintain Cytc activity. Concluding, Cytc is able to convert DAC at least to a rate of 35 min^{-1}. If DAC is added at a higher molar rate, DAC

is likely to accumulate, leading to Cytc deactivation. If activity loadings are known, the convertible molar feed rate can be calculated without risking a DAC accumulation.

In summary, the fed-batch application in the 500 mL scale enabled additional improvements particularly with an elevated OB_{final}. After increasing the Cytc concentration as well as the added substrate amount, the product concentration rises in a linear rate, limited by the presence of DAC. Hence, DAC-induced deactivation of Cytc is minimized, also after a second feed for another rise in OB concentration. The deactivation can thus be delayed and is not related directly to the reaction time, but is instead depending on the period where DAC is available in significant concentrations. Since these can be controlled with an adapted dilution rate, the fed-batch brings opportunities for even higher OB contents and TTN. In the end, OB_{final} reaches 33.4 mM which are 3.5 $g \cdot L^{-1}$ and thereby a step towards an industrially relevant process. The TTN of 2760 $mol \cdot mol^{-1}$ at the final OD 30 fed-batch test can be boosted further to open higher product concentrations.

3.3.3 Continuous Mode

The continuous operation mode is the third possibility to run a process and can provide a constant product synthesis over days and weeks to months. However, catalytic activity has to be maintained over a prolonged period to secure an efficient reaction. Since previous fed-batch results demonstrate the extension of Cytc activity with an adapted feed of DAC, the application of a continuous stirred tank reactor (CSTR) can be considered as an opportunity to further enhance TTN and STY of biocatalytic borylation.

3.3.3.1 CSTR Characterization

In addition to instant and complete mixing, which are also provided by batch and fed-batch operation modes, the CSTR is operating under outflow conditions. This enables a maximum conversion at minimal substrate concentrations, which is important to reduce DAC-induced deactivation of Cytc. However, to carry out contiuous biocatalytic OB synthesis under defined conditions, a characterization of the utilized reactor is required. Here the real volume as well as the residence time distribution (RTD) embody important parameters to describe the mixing conditions within a CSTR.

Thus, investigations targeted the determination of the real volume of the applied reactor model. This was executed by recording a RTD of a tracer fed to the CSTR at a known dilution rate. Since the input signal of the tracer was a jump function, the response or output signal at the outlet of the reactor was already the cumulative RTD (fig. 3.33 A) [114]. From

here, a graphical estimation of the residence time τ for reactors with real mixing behaviour is possible [115]. Therefore, the residence time can be determined, where the areas A_1 and A_2 are equal (fig. 3.33 B). This procedure was done for a feed rate of 400 and 600 μL·min^{-1} and τ_{400} and τ_{600} were taken to calculate the reactor volume as a mean.

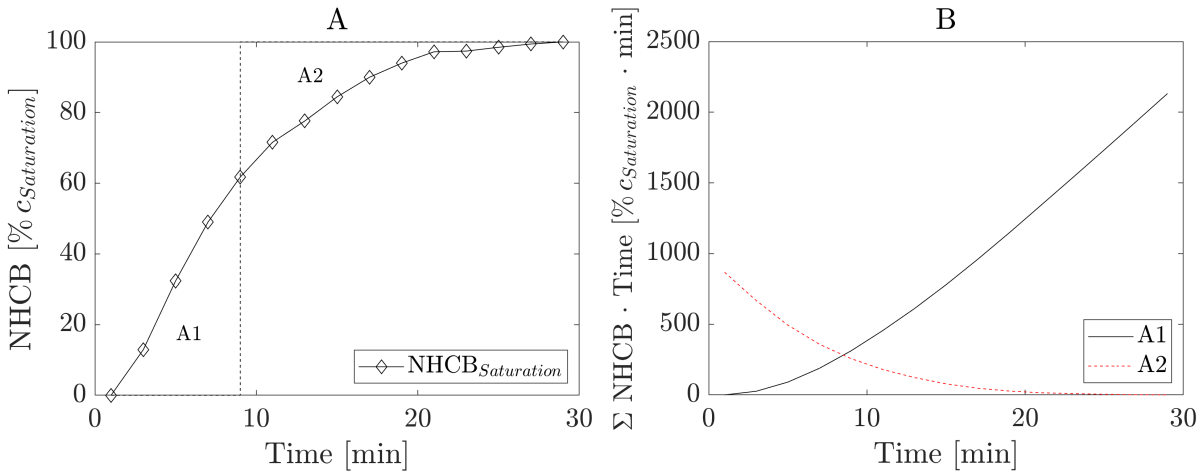

Figure 3.33: Cumulative RTD of a CSTR with 6 mM NHCB as tracer in M9-N buffer with 5 % (v/v) MeCN fed as a jump function at the reactor inlet at 400 rpm stirring with a feed rate of 400 μL·min^{-1}. NHCB at the outlet was normalized to NHCB$_{max}$ and monitored in dependence on feed time (A). The residence time τ was determined graphically, where A_1 and A_2 are equal (B). τ_{400} was calculated to 8.5 min and τ_{600} to 5.4 min, leading to a reactor volume of 3.32 mL.

The cumulative RTDs at 400 and 600 μL·min^{-1} show a real mixing behaviour [115]. The response signals reach 100 % inlet tracer concentration after 29 and 19 min, respectively. The area of A_1 and A_2 as pictured in figure 3.33 B were used to locate τ. Here, τ_{400} was calculated to 8.5 min and τ_{600} to 5.4 min. Moreover, the real reactor volume V_{real} was determined for the feed rate F according to equation 3.8.

$$V_{real} = \tau_F \cdot F \tag{3.8}$$

As a result, V_{real} is at 3.4 mL for τ_{400} and at 3.24 mL for τ_{600}, averaged to 3.32 mL. Since an estimation via gravimetric dimensioning approximated a volume around 3 mL, the determination via the residence time seems to give a realistic value for V_{real}. The deviations probably have been caused by stretching of the reactor dimensions under process conditions. Due to two assembled flexible O-ring rubber sealings, an expansion of the height of the reaction space is likely by pressure build-up during feeding. Based on the deviation of 0.32 mL, this is a vertical stretching of 1.02 mm being in a reasonable range.

In addition, the cumulative RTD was recorded for different flow rates. The CSTR was

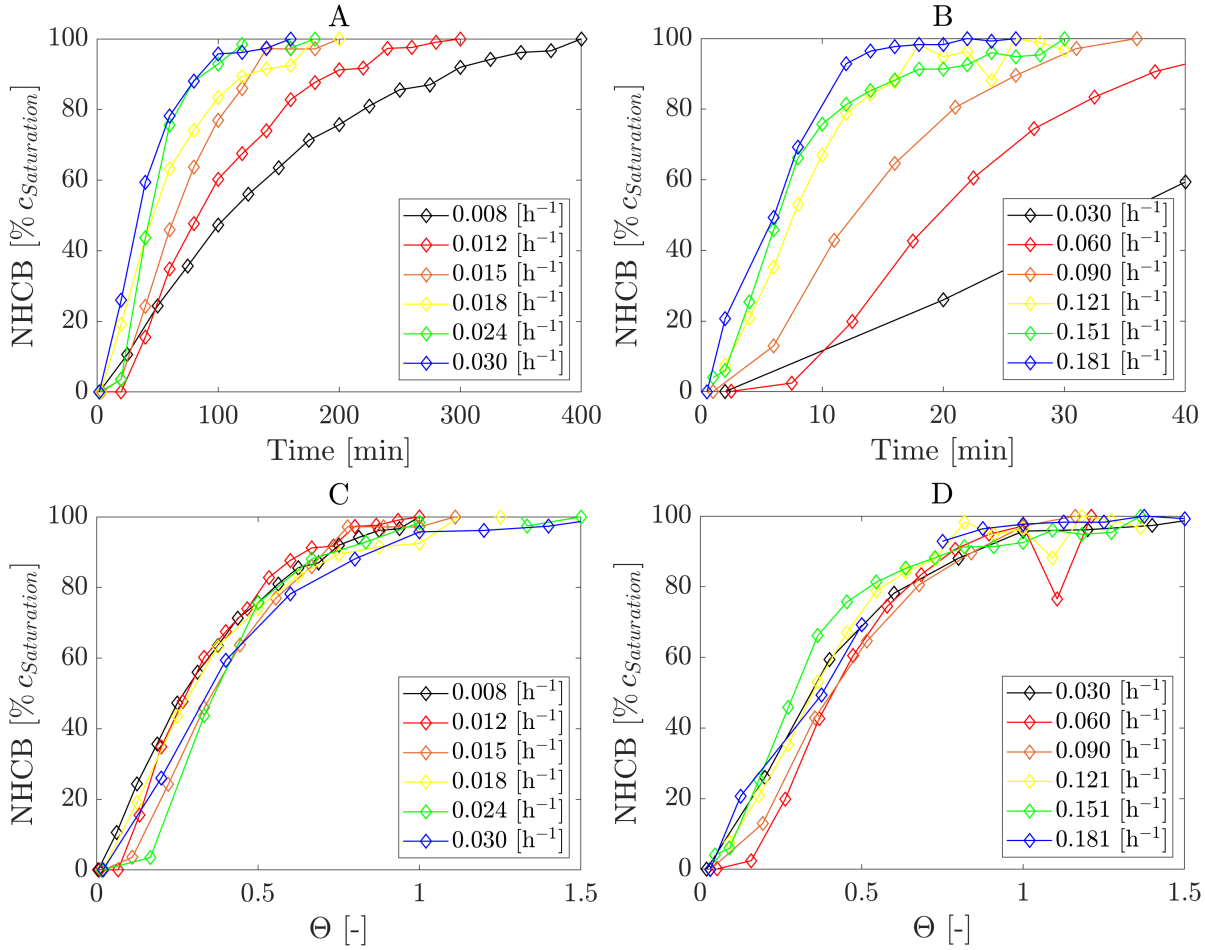

Figure 3.34: Cumulative RTD of a CSTR for different dilution rates with 6 mM NHCB in M9-N buffer with 5 % (v/v) MeCN as tracer fed as a jump function at the reactor inlet at 400 rpm stirring. NHCB at the outlet was normalized to NHCB$_{max}$, depending on feed time (A + B) and to numbers of residence times θ(C + D). A lower dilution rate increases residence time, but does not change the mixing behaviour.

filled and flushed with M9-N buffer containing 5 % (v/v) MeCN for comparative reasons. Afterwards, NHCB served as tracer as a 6 mM solution in M9-N buffer with 5 % (v/v) MeCN as co-solvent, being fed by a syringe pump in dilution rates of 0.01 to 0.24 min^{-1} as a jump function. NHCB content was measured at the outlet, normalized to NHCB$_{max}$ and plotted in dependence of the feed time as well as residence time and normalized to the residence time (fig. 3.34).

The collected data stated that lower dilution rates require more time to reach NHCB$_{max}$. This could be expected due to less tracer being injected per time in the same reactor volume. While only 16 min elapsed at D of 0.24 min^{-1} to reach NHCB$_{max}$, a D of 0.01 min^{-1} caused an elongation of the necessary feed time to 400 min. However, if the time to reach NHCB$_{max}$

is normalized to the residence time number θ, the increase of NHCB is identical for all dilution rates, which characterizes a constant and immediate distribution of fed substances along the investigated dilution rates [116].

In summary, the utilized CSTR model was characterized by determining V_{real} to 3.32 mL under process conditions via RTD-based calculated of τ. In addition, the reactor shows an equal mixing behaviour for different dilution rates from 0.01 to 0.24 min^{-1}, when depending on to the numbers of residence time θ.

3.3.3.2 Continuous OB Synthesis

With a successfully characterization of the CSTR reactor, biocatalytic OB synthesis in a continuous mode was investigated. Here, the residence time needed to be checked for impacting the overall amount of OB formed. *E. coli* BL21 DE3 cells harbouring Cytc BOR^{R1} were retentated with an ultrafiltration membrane with a 5 kDA MWCO and were flushed with anaerobic M9-N buffer prior to substrate feeding.

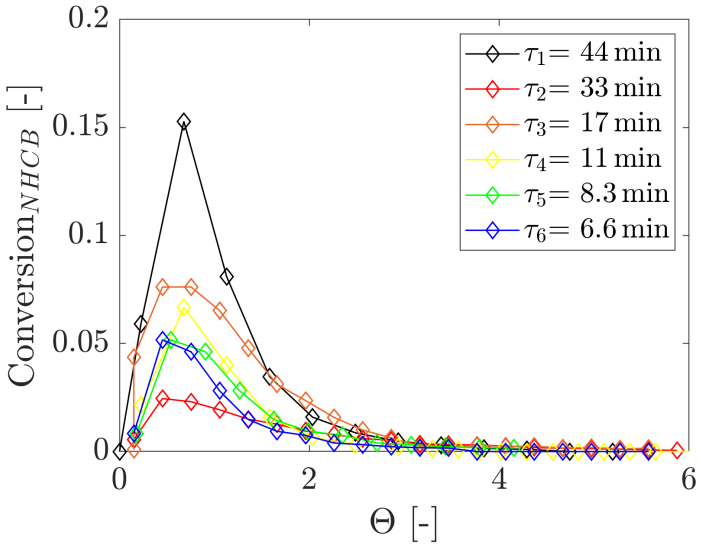

Figure 3.35: Conversion of NHCB to OB for different τ from 6.6 to 44.3 min for biocatalytic borylation catalyzed by Cytc BOR^{R1} harboured in *E. coli* BL21 DE3 at OD 5 in M9-N buffer at pH 7.4 with 5 % (v/v) MeCN as co-solvent in a CSTR depending on the number of residence times θ. The conversion increases with decreasing τ.

Continuous biocatalytic OB synthesis was executed under anaerobic conditions at 40 °C with *E. coli* BOR^{R1} whole cells, set to OD 5 (1.5 μM Cytc) in M9-N buffer at pH 7.4 with 5 % (v/v) MeCN as co-solvent. Substrates were supplemented in concentrations of 6 mM NHCB and 12.5 mM DAC in M9-N buffer at pH 7.4 with 5 % (v/v) MeCN and fed via a syringe

piston pump in dilution rates from 0.03 to 0.20 min^{-1}. OB formation was recorded during varying feed periods adapted to the different D. The conversion was calculated based on the NHCB content at the inlet and plotted against the numbers of residence times θ for each D (fig. 3.35).

The measurements show an increasing conversion of NHCB with decreasing τ. For a τ of 44.3 min up to 15 % conversion are reached, while a faster feeding at a τ of 6.6 min leads to a maximum of 5 % conversion. After reaching maximum conversion after 1 θ, conversion declined due to Cytc deactivation by DAC leading to a lack of OB formation. This behaviour is observable over the span of 3 θ for all D. Since substrates and DAC in particular is added slower at higher τ, Cytc has less difficulties to reduce the DAC content. Higher D leads to fast increasing substrate concentrations enabling an accelerated Cytc deactivation. However, instead of increasing τ to raise NHCB concentration and Cytc activity, a reduction of τ combined with an increase of the stock concentration of NHCB is more effective. Thereby, activity would increase by a rise of NHCB content without feeding additional DAC, leading to a reduced Cytc deactivation. Nevertheless, the data demonstrates, that a limited feed of DAC is required to improve conversion, maximum product concentration and thereby an improved STY.

In order to compare additional parameters with respect to the residence time (Eq. 2.6), STY (Eq. 2.2) as well as the molar OB synthesis n_{OB} were determined (fig. 3.36).

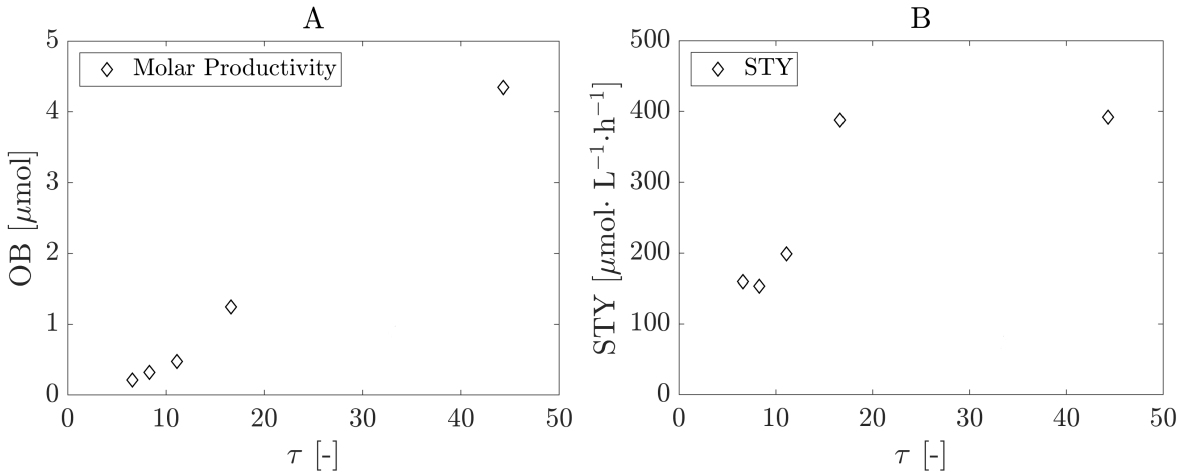

Figure 3.36: Molar OB synthesis n_{OB} and STY for different τ from 6.6 to 44.3 min for biocatalytic borylation catalyzed by Cytc BOR^{R1} harboured in *E. coli* BL21 DE3 at OD 5 in M9-N buffer at pH 7.4 with 5 % (v/v) MeCN as co-solvent in a CSTR depending on the number of residence times θ. N_{OB} and STY increased with decreasing τ.

The calculations show, that n_{OB} rises nearly linearly with increasing τ, underscoring the

effect of a limited presence of DAC to minimize Cytc deactivation to boost product formation to 4.35 μmol OB. Moreover, the STY is additionally elevated at τ of 44.3 and 16.6 min to almost 400 μmol·L^{-1}·h^{-1}. This incorporates a TTN of up to 873, which is a low value, in comparison to a TTN of over 3000 in the fed-batch mode.

In summary, the application of OB synthesis in a continuous mode reveals important information for biocatalytic borylation. As already shown for the dilution rate in the fed-batch mode, an adjusted residence time is crucial to reduce DAC-induced Cytc deactivation and to maintain product formation. However, since only tests with low catalytic activity at OD 5 were examined, further investigations at higher activity loads at unchanged molar feed rates could achieve improved STY and molar OB synthesis. An adaption of residence time and substrate stock concentrations can improve the OB synthesis in a CSTR by far. In particular, TTN can still be increased and can lead to elongated process times without frequently renewing the biocatalyst. With additional developments of the CSTR, enhanced TTN and OB_{final} compared to the fed-batch mode are possible to evolve an industrial relevant approach of biocatalytic OB synthesis.

3.3.4 Process Parameter Comparison

The reaction engineering investigation of biocatalytic borylation evolved the approach of Cytc-driven OB synthesis stepwise. In order to present the evolution of the yielded results more concise, a short summary is given with figure 3.37 with respect to the collected relevant process data (tab. 3.2).

The batch mode was applied due to comparability reasons with the work of Kan *et al* (2017). First tests revealed, that only Cytc in whole cells maintain Cytc activity to yield elevated product concentration and TTN. As a results, the OD was increased from 5 to 30 to enhance OB_{final} to 12.9 mM and the TTN to 1397 mol·mol^{-1}. Here, a too slow conversion of DAC in OD 5 syntheses results in DAC accumulation and subsequent Cytc deactivation and prevents especially higher TTNs. Thus, a controlled DAC supplementation in a fed-batch set-up was checked in addition. This prevents DAC accumulation, which causes the rise of TTN and OB_{final} especially at OD 5 tests to 1955 mol·mol^{-1} and 2.76 mM particularly at low D of 0.012 h^{-1}. Here, an addition of 50 mM glucose elevates the TTN and OB_{final} even further. The effect of the adjustment of D is less pronounced at OD 15 and 30, but still improves process parameters compared to the batch experiments. While TTN and OB_{final} rise with falling D, the opposite effect is observed for the STY. Since this parameter was calculated according to the duration of the feed phase, this effects was

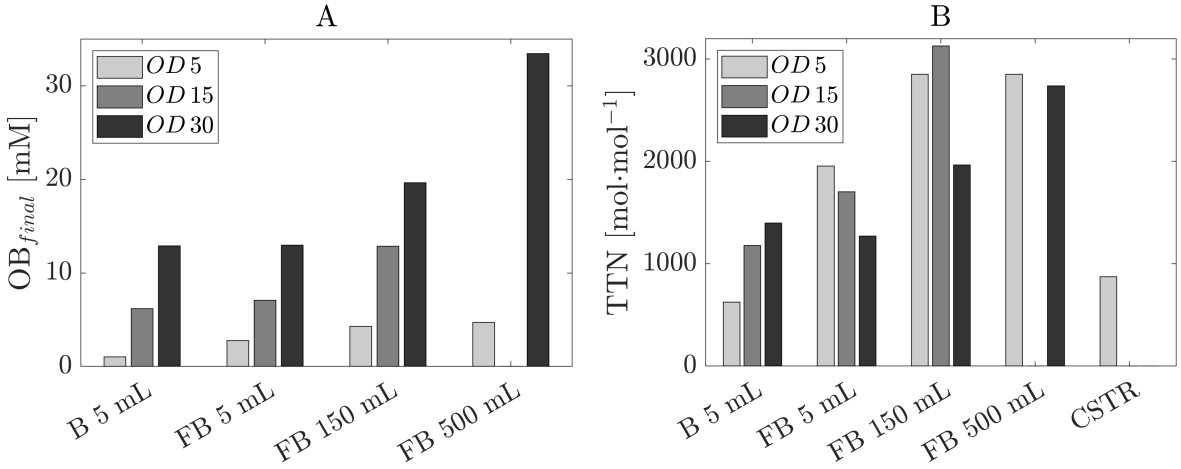

Figure 3.37: Evolution of OB$_{final}$ (A) and TTN (B) within this thesis for biocatalytic borylation catalyzed by Cytc BOR^{R1} harboured in *E. coli* BL21 DE3 at OD 5, 15 and 30 in M9-N buffer at pH 7.4 and 40 °C with 5 % (v/v) MeCN as co-solvent in batch (B), fed-batch (FB) or continuous mode (CSTR). D in fed-batch mode: 0.12 (OD 5 and 15) and 0.24 (OD 30). OB$_{final}$ and TTN increases particularly due to fed-batch application with a limited DAC supplementation.

expected, as a higher D causes a shorter feed phase. Nevertheless the productivity increases up to 28.65 g·L^{-1}·h^{-1} for OD 30 tests at 0.96 h^{-1} and 12.5 mM NHCB, but due to the high Cytc content the TTN do not exceed 1236 mol·mol^{-1}. Subsequently, a 30-fold scale-up to 150 mL reaction volume was established where results from the 5 mL scale were proven. At to a D of 0.012 h^{-1}, OD 15 tests reach the highest TTN within this thesis of 3129 mol·mol^{-1}. Moreover, OD 30 tests with 20 mM substrates and a D of 0.024 h^{-1} reach the highest OB$_{final}$ of 19.64 mM in this study until this point. Moreover, the syntheses at OD 15 and 30 show a linear increase of OB limited to the feed, which proved the instant and full conversion of added DAC to minimize Cytc deactivation. The same behaviour show tests at OD 30 in 500 mL reactors. Additionally, a secondary feed causes the rise of OB$_{final}$ to 33.4 mM. Moreover, the continuous mode was investigated to identify comparable effects regarding benefits in Cytc activity by limited DAC addition. Here, a reduction of D, described by an increase of θ, causes molar OB synthesis to rise up to 4.35 μM at 44.3 min retention time. However, due to a TTN of 873 mol·mol^{-1}, the continuous OB synthesis is improvable.

Table 3.2: Overview of all collected data of reaction engineering experiments for biocatalytic borylation catalyzed by Cytc BOR^{R1} harboured in *E. coli* BL21 DE3. STY calculated for batch mode with 2 h reaction time, for fed-batch mode with feed-phase duration and for continuous mode with 5θ. *additional 50 mM Glucose, ** synthesized OB [μmol], F: free Cytc, I: immobilized Cytc.

Parameter	Volume	D/τ	OD_{600}	Cytc	NHCB	OB_{final}	TTN	STY
Unit	mL	h^{-1}/min	-	μM	mM	mM	mol·mol^{-1}	g·L^{-1}·h^{-1}
Batch	5	-	5	1.67	6.0	1.04	624	-
Batch	5	-	F	1.90	6.0	0.45	76	-
Batch	5	-	I	0.50	6.0	0.09	180	-
Batch	5	-	15	5.24	6.0	6.19	1180	-
Batch	5	-	30	9.23	6.0	8.87	961	-
Batch	5	-	30	9.23	12.5	12.90	1397	-
Fed-batch	5	0.012	5	1.41	6.0	2.76	1955	0.23
Fed-batch	5	0.036	5	1.41	6.0	2.66	1889	0.55
Fed-batch	5	0.360	5	1.41	6.0	1.91	1357	1.61
Fed-batch	5	0.960	5	1.41	6.0	1.95	1380	2.95
Fed-batch*	5	0.012	5	1.49	6.0	3.39	2273	0.25
Fed-batch*	5	0.036	5	1.49	6.0	2.42	2132	0.69
Fed-batch*	5	0.360	5	1.49	6.0	1.96	1621	1.98
Fed-batch*	5	0.960	5	1.49	6.0	1.95	1304	2.93
Fed-batch	5	0.012	15	4.16	6.0	7.09	1704	0.55
Fed-batch	5	0.036	15	4.16	6.0	7.09	1704	1.55
Fed-batch	5	0.360	15	4.16	6.0	6.73	1619	6.19
Fed-batch	5	0.960	15	4.16	6.0	6.42	1542	10.65
Fed-batch	5	0.012	30	9.47	6.0	10.20	1078	0.85
Fed-batch	5	0.036	30	9.47	6.0	10.51	1100	2.54
Fed-batch	5	0.360	30	9.47	6.0	10.29	1086	13.53
Fed-batch	5	0.960	30	9.47	6.0	10.00	1056	24.15
Fed-batch	5	0.012	30	10.19	12.5	11.56	1134	0.90
Fed-batch	5	0.036	30	10.19	12.5	12.96	1271	2.98
Fed-batch	5	0.360	30	10.19	12.5	12.73	1249	19.27
Fed-batch	5	0.960	30	10.19	12.5	12.59	1236	28.65
Fed-batch*	150	0.012	5	1.50	6.0	4.28	2851	0.38
Fed-batch*	150	0.012	15	4.10	12.5	12.83	3129	1.24
Fed-batch*	150	0.024	30	12.1	12.5	13.08	1081	2.46
Fed-batch*	150	0.024	30	10.0	20.0	19.64	1964	3.69
Fed-batch*	500	0.012	5	1.50	6.0	4.71	2851	0.47
Fed-batch*	500	0.024	30	9.45	20.0	20.02	2118	4.07
Fed-batch*	500	0.024	30	12.20	40.0	33.42	2739	2.73
CSTR	3.3	44.3	5	1.50	6.0	**4.35	873	0.08
CSTR	3.3	16.6	5	1.50	6.0	**1.24	250	0.08
CSTR	3.3	11.1	5	1.50	6.0	**0.48	95	0.04
CSTR	3.3	8.3	5	1.50	6.0	**0.32	65	0.03
CSTR	3.3	6.6	5	1.50	6.0	**0.21	43	0.03

4 Discussion and Outlook

After presenting and discussing the results stepwise for each experiment, a general discussion is important to interconnect the learnings from single tests for the evolution of whole project. At this point, common limitations of the approach but also opportunities can be identified to give an outlook about possible targets to further develop biocatalytic borylation in coming theses.

4.1 Starting Material Investigation

Since the state of a substrate can effect a reaction decisively, investigations focused on the condition of the starting materials under various conditions. Here, DAC stated an instable substance, as several parameters were proven to lead to a decay by cleavage of its diazo moiety as N_2. Experiments demonstrated clearly, that DAC decays at elevated temperatures above 60 °C after 15 min and due to UV-light stimulation latest after 24 h.

The study of the UV-light-induced impact on DAC decomposition was influenced by non-controllable effects. During the UV-light exposure the intensity varied during day and night and due to cloud coverage. Although an UV-meter was intended to quantify the UV-light intensity during the experiment, its sensitivity was not sufficient. Thus, the measurements were error-prone and too inaccurate to serve as reliable reference. Instead, an adjustable UV-light source can provide constant conditions. Since not only the light intensity can be adapted, but also the wavelength can be varied, precise investigations are possible. In addition, both peak wave lengths $\lambda_{DAC,1}$ of 220 nm and $\lambda_{DAC,2}$ of 270 nm within the fingerprint region can be stimulated separately. Thereby, an identification of the peak for diazo moiety separation seems possible.

Tests investigated UV-light and temperature separately, but side-effects could not always be prevented. As an example, DAC samples were covered with aluminium foil during incubation in the thermo shaker to reflect UV-light during the experiment. In contrast, DAC samples positioned at the window for the UV-light were at room temperature, which varied during the experiment. Although temperatures did not extend 60 °C, r.t. might also had a measurable effect on the decomposition due to the enlarged incubation time of one month. A sample storage on ice or in a thermostated water bath can exclude this effect. If it is not possible to block the single parameters, a study with all effecting parameters is possible in form of a design of experiment (DOE). Several parameters like temperature, UV-light and water content can be investigated simultaneously, where experiments in a previously determined pattern reduce the amount of single tests needed. Nevertheless, the impact of

each effect alone can be yielded.

Overall, the examined tests showed qualitative hints on the impact of different conditions on DAC decay. However, studies need to find a way to maintain constant conditions and to minimize cross-effects. Moreover, a comparison with a sample stored at -20 °C is necessary to compare the condition of exposed DAC with an undecayed stock.

4.2 Kinetic Characterization

This thesis characterized the biocatalytic borylation in terms of temperature and pH towards Cytc activity and cell stability. The reaction was mathematically described along Michaelis-Menten kinetics to simulate and forecast the reaction process. A detailed temperature screening demonstrated an increased initial reaction rates for syntheses at elevated temperatures up to 40 °C . The same was possible for the pH value, that was screened between pH 5 and 9.

The pH-value effects Cytc activity negatively in acidic and alkaline milieus. However, the molecular and structural effect induced by a lowered or heightened pH is unknown. For one, the conformation of Cytc might be influenced according to its pI leading to changes in activity, stability and solubility [117]. Since Cytc is a basic protein with a pI of 9.3 to 10.3, all checked pH values led to an net positive electric charge of Cytc [118]. Nevertheless not the whole protein has to be positively charged, since single amino acids have their own pI and lead thereby to a stepwise increase of the net charge with a falling pH and fluctuations across the proteins surface occur [119]. A limited transport of substrates is also imaginable due to pH variations. The titration of NHCB proved, that NHCB is prominently protonated below pH 6.12 and can thereby be hindered to associate to the active site. Consequently, Cytc deactivation would occur easier with DAC already bound as carbene to the active site, awaiting the delayed borane compound and thus leading to a lowered initial reaction rate. Furthermore, active site amino acids also change their charge in dependence of the pH. For example, threonine 103 has a pI of 5.6 being negatively charged at pH 6, 7.4 and 9 [120]. In contrast, pH 5 leads to a positive charge which can additionally block attacking NHC-BH_2 as well as the carbene, resulting in a drop of the reaction rate. This effect can be additionally supported by foaming and an assumed cell lysis, that disables cell homeostasis and enables the effects described above.

The studies investigated both parameters separately, where one parameter stayed constant while the other increased or decreased. In particular, the pH screening was executed at 40 °C, which could have stressed the host cells in addition to acidic or alkaline milieus,

as 40 °C lays slightly above the optimum growth temperature of *E. coli* of 37 °C [121, 122]. Despite the minor difference of 3 °C, a severe damage can be assumed, since growth rates and protein stability decrease exponentially a few degrees above their optimum [123]. Therefore, temperatures at 35 or even 30 °C might result in a more pH-resistant behaviour of the host strain, preserving Cytc activity. In general, dependencies of Cytc activity on pH and temperature can be studied in coming studies simultaneously, where both parameters vary in one experiment. As describe for the effects on DAC decomposition, a DOE can help to minimize the number of experiments needed to gain valid statements for the effect of both parameters on Cytc activity during biocatalytic borylation. As algorythm-based option, machine learning can identify patterns and linkages between experimental parameters by using artificial intelligence [124]. This method is projected to be significant in future research [125].

Aside from the the investigated parameters a third characteristic is known to influence heme enzymes in particular. The ionic strength describes the concentration of ions in a solution [126]. Present ions effect the ionic strength where the concentration of each ionic compound c is factorized with their charge z (Eq. 4.1).

$$I = \frac{1}{2} \cdot \sum_{i=1}^{n} c_i \cdot z_i^2 \tag{4.1}$$

Since Cytc belongs to the enzyme class of oxidoreductases, the electron transport is the main catalytic task of active Cytc. At this point the ionic strength can interfere with the biocatalyst in protonating or deprotonating reactants. The required formation of an electron transfer complex between the heme and the carbene can be hampered. This can be assumed, since comparable studies between ferricytochrome c and oxymyoglobin showed, that for high ionic strengths the electron transfer rate can be neglected and an ionic strength of 0.01 inhibits the electron transfer [127]. Thus, this parameter needs to be included in further studies and can be incorporated in the aforementioned DOE.

Aside from the interpretation of the results, the acquisition of experimental data is discussable. Here, the initial reaction rate is particularly arguable, since the host strain itself is a living organism and is thereby as controllable as pure enzyme. The recombinant expression of Cytc is thus not reproducible to 100%. Although the OD was set before each initial rate measurement and inducer stocks were prepared equally, deviations occurred in the Cytc content between 1 and 2 μM, being a wide range for comparable test. Here, cell suspensions had to be utilized immediately after OD adjustment to minimize the risk of cell lysis at storage in harsh conditions e.g. non-neutral pH. Thus, the Cytc content was determined afterwards and initial reaction rates were normalized to the Cytc concentration to eliminate

this aspect mathematically. However, initial reaction rates varied under the same reaction conditions for different cell suspensions and could not be correlated mathematically. Thus, the ratio between OD and enzyme content is crucial and probably influences the intracellular mass flow. The DAC transport to the periplasm is probably comparable for all host cells. However, a doubled content of Cytc inside the periplasm can maintain the present DAC concentration at a lower level leading to variations of the initial rate as well as of the deactivation.

In addition to the biological aspect, deviations in the quality of substrates can lead to variations in the convertible amount of substrate added. Here, impurities of NHCB due to self-synthesis are in general possible, but can be excluded, due to recrystallization of crude NHCB. The decomposition of DAC is a further decisive issue. The purchased stocks and the prepared substrate solutions were stored at -20 °C under Ar atmosphere, which minimized the decay of DAC. However, the commercially received stocks arrived in different conditions, which were marked by a more reddish instead of a yellowish color. Moreover during storage at -20 °C some stocks stayed liquid while other stocks solidified. For the solidifying as well as the reddish stocks only trace activities could be measured. This can be caused by a reduction in intact DAC concentration and a followed decrease of the initial reaction rate according to Michaelis-Menten theory. Although it was possible to determine DAC content in MeCN for the decomposition studies, the samples need to originate from one stock, which is not applicable for the experiments done every week using different substrate stocks. Due to overlapping absorption spectra with the M9-N buffer, fingerprint peaks of DAC can not be quantified in the reaction mixture.

As demonstrated in literature, oxygen effects biocatalytic borylation by reducing Cytc acitivty, due to oxidization of the heme [21]. Thus, small scale synthesis up to 1 mL reaction volume were carried out in an anaerobic chamber. Here, the oxygen content can be maintained within the ppm region. Since kinetic studies were executed without an oxygen measuring device, oxygen accumulation due to leaks in the rubber septa could have occurred without being noticed. However, since reactors, syringes and substrate stocks were flushed multiple times with N_2 and Ar, oxygen contaminations are less pronounced, than DAC stock decomposition for example.

Concluding, a variety of possible reasons for errors in initial rate measurements is imaginable, which caused measurements to be neglected for kinetic parameter estimation at first. Despite, established benchmark reactors helped to minimize this deficit, which were conducted at 6 mM NHCB, 12.5 mM DAC at 40 °C and pH 7.4 in each set of experiments and each cell culture. This erased the error of Cytc-to-OD ratio as well as fluctuations in the

DAC quality, since investigated effects were correlated to the benchmark conditions. For example, when determining initial reaction rates depending on DAC at 35 °C the benchmark reactors at 40 °C, which were run with the same cell suspension and substrate stocks as the 35 °C tests, were considered as reference. Here, fluctuations in initial reaction rate due to Cytc content or substrate quality led to changes in determined initial reaction rate also for the benchmark reactors. The set of data for the 35 °C study was then multiplied with the factor of activity loss between the benchmark reactors at 40 °C within this set and the benchmark reactors that had optimal reaction conditions. As a results, the error in the initial reaction rates of the 35 °C study was erased. After all data from one set was collected and multiplied according to the benchmark reactors, the data points with still remaining activity deficits due to contaminations with oxygen, off track substrate concentrations or visible foaming were excluded. The left-over data founded the mathematical kinetic model.

A numerical fitting determined kinetic parameters with non-linear regression to setup a Michaelis-Menten model. The simulations of the reaction process based on this model stayed in a reasonable range but were not able to reproduce the experimental data over the whole reaction process. Here, biological effects can impact the OB synthesis over time, which is important when investigating whole cells instead of free enzymes. Whole cells provide a maintenance metabolism, build inclusion bodies and can grow as well as duplicate. Factors, which are not covered within the conducted experiments for kinetic characterization and would also lead to a more complex kinetic model [128]. Additionally, and as already mentioned in the results section 3.2.3.2, Cytc-deactivation by DAC is simulated too fast as it follows an exponential first order decline. This does not represent the experimental measured process, where activity is longer available than the model forecasts. Here, a detailed study is necessary to determine the dependency of the deactivation constant K_{dea} relative to the DAC concentration. Since the assumptions made during the fed-batch studies considered the deactivation to be less pronounced at low or close-to-zero concentrations, deactivation studies need to be examined at different concentrations. The experiments that had been conducted at 12.5 mM DAC have to be repeated additionally at 9, 6, 3, 1 and 0.1 mM for instance. According to the assumption, the decline of activity over time is reduced at low concentration as shown in figure 4.1A.

If normalized to the initial reaction rate without pre-incubation at a specific DAC content, different K_{dea} can be estimated for different concentrations (fig. 4.1B). The plotting of the determined K_{dea} against the concentration would create a term with two additional constants A_{dea} and B_{dea} that have to be calculated (fig. 4.1C). Since the term has the same structure as the Michaelis-Menten equation, the constants can be fitted according to v_{max} and $K_{m,NHCB}$.

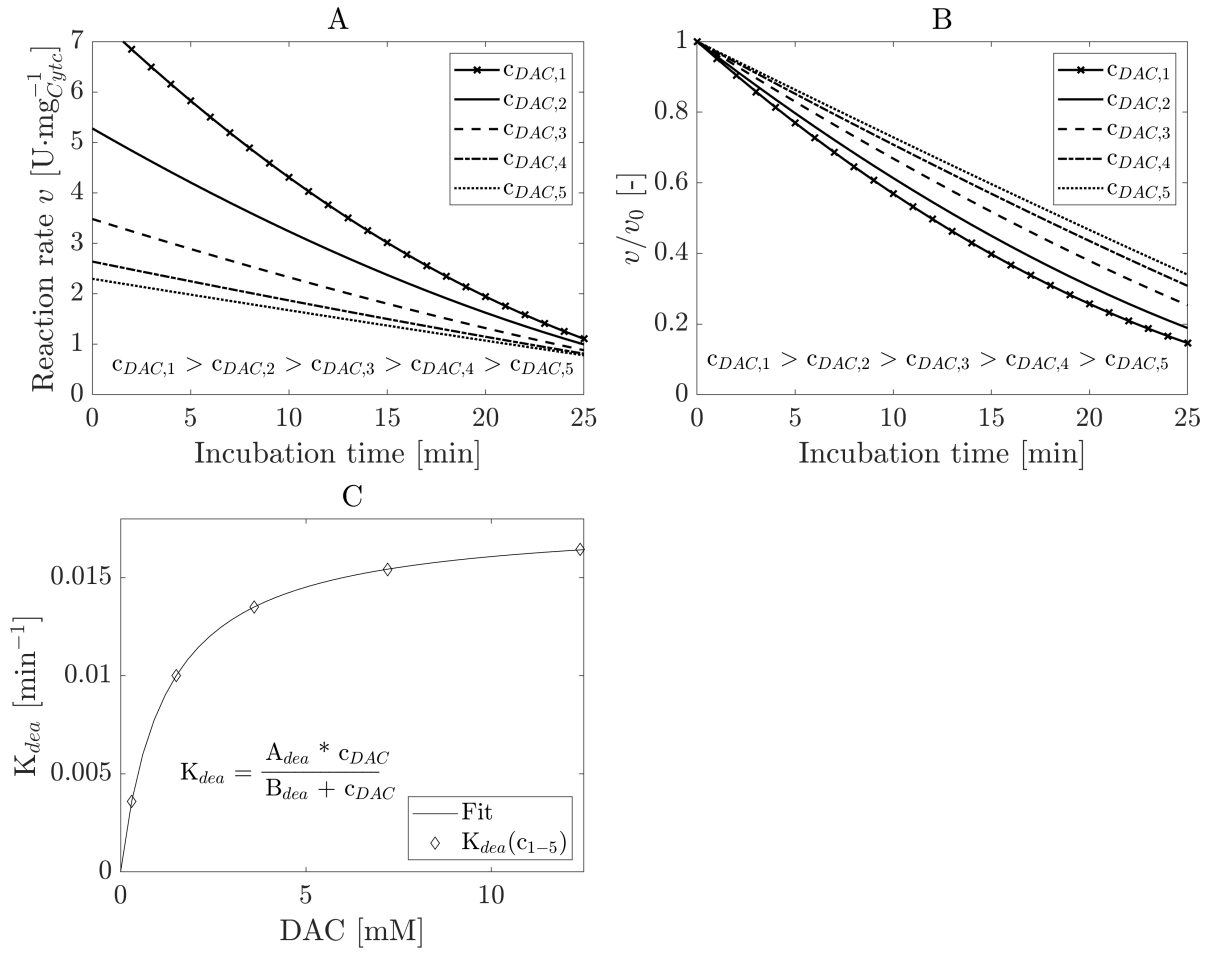

Figure 4.1: Presumable plots of experimental data for the determination of a mathematical expression of K_{dea} in dependency of DAC content. Cytc deactivation in depending on DAC content is recorded (A) and normalized (B), before the term for $K_{dea}([DAC])$ is derived by plotting against DAC concentration and determination of A_{dea} and B_{dea}.

The result is an expression, which can be implemented into the overall substrate surplus inhibited double-substrate Michaelis-Menten model and describes K_{dea} as a function of the DAC concentration.

Non-linear regression estimated kinetic parameters utilized in the Michaelis-Menten model successfully. The fitted kinetic constants allow to recreate the dependency of the initial reaction rate to the substrate concentration for both substrates precisely. Although the experimental data hit the simulated progress of the plots nearly without optical deviations, the resulting kinetic constants had relatively wide confidence intervals. At this point other fitting functions can be tried to minimize the the confidence interval. Here, a weighted non-linear regression increases the mathematical weight on specific data points. The fitting lays more focus on these weighted data and reduces the error especially there. This reforms

the progress of the simulated Michaelis-Menten plot for instance and changes the confidence intervals likewise.

In addition to measure the activity of Cytc under defined conditions by initial reaction rates, a process curve analysis might be possibly against early assumptions based on deactivation issues. If the deactivation can be described correctly, it can be implemented in the overall model and allows thereby the process curve analysis. Nevertheless, initial measurements for the deactivation studies are required. However, afterwards correlations between the initial reaction rate and the substrate concentration can get more precise as reaction rates at supplementary concentrations are determinable. This creates an expanded data set also from one reaction with exactly the same conditions and improves the precision of the kinetics parameters. Moreover, the reaction simulation an anneal to the progress curve, as the data originates from a complete reaction.

4.3 Reaction Engineering

The reaction engineering studies enhanced process parameters in Cytc-driven biocatalytic borylation. In particular TTNs as well as OB_{final} rose by over a magnitude with applying different operation modes.

OB_{final} reached a maximum of 33.4 mM, being the highest concentration of OB accomplished in biocatalytic borylation in this thesis. However, OB_{final} was sometimes higher, than the mole amount of NHCB added, which can indicate an error-prone calibration of OB. Here, the efficiency of the extraction used for calibration of the aqueous samples can vary. Furthermore, impurities of the chemical OB standard are possible due to chemical self-synthesis, which is additionally applicable on NHCB calibration. For the chemically synthesized OB racemic standard, ^{1}NMR spectra available in literature do not show many differences in peak amounts or peak size (supplementary information fig. 6.5 and 6.6). In addition, the measured GC spectra for the standard do not give any advice for decisive impurities which can influence the calibration in the ratio noticed in the experimental data. Undiscovered impurities could have occurred and still not been recognized. Either their concentration was not significant to effect the peaks in the ^{1}NMR spectra or they decay like DAC at elevated temperatures and are thereby not detectable by GC. Furthermore, DAC and NHCB were both separated after chemical OB synthesis by applying reversed phase chromatography. Aside, water states a reasonable impurity, as well as CH_2Cl_2 as synthesis solvent. But since OB is not known to be hygroscopic and intesive drying at 40 °C over 24 h after standard synthesis was executed, both candidates can be excluded. In contrast, the calibration with

chemically synthesized NHCB can cause errors due to impurities. Here, assumptions can be made on possible contaminations visible in the ^{1}NMR spectra, since no reference is given in literature. Divergent from the chemical OB synthesis from NHCB and DAC, the chemical NHCB synthesis is based on additional chemicals like the salts $NaBH_4$ and 1,3-dimethyl-1H-imidazol-3-ium iodide. Here, the 1,3-dimethyl-1H-imidazol-3-ium iodide causes additional or slightly shifted peaks in the ^{1}H-NMR spectra of the synthesis product (supplementary information fig. 6.7). Moreover, $NaBH_4$ is not visible in the GC since it is not soluble in organic solvents, which are used for the applied extraction before GC quantification. However, contaminations would have led to a lowered peak area of NHCB in the calibration, resulting in less NHCB added and less OB formed. But since more OB was synthesized biocatalytically, this might not be the reason. Aside, substrate addition can be error-prone. NHCB substrate stocks were prepared freshly one day before each experiment. Here, the solvent MeCN could have evaporated partially during storage at 4 °C, or dissociated into the material of the micro reaction tube. As a result, the concentration of NHCB in the stock rose over night. Moreover, due to the storage temperature at 4 °C, stocks needed to warm up to r.t. before the substrates can be added volumetrically with pipettes. If the NHCB stock was added too early, the solution was denser leading to more NHCB added. Thus, inconsistent addition of the NHCB stock in combination with evaporation of the solvent is possibly the reason for too high OB concentrations, which only appeared rarely. The recording of NHCB during the reaction showed fluctuations 100 μM range, providing no reliable source to calculate product concentrations. Concluding, too high OB contents are likely a result of inconsistent substrate addition instead of calibration issues due to contaminations. Thus, the fed-batch experiments, particularly with the detailed sampling during the feed phase, are reliable since the molar product formation rate agreed with the calculated molar feed rate to around 99 %. Moreover, OB_{final} in OD 15 and 30 reactors in the 150 ml and 500 ml scale reached the amount of added substrate to a final concentration 20 mM exactly. The maximum OB_{final} of 33.4 mM is therefore overall still valid.

The reaction engineering studies increased TTN of Cytc in biocatalytic borylation. Improvements in the batch mode from 620 to 1400 mol·mol^{-1} were achieved by an increase of the Cytc concentration. However, these TTNs are below the TTNs yielded in the study of Kan *et al.* (2017) at 2490 mol·mol^{-1} [21]. Although the conditions at studies from Kan *et al.* (2017) were at 10 NHCB, 10 mM DAC and 25 °C, and are thereby not adjusted to kinetic influences as substrate inhibition or temperature-improved activity, the corresponding OB_{final} as well as the TTN were higher. Thus, it has to be differentiated between the activity of Cytc during the initial phase of the reaction and Cytcs performance and endurance over the

whole reaction progress. The kinetic characterization mainly focused on the optimization of the initial reaction rate during the first minutes of OB synthesis. In contrast, the identified beneficial conditions are probably not optimal for the overall reaction. Particularly, temperature screenings revealed advantageous improvements at 40 °C regarding the reaction rate. However, the deactivation can behave differently on temperature changes. For example, the deactivation mechanism could be accelerated by a factor of 5 or higher for instance, while the reaction rate only enhances 3.5-fold by an increase from 25 to 40 °C. This would result in a lower but an elongated activity of Cytc at e.g. 25 °C, leading to higher OB_{final} and TTN. Additional studies should therefore investigate the deactivation at 25°C or examine an overall temperature screening for the deactivation mechanism of Cytc by DAC. These tests need to target especially the range between 20 and 40 °C. Particularly, process parameters in batch processes can be enhanced with a temperature that is adapted to the overall reaction instead of increasing the activity, thus aiming for a more holistic optimization. Together with the learnings from the kinetic characterization, substrate concentrations can be varied in additional studies to increase conversion, STY and OB_{final}. Regarding NHCB, the range around 6 mM is interesting, whereas DAC concentrations between 3 and 12.5 mM influence Cytc activity strongly. The combined effect of lowered deactivation and catalytic activation is especially interesting. In order to be time efficient, a DOE is suggested to vary all three effects to determine their impact on the process parameters STY, TTN and OB_{final}.

Although the discovered discrepancies for TTNs between this study and Kan *et al.* (2017) can be explained for the batch process, same conclusions are not equally transferable to fed-batch and continuous modes. Here, DAC is added according to an adjusted dilution rate to minimize the deactivating effect on Cytc by direct and full conversion. Thus, a long incubation of Cytc with DAC as present in the batch mode is prevented. Although TTNs multiplied compared to batch mode, the TTN reached within studies of Kan *et al.* (2017) with up to 12000 $mol \cdot mol^{-1}$ are 3 to 4 fold higher. Since the Dac-driven deactivation is reduced in fed-batch mode due to the adapted dilution rate, the hypothesis of faster deactivation at 40 °C is not observable. There is a lack of experimental data for 25 °C which proof the deceleration of the deactivation compared to 40 °C. Thus, experiments with a constant dilution rate are required, which feed DAC until the molar OB synthesis rate decreases in comparison to the molar DAC feed rate, resulting in DAC accumulation. This moment marks a reference point $t_{Deac,40}$ for the fed-batch tests at 25 °C. At the time, where at 25 °C the molar OB synthesis rate decreases and stops to be linear, the corresponding reference point $t_{Deac,25}$ is reached. If $t_{Deac,25}$ is bigger than $t_{Deac,40}$, the made assumption towards an accelerated deactivation at 40 °C is proven. Therefore, the Cytc concentration

has to be equal and the dilution rate has to be low enough. Then, the activity at 40 and particularly at 25 °C is sufficient to convert DAC during the feed phase to prevent DAC from accumulating until $t_{Deac,25}$.

OB syntheses in a CSTR yielded TTNs in the range of the batch experiments at 873 mol·mol^{-1} for the highest investigated retention time of 44.3 min. Thereby, the CSTR does not reach TTNs achieved in the fed-batch mode yet. One reason is the substrate concentration in the CSTR itself. As DAC is added in comparable dilution rates as in the fed-batch mode, NHCB is supplemented in an equal ratio. Hence, NHCB does not start at a high concentration of 6, 12.5 or even 20 mM as in the fed-batch, but rises slowly after feed initiating. Since NHCB is provided in a lower concentration than DAC, this leads to an even meagerer increase than for DAC and the reaction rate is critically reduced in the beginning as it takes time to reach half of v_{max} at $K_{m,NHCB}$ of close to 6 mM. Due to $K_{m,NHCB}$ being higher than $K_{m,DAC}$ at 1.1 mM, a sufficiently high reaction rate is probably never reached to convert the fed substrates (Fig. 4.2 B) .

Thus, DAC accumulates and deactivates Cytc within ongoing incubation time as shown in figure 4.2 A, leading to a lack of OB formation after $3\,\theta$. In order to reduce the accumulation of DAC, an initial reaction rate around 5 to 7 U·mg^{-1} has to be achieved. For instance, a NHCB supplementation to 6 mM close to $K_{m,NHCB}$ after addition of the cell suspension during reactor preparation, but prior to substrate feeding is possible to provide an initial elevated reaction rate. After feed initiation, the feed containing 6 mM NHCB maintains the NHCB concentration (Fig. 4.2C). As an other option, NHCB and DAC can be added separately from two reservoirs, where NHCB is fed first to establish a NHCB content of 6 mM, before DAC is feeded to the CSTR secondly. Both options provide an initial reaction rate of 5 to 7 U·mg^{-1} due to substrate concentrations close to $K_{m,DAC}$ and $K_{m,NHCB}$, but hold DAC at reduced levels which minimize Cytc deactivation. This set-up additionally enables a stepwise increase of DAC. Here, DAC can be conveyed in a low molar rate to be instantly fully converted and holding the actual concentration inside the CSTR at zero. Subsequently, the molar DAC feed rate can be increased, until DAC is again at a concentration close to or at zero. During this stepwise elevation of the molar feed rat of DAC, the DAC concentration in the CSTR only varies between zero and a low content during the short time of dilution rate increase. Thus, Cytc notices only those low DAC concentrations, which minimizes the deactivation. This characteristic is comparable to the conversion of added DAC by Cytc in the fed-batch mode, where DAC entered the reactor droplet-wise or with changing molar feed rates. However, this procedure needs a Cytc concentration of at least 5 μM to convert entering DAC fast and requires a careful increase of the molar feed rate of DAC, but can

enhance the TTNs as well as the STY.

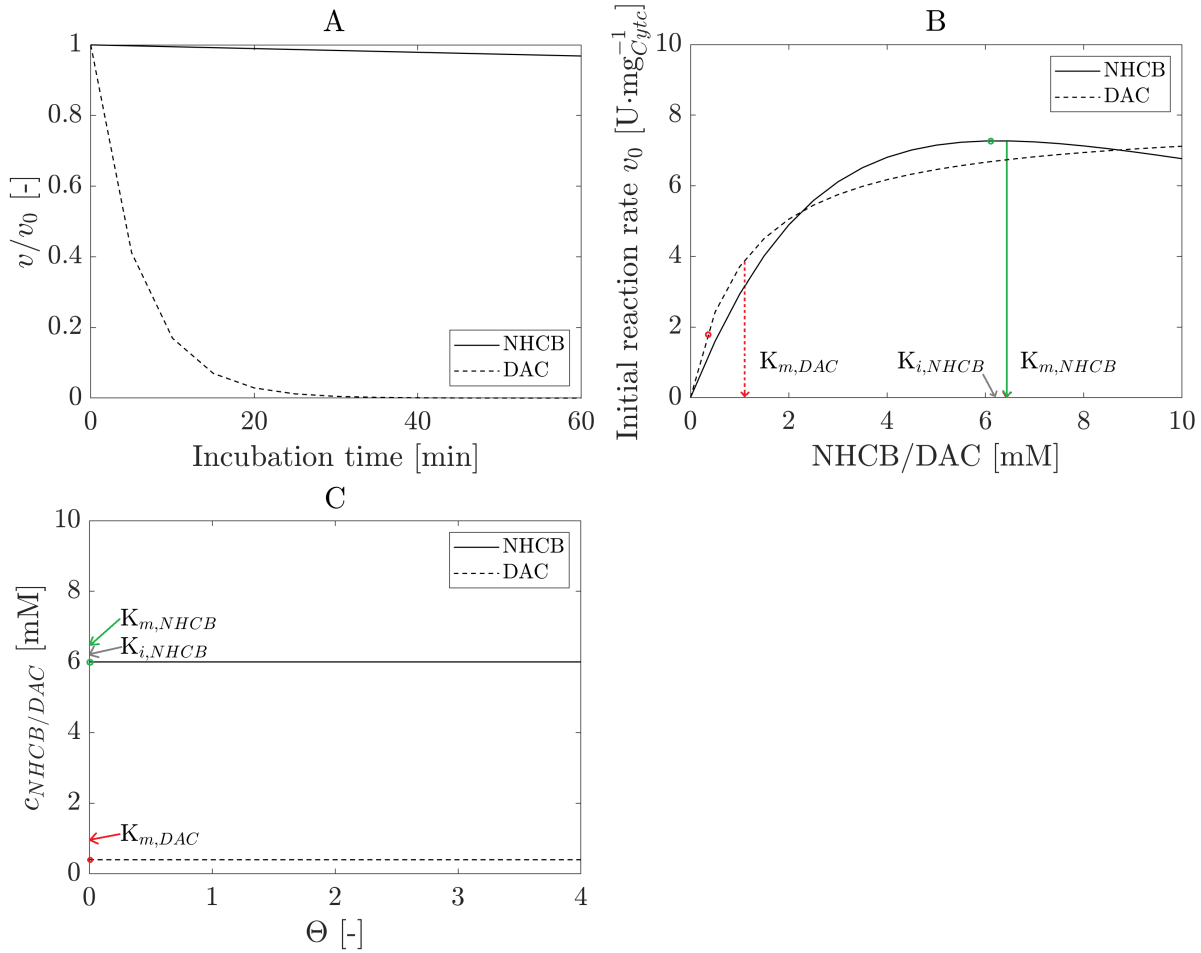

Figure 4.2: Derivation of suitable operating points for substrate concentrations for biocatalytic borylation in a CSTR. Cytc is deactivated by 12.5 mM DAC after 20 min incubation time (A) demanding a low applied concentration during CSTR operation (C). A concentration of 6 mM NHCB close to $K_{m,NHCB}$ increases the initial reaction rate without risking a substrate surplus inhibition below $K_{i,NHCB}$(B).

Although TTN and STY can be enhanced by the suggested set-up changes for the CSTR, other process parameters may suffer instead. DAC is converted completely with an optimized dilution rate, leading to a conversion of 100 %. This is economically important as DAC is the most expensive substrate participating in this reaction with a price of 1000 $ per 25 g. In contrast, NHCB has to be held constant at 6 mM to conserve a high reaction rate of Cytc. This incorporates, that beside the formed OB, NHCB leaves the CSTR constantly at this concentration. Thus, a high conversion of NHCB is not possible. In terms of economy and ecology, NHCB conversion needs to be improved, which can be achieved with a continuous separation and a recycle of the recovered NHCB into the supply reservoir.

When installing a recycle stream, a purge stream is essential to prevent accumulation of side products. Possible contaminations can be hydrolysis and decomposition products of DAC like EL and its consecutive hydrolysis products EtOH and LA. Contaminations from NHCB synthesis like $NaBH_4$ and 1,3-dimethyl-1H-imidazol-3-ium iodide are plausible. Proteinogenic impurities can occur during continuous synthesis due to cell lysis or leakage of the membrane. Concluding, different contaminations are possible, which need to be eliminated to receive an OB product above 95 (w/w)% purity. With a successfully established CSTR, additional studies can investigate different methods to continuously purify OB and to separate NHCB by different downstream operations, recycling this substrate and to minimize the risk of accumulation of impurities. Filtration is a promising technique, which is able to split the main components of the product stream NHCB and OB according to their molecular weight and size. Particularly nanofiltration is utilized for a separation of molecules with a molecular mass of 200 - 1000 $g \cdot mol^{-1}$, where OB with a molecular mass of 209,9 $g \cdot mol^{-1}$ provides a suitable size to stay in the retentate [129]. The solutes in the permeate can further be divided via extraction with ethyl acetate to extract NHCB into the organic phase, while leaving salts, LA, EtOH and EL in the aqueous phase. Subsequently, NHCB can be recycled to the reservoir. OB can probably be received in the solvent mix of the retentate without major impurites, where a following continuous pervaporation or spray drying can be applied to isolate OB without exposing the product to elevated temperatures. Here, especially spray drying gets more and more recognized in pharmaceutical industry as efficient and economic technique for drying temperature sensitive products and is thereby applicable for OB as well [130]. Concluding, the implementation of further process units were not the scope of this thesis, but are required in order to receive OB in purities above 95 (w/w)% and to develop an economic process. The described process is schematically presented in a flowcharts in the supplementary information (fig. 6.8).

A solution to diminish the loss of native Cytc to deactivation, is the replacement of denaturated Cytc with continuously expressed Cytc. The conducted studies in section 3.3 investigated *E. coli* strains as resting cells in a buffer as liquid phase without a nitrogen-source to suppress cell growth. But in addition, expression studies revealed, that a supplementation of 12.5 mM DAC and 6 mM NHCB as well as MeCN lead to a nearly full stop of Cytc expression, as shown in the supplementary information (Fig. 6.9). However, these results are only valid for the applied substrate contents. Thus, studies with lower substrate concentrations could enable Cytc expression. If those conditions can be employed with respect to the selected operation mode, further improvements of conversion and STY are imaginable.

Independent from the applied operation mode and biological aspects, a reliable technique

to measure the reactant concentrations during synthesis is important to react on accumulations or limitations. Offline measurements with chromatography can not respond to fluctuations in the system in appropriate time. Instead inline analytics are able to quantify reactants in real time in the reaction mixture. Here fourier-transformation infra-red spectroscopy is a suitable candidate, quantifying analytes according to vibrations between specific bonds. OB can be identified according to the wavenumber of the carbon-boron heteroatomic bond at $1020\,\mathrm{cm}^{-1}$ [131]. In addition, DAC should also show a noticeable infra-red absorption in the range of 1950 to $2300\,\mathrm{cm}^{-1}$, which can be assigned to the N-N stretching [68]. Finally, NHCB might be identified by its C-N bonds between 1000 to $1400\,\mathrm{cm}^{-1}$ [132]. In summary, FTIR has to be investigated closely within coming studies as inline analytic technique to improve process control.

5 Summary

This thesis aimed for the deep understanding and the improvement of biocatalytic OB synthesis catalyzed by Cytc with whole cell biotransformation. Therefore, experiments investigated the conditions of starting materials and developed a kinetic model. Reaction engineering enhanced process parameters to develop this approach towards industrial relevance.

The substrate investigation focused on NHCB and DAC to describe their behaviour during reaction relevant conditions. The titration determined protonation state of NHCB, the pK_b value to 6.12, where NHBC and NHC-B_2^+ are in equilibrium. This identifies NHCB as semi-strong base and verifies, that the substrate is present in a non-protonated state under reaction conditions at pH 7.4. DAC is a less stable compound compared to NHCB, which was evaluated in hydrolysis and decomposition studies. While the hydrolysis in water can be neglected, the decomposition of DAC to EL reaches a ratio of 10 % of the former DAC concentration. UV-Vis spectrophotometry demonstrated conformational changes of the diazo moiety at temperatures above 60 °C. Here, elongated incubation times and especially temperature elevation up to 80 °C result in an even more severe and faster decay of DAC. Moreover, exposures to daylight lead to a decay of 50% of DAC after 24 h, while after 30 d DAC is completely decayed. Concluding, DAC needs to be stored at -20 °C in a UV-light-proved vessel. Reaction temperatures should not exceed 60 °C during biocatalytic borylation in order to minimize the loss of convertible DAC.

This thesis gave the first mathematical description of biocatalytic borylation with a kinetic reaction model. A temperature screening achieved a 3.25-fold improvement the initial reaction rate with a temperature increase from 25 to 40 °C. Cytcs activity is still present above 40 °C, but decreases exponentially as simultaneously observed foaming indicated cell lysis. Alkaline pH 9 and acidic pH 5 and 6 reduce the initial reaction rate by 15 to 40 % compared to neutral pH 7.4. The kinetic model was based on to the Michaelis-Menten theory and initial reaction rates were determined in dependency of both substrate concentrations. Here, conditions of 6 mM NHCB, 12.5 mM DAC at pH 7.4 and 40 °C result in the highest initial reaction rate of 7.5 $U \cdot mg^{-1}$. A reversible substrate-surplus inhibition was discovered for NHCB leading to significantly reduced initial reaction rate above 6 mM. Although no reversible inhibition by DAC could be identified below 12.5 mM, the DAC-driven deactivation described for P450 was also proven for Cytc, which causes an irreversible inhibition and a complete loss of activity after 30 min incubation at 12.5 mM DAC. No hints for a product inhibition were found below 5 mM OB. A substrate-surplus inhibited double-substrate Michaelis-Menten model determined the kinetic constants v_{max}, $K_{m,NHCB}$, $K_{m,DAC}$ and $K_{i,NHCB}$ by numerical fitting with non-linear regression in Matlab. At 40 °C, kinetic

constants were estimated to v_{max} of 24.1 ± 15.6 U·mg^{-1}, $K_{m,NHCB}$ of 6.4 ± 5.8 mM, $K_{m,DAC}$ of 1.1 ± 0.5 mM and $K_{i,NHCB}$ of 6.2 ± 5.6 mM. The deactivation constant K_{dea} was fitted to 0.165 ± 0.056 min^{-1}. Reaction process simulations evaluated the developed kinetic model, which predicted the biocatalytic OB synthesis reasonably. Initial reaction rates and OB_{final} were estimated precisely, while deviations occurred during broken-order reaction kinetics.

The reaction engineering of biocatalytic borylation aimed for improvements of TTN, OB_{final} and STY. Initial batch mode experiments showed, that purified Cytc, applied in free or immobilized form, is deactivated immediately by DAC. Thus, further experiments focused on whole cell biotransformation. An increase of Cytc content from 1.67 to 9.23 μM enhanced the TTN from 624 to 1397 mol·mol^{-1}, due to immediate conversion of deactivating DAC and yielded an OB_{final} of 12.9 mM. The fed-batch mode minimized the deactivation at different dilution rates D of 0.012 to 0.96 h^{-1}. Here, lower D led to an increase of OB_{final} of 2.76 mM, which meant a 2.5-fold enhancement compared to the full addition of DAC to a content of 12.5 mM in batch mode. The observed effect is particularly prominent at low Cytc contents, since these reactors benefit more from a reduced DAC supply due to their limited conversion of DAC in contrast to reactors with more Cytc, which were capable to convert even higher DAC contents fast enough. As a result, TTNs could be further enhanced to 2273 mol·mol^{-1} by a supplementation of 50 mM glucose, stating an almost 4-fold improvement compared to TTNs at batch synthesis. Moreover, the STY at a D of 0.96 was increased by a factor of over 20 for OD 30 syntheses referred to batch experiments. The results were transferred to scales of 150 and 500 mL and an OB synthesis limited to the molar feed rate of DAC was recorded, holding the present DAC content at zero. Therefore, TTNs increased to 3129 mol·mol^{-1} as well as OB_{final} to 33.4 mM. Experiments in a continuous mode showed elevated molar OB synthesis for reduced residence times, but maximum TTNs of 873 mol·mol^{-1} leave room for further improvements.

Overall, the substrate investigation showed critical behaviour especially of DAC towards temperature and UV-light induced decay. The developed substrate-surplus inhibited double-substrate Michaelis-Menten model with numerically approximated parameters simulated OB synthesis reasonably. Reaction engineering improved TTNs, STY and OB_{final} by the establishment of an adjusted DAC supply to minimized Cytc deactivation.

6 Supplementary Information

6.1 Materials and Methods

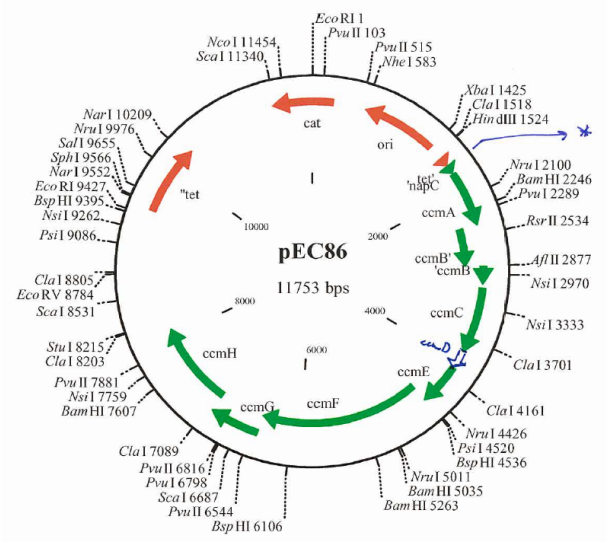

Figure 6.1: Plasmid card of pEC86 with Cytc maturation genes ccmABCDEFGH and a Chl-resistance.

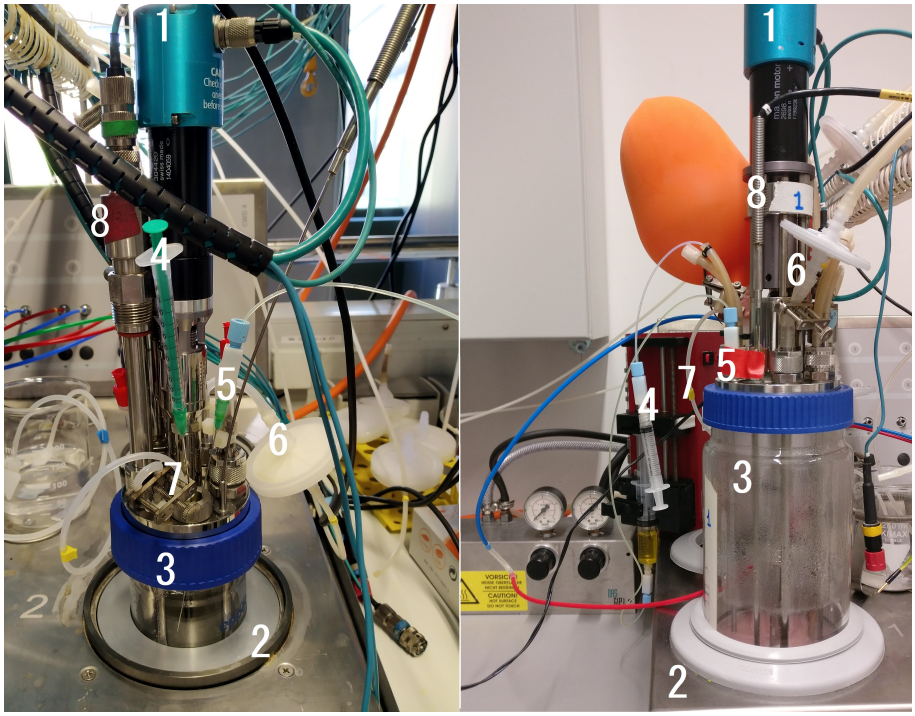

Figure 6.2: DASGIP reactor setup for biocatalytic borylation in 150 mL and 500 mL scale. Equipment consists of 1: stirring motor, 2: heating/cooling unit, 3: reaction vessel, 4: sampling syringe, 5: feed inlet, 6: Ar/N_2 gassing inlet with 0.22 μm sterile filter, 7: gassing outlet, 8: thermo couple.

6.2 Results

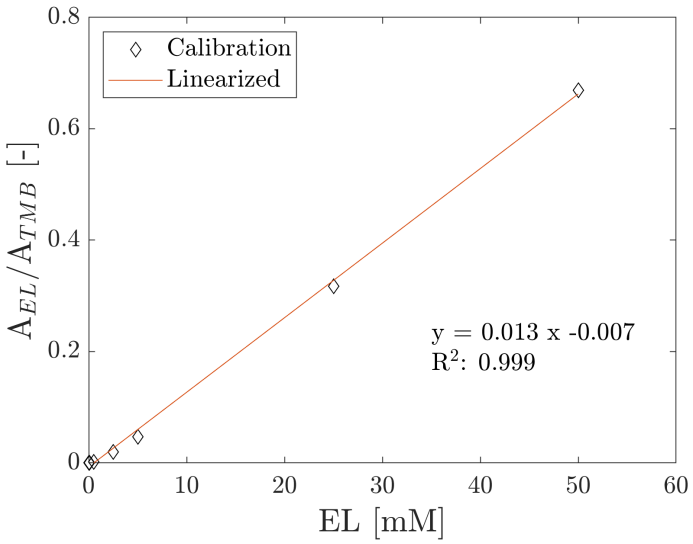

Figure 6.3: Calibration curve of ELfor GC analysis.

Table 6.1: Ratio of peak heights of $\lambda_{DAC,1}$ and $\lambda_{DAC,12}$ for temperatures from r.t. to 85 °C within fingerprint region of DAC in UV-spectroscopy.

Temperature [°C]	$\frac{\lambda_{DAC,1}}{\lambda_{DAC,2}}_{0,min}$	$\frac{\lambda_{DAC,1}}{\lambda_{DAC,2}}_{120,min}$
R.T.	0.412	0.407
55	0.411	0.410
60	0.420	0.430
65	0.429	0.890
75	0.418	1.090
85	0.417	1.190

Kinetic_Parameter_Estimation.m

$File =' Kinetic\_Data.xlsx'$; **%Excelfile**

%Loading of experimental data
$disp('...Loadingexperimentaldata...')$
$C = [xlsread(File,' Summary',' I8 : I21'),$
$xlsread(File,' Summary',' J8 : J21')];$

%Substrate concentration matrix
$cNHCB = C(:, 1)$; **%NHC-borane concentration vector**
$cDAC = C(:, 2)$; **%Diazo-compound concentration vector**
$v\_m = [xlsread(File,' Summary',' K8 : K21')]$; **%Activity matrix**

%Starting parameters
$vmax = 21$; **%U/mg**
$km\_NHCB = 8$; **%[mM]**
$km\_DAC = 4$; **%[mM]**
$ki\_NHCB = 4$; **%[mM]**
$start\_parameter = [vmaxkm\_NHCBkm\_DACki\_NHCB]$; **%As vector 1x4, for easier startparameter reading for functions**

%Non linear regression: For fitting of kinetic parameter
$disp('...FittingofkineticParameter...')$
$[parfit, Res, Jac, Sigma] = nlinfit(C, v\_m, @MMKinetik, start\_parameter)$;
$CInt = nlparci(parfit, Res,' jacobian', Jac)$;
$CInt = abs((CInt(:, 1) - CInt(:, 2))/2)$;
%Display of fitted kinetic parameter
$fprintf('Parameters : \n\t\t, InitialCalculated\t Confi.Int\t Unit\n')$
$formatSpec =' \%s\t\%2.1f \t\%1.3f \t + - \%1.3f \t\%s \n'$;
$kinpara\{`vmax` `kmNHCB` `kmDAC` `kiNHCB`\}$;
$paraunit = \{`U/mg` `mM` `mM` `mM`\}$;
$for\, i = 1 : 4$
$fprintf(formatSpec, kinpara\{i\}, start_parameter(i), parfit(i), CInt(i), paraunit\{i\})end$

%%FUNCTIONS:

%Michaelis-Menten_Equation (Two-Substrates)

$function\, v = MMKinetik(start\_parameter, C)$

$cNHCB = C(:,1);$

$cDAC = C(:,2);$

%Startparameter:

$vmax = start\_parameter(1);$ **%U/mg**

$km\_NHCB = start\_parameter(2);$ **%[mM]**

$km\_DAC = start\_parameter(3);$ **%[mM]**

$ki\_NHCB = start\_parameter(4);$ **%[mM]**

$v = vmax.*cNHCB.*cDAC./(km\_NHCB + cNHCB.*(1 + cNHCB/ki\_NHCB))./$
$(km\_DAC + cDAC);$

end

Inactivation.m

$File =' Kinetic\_Data.xlsx';$**%Excelfile**

%Loading of experimental data

$disp('...Loadingexperimentaldata...')$

$T = [xlsread(File,' Summary',' D202 : D207')];$ **%Substrate concentration matrix**

$t = T(:,1);$ **%DAC concentration vector**

$v\_m = [xlsread(File,' Summary',' F202 : F207')];$ **%Activity matrix**

%Starting parameters

$k = 0.001;$ **%[1/s]**

$start_parameter = [k];$

%Non linear regression: For fitting of kinetic parameter

$disp('...FittingofkineticParameter...')$

$[parfit, Res, Jac, Sigma] = nlinfit(T, v_m, @MMKinetik, start_parameter);$

$CInt = nlparci(parfit, Res,' covar', Sigma);$

$CInt = abs((CInt(:,1) - CInt(:,2))/2);$

%Display of fitted kinetic parameter

$fprintf('Parameters : \n\t\tInitialCalculated\tConfi.Int\tUnit\n')$

$formatSpec =' \%s\backslash t\%2.4f\backslash t\%1.5f\backslash t + -\%1.5f\backslash t\%s\backslash n';$
$kinpara = \{`k`\};$
$paraunit = \{`1/s`\};$
$for\, i = 1$
$fprintf(formatSpec, kinpara\{i\}, start\_parameter(i), parfit(i), CInt(i), paraunit\{i\})$
end

%% FUNCTIONS:
$functionv = MMKinetik(start\_parameter, T)$
$t = T(:, 1);$
$k = start\_parameter(1);$
$v = 7.1 * exp(-k. * t);$
end

OBS.m

$[t, x] = ode45(@Sim, [0\ 120], [6\ 12.5\ 0]);$
$Z = [1, 2, 3, 4, 5, 6, 7, 10, 20, 40, 75, 120];$
$O = [0.156, 0.25, 0.324, 0.389, 0.423, 0.464, 0.494, 0.557, 0.849, 0.866, 0.987, 1.042];$

%%FUNCTIONS
$function[f] = Sim(t, x)$
%Concentration vector x
$NHCB = x(1);$
$DAC = x(2);$
$OB = x(3);$
$e = 24.6882;$
$v = 24.1 * exp(-0.1596 * t) * NHCB * DAC/((6.4 + NHCB * (1 + NHCB/6.2)) * (1.1 + DAC));$
$dNHCBdt = -v * e * (1/1000);$ **%[μmol/min/mg]*[mg_enz]*[(1/1000μM/mM)]**
$dDACdt = -v * e * (1/1000);$
$dOBdt = v * e * (1/1000);$
$f = [dNHCBdt; dDACdt; dOBdt];$
end

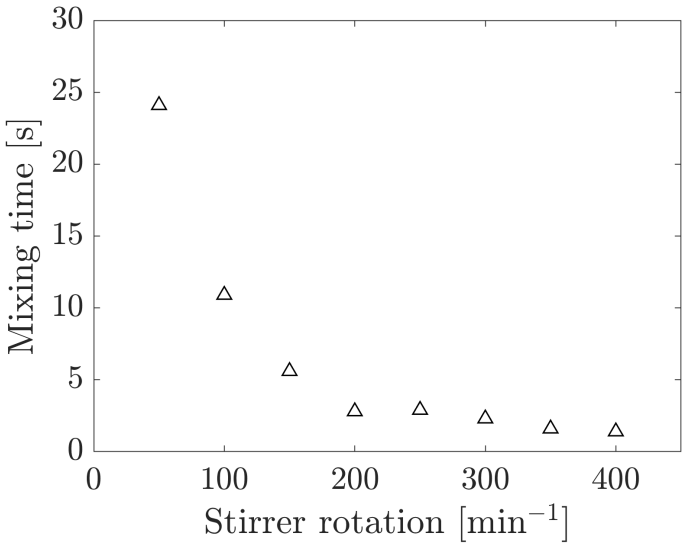

Figure 6.4: Mixing time in dependence of stirrer revolutions in a 500 mL DASGIP reactor with 150 mL liquid reaction volume. Mixing times were determined by adding 1 mL of 1 M NaOH or 1 M HCl into M9-N buffer supplemented with 0.2 mL phenylalanine (1 % (w/v) in EtOH).

6.3 Discussion and Outlook

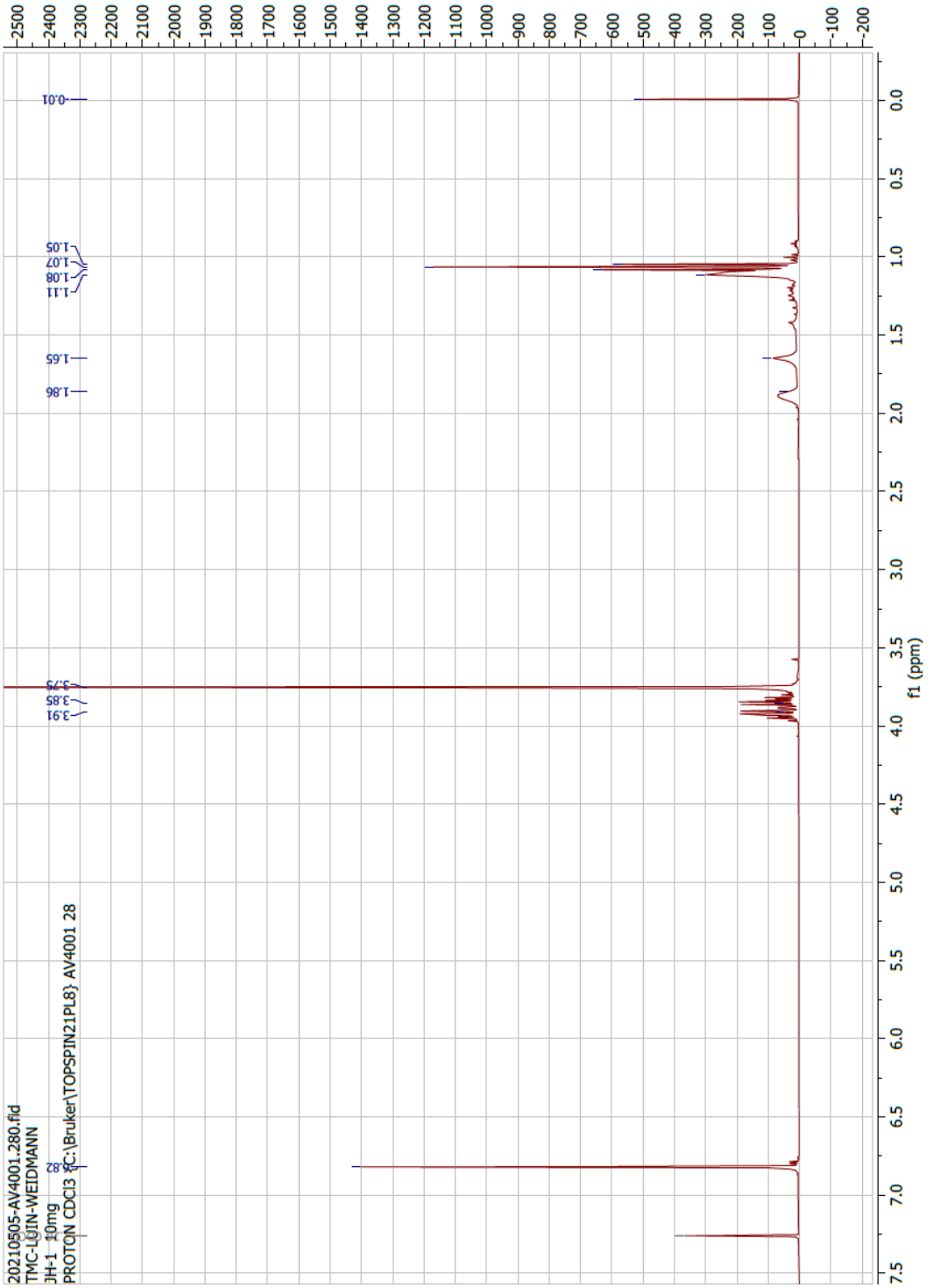

Figure 6.5: ^{1}H-NMR spectra of OB synthesized at the Institute of Technical Biocatalysis, recorded with a Bruker Topspin (Bruker Corporation, Billerica, USA) at 400 MHz in Chloroform-δ) at the University of Hamburg (Hamburg, Germany).

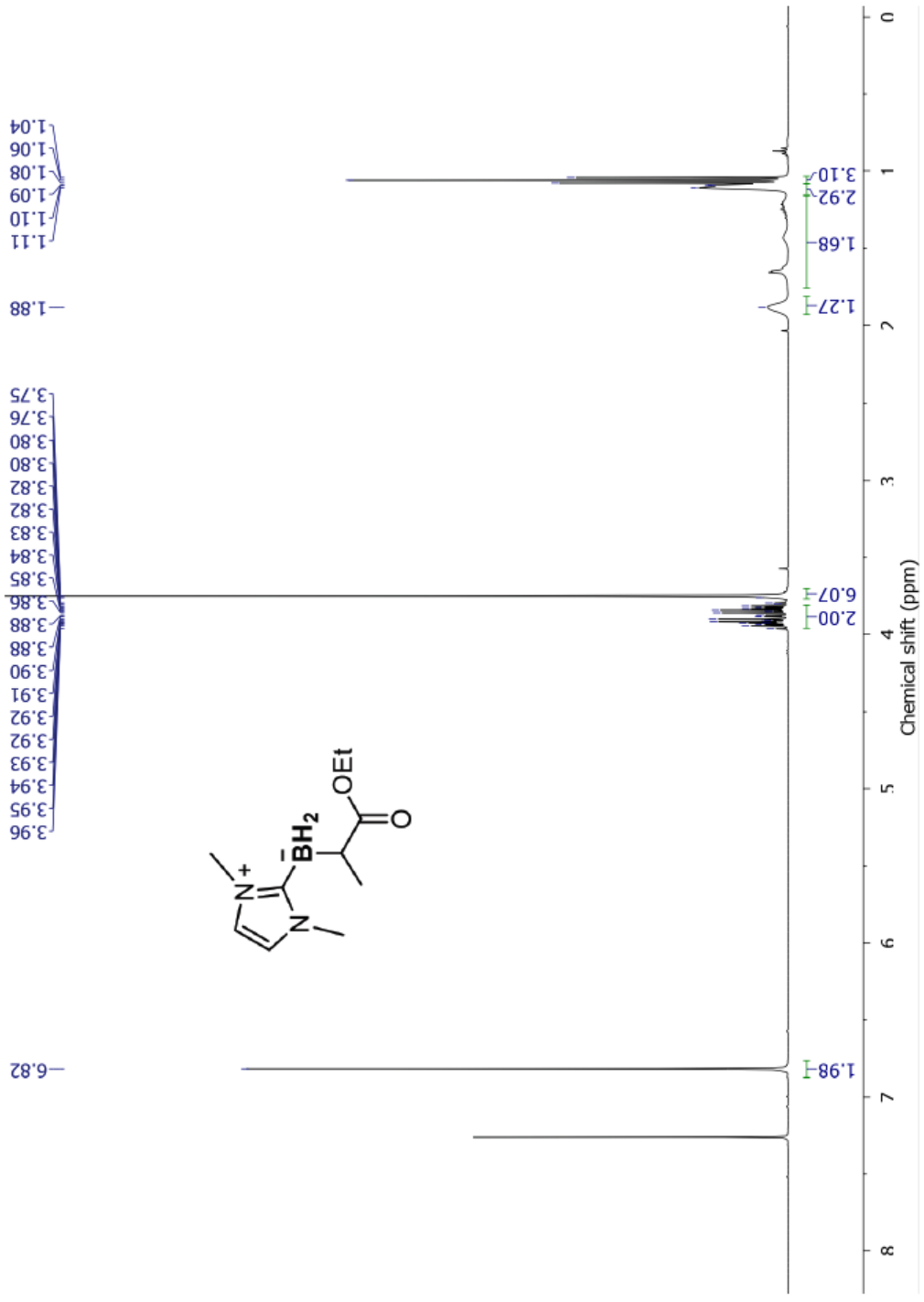

Figure 6.6: ^{1}H-NMR spectra of OB synthesized at the California Institute of Technology, recorded at 400 MHz in Chloroform-δ).

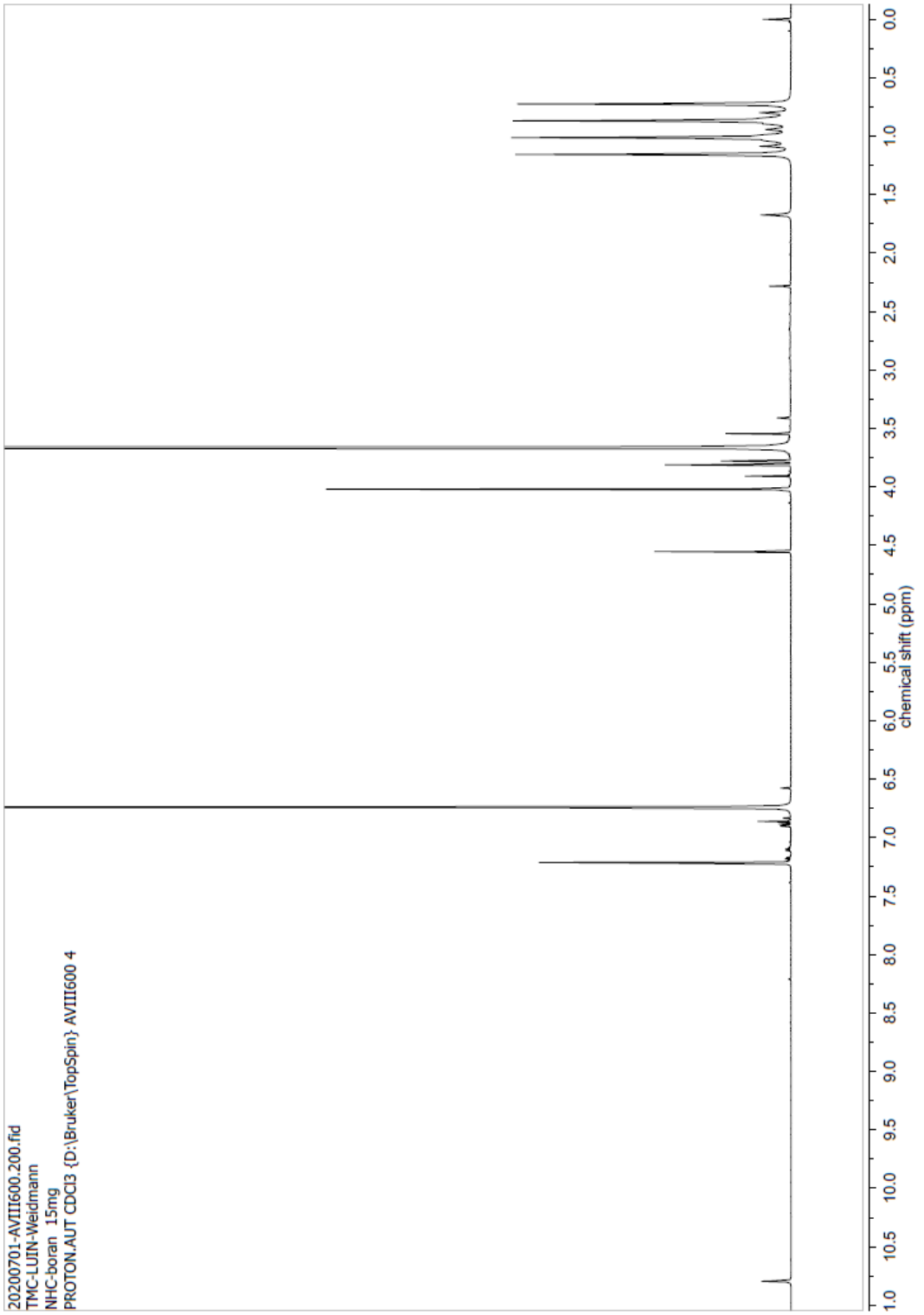

Figure 6.7: ^{1}H-NMR spectra of NHCB synthesized at the Institute of Technical Biocatalysis, recorded with a Bruker Topspin (Bruker Corporation, Billerica, USA) at 400 MHz in Chloroform-δ) at the University of Hamburg (Hamburg, Germany).

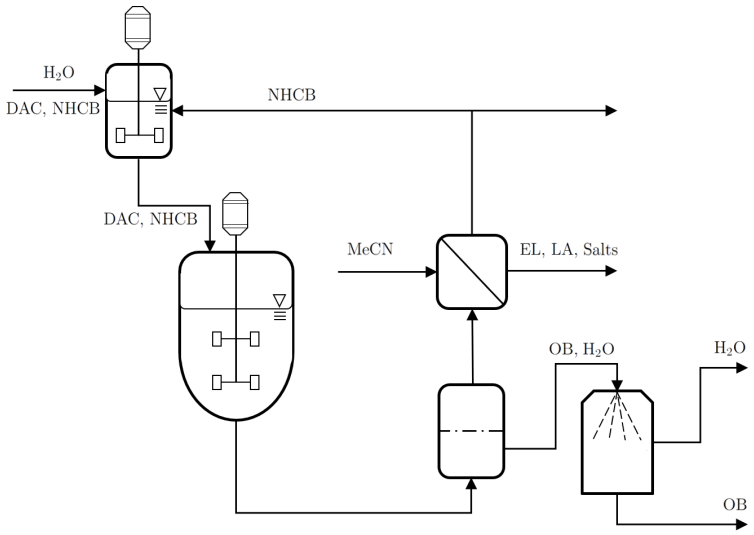

Figure 6.8: Flowchart of a desired continuous process for biocatalytic borylation of OB.

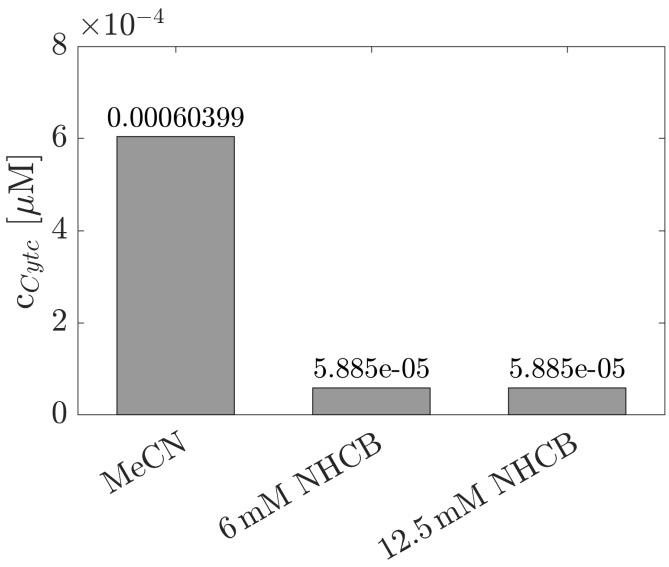

Figure 6.9: Expression of Cytc BOR^{R1} in *E. coli* BL21 DE3 under presence of either 12.5 mM DAC (OD 1.7), 6 mM NHCB (OD 1.7) or 5 % (v/v) MeCN (OD 3.7). Final c_{Cytc} reached only trace amount, compared to expression without added species (1 - 2 μM at OD 5).

Bibliography

[1] D. Mattanovich, M. Sauer, and B. Gasser. Yeast biotechnology: teaching the old dog new tricks. *Microbial cell factories*, 13(1):34, 2014.

[2] K. Nemcová, E. Breierová, R. Vadkertiová, and J. Molnárová. The diversity of yeasts associated with grapes and musts of the strekov winegrowing region, slovakia. *Folia microbiologica*, 60(2):103–109, 2015.

[3] H. Klefenz. *Industrial pharmaceutical biotechnology*. Wiley-VCH, Weinheim, 1. reprint edition, 2005.

[4] T. J. Laughlin and T. M. Ferrell. Biotechnology in the cosmetics industry. *Nature Biotechnology*, 5(10):1035–1037, 1987.

[5] H. Wang, Y. Tao, M. Temudo, M. Schooneveld, H. Bijl, N. Ren, M. Wolf, C. Heine, A. Foerster, V. Pelenc, J. Kloek, J. B. van Lier, and M. de Kreuk. An integrated approach for efficient biomethane production from solid bio-wastes in a compact system. *Biotechnology for biofuels*, 8:62, 2015.

[6] O. V. Singh and S. P. Harvey. *Sustainable Biotechnology*. Springer Netherlands, Dordrecht, 2010.

[7] M. Cornelissen, A. Małyska, A. K. Nanda, R. K. Lankhorst, M. A. J. Parry, V. R. Saltenis, M. Pribil, P. Nacry, D. Inzé, and A. Baekelandt. Biotechnology for tomorrow's world: Scenarios to guide directions for future innovation. *Trends in biotechnology*, 39(5):438–444, 2021.

[8] Fritsche, U., Brunori, G., Chiaramonti, D., Galanakis, C., Hellweg, S., Matthews, R. and Panoutsou, C. *Future transitions for the Bioeconomy towards Sustainable Development and a Climate-Neutral Economy - Knowledge Synthesis Final Report*.

[9] United Nations. *Transforming our World: The 2030 Agenda for Sustainable Development*. 2015.

[10] L. Lange, V. Parmar, and A. Meyer. Biocatalysis. In *Encyclopedia of Sustainable Technologies*, pages 663–673. Elsevier, 2017.

[11] J.-P. Meijnen, H. de Winde, and H. Ruijssenaars. Sustainable production of fine chemicals by the solvent-tolerant pseudomonas putida s12 using lignocellulosic feedstock. *INTERNATIONAL SUGAR JOURNAL*, 113(1345), 2011.

[12] G. M. Cooper. *The cell: A molecular approach*. ASM Press and Sinauer Associates, Washington, DC and Sunderland, Mass., 2. ed. edition, 2000.

[13] E. L. Bell, W. Finnigan, S. P. France, A. P. Green, M. A. Hayes, L. J. Hepworth, S. L. Lovelock, H. Niikura, S. Osuna, E. Romero, K. S. Ryan, N. J. Turner, and S. L. Flitsch. Biocatalysis. *Nature Reviews Methods Primers*, 1(1):46, 2021.

[14] S. E. Thomas. *Organic synthesis: The roles of boron and silicon*, volume 1 of *Oxford chemistry primers*. Oxford Univ. Press, Oxford, reprinted. edition, 1994.

[15] *Mechanism and Synthesis*, volume 10 of *Open University course S205, molecular world*. Royal Society of Chemistry, Cambridge, 2002.

[16] Stephen K. and Ritter. Boron chemistry branches out: Electron poor but chemically rich element with a storied past continues to surprise with a surge of new developments. *Chemical & Engineering News*, 94(30), 2016.

[17] R. Zenk and S. Partzsch. Organic boronic acids and boronic acid esters in industrial synthesis. *ChemInform*, 35(25), 2004.

[18] J. W.B. Fyfe and A. J.B. Watson. Recent developments in organoboron chemistry: Old dogs, new tricks. *Chem*, 3(1):31–55, 2017.

[19] T. Onak. *Organoborane chemistry*. Organometallic chemistry. Academic Press, New York, 1975.

[20] C. Alayrac, S. Lakhdar, I. Abdellah, and A.-C. Gaumont. Recent advances in synthesis of p-bh3 compounds. *Topics in current chemistry*, 361:1–82, 2015.

[21] S. B. J. Kan, X. Huang, Y. Gumulya, K. Chen, and F. H. Arnold. Genetically programmed chiral organoborane synthesis. *Nature*, 552(7683):132–136, 2017.

[22] E. Negishi. Aliphatic organoboron compounds. In *Comprehensive Organometallic Chemistry*, pages 265–301. Elsevier, 1982.

[23] D. G. Hall. *Boronic Acids*. Wiley-VCH Verlag GmbH & Co. KGaA, Weinheim, Germany, 2011.

[24] T. Ishiyama, Y. Nobuta, J. F. Hartwig, and N. Miyaura. Room temperature borylation of arenes and heteroarenes using stoichiometric amounts of pinacolborane catalyzed

by iridium complexes in an inert solvent. *Chemical communications (Cambridge, England)*, (23):2924–2925, 2003.

[25] N.. Miyaura and A. Suzuki. Palladium-catalyzed cross-coupling reactions of organoboron compounds. *Chemical Reviews*, 95(7):2457–2483, 1995.

[26] T. König, D. Männel, W. D. Habicher, and K. Schwetlick. Organoboron antioxidants: Part 1—boric acid derivatives as primary antioxidants. *Polymer Degradation and Stability*, 22(2):137–145, 1988.

[27] P. S. Coghi, Y. Zhu, H. Xie, N. S. Hosmane, and Y. Zhang. Organoboron compounds: Effective antibacterial and antiparasitic agents. *Molecules (Basel, Switzerland)*, 26(11), 2021.

[28] A. F. Littke and G. C. Fu. Palladium-catalyzed coupling reactions of aryl chlorides. *Angewandte Chemie International Edition*, 41(22):4176–4211, 2002.

[29] L. Jia, X. Yang, C. L. Stern, and T. J. Marks. Cationic metallocene polymerization catalysts based on tetrakis(pentafluorophenyl)borate and its derivatives. probing the limits of anion "noncoordination" via a synthetic, solution dynamic, structural, and catalytic olefin polymerization study. *Organometallics*, 16(5):842–857, 1997.

[30] N. Corrigan, K. Jung, and C. Boyer. Merging new organoborane chemistry with living radical polymerization. *Chem*, 6(6):1212–1214, 2020.

[31] H. C. Brown. Hydroboration—a powerful synthetic tool. *Tetrahedron*, 12(3):117–138, 1961.

[32] H. DeFrancesco, J. Dudley, and A. Coca. Boron chemistry: An overview. In A. Coca, editor, *Boron Reagents in Synthesis*, volume 1236 of *ACS Symposium Series*, pages 1–25. American Chemical Society, Washington, DC, 2016.

[33] R. S. MONSON. Hydroboration. In *Advanced Organic Synthesis*, pages 31–38. Elsevier, 1971.

[34] J. M. Clay and E. Vedejs. Hydroboration with pyridine borane at room temperature. *Journal of the American Chemical Society*, 127(16):5766–5767, 2005.

[35] J. A. Souto, R. A. Stockman, and S. V. Ley. Development of a flow method for the hydroboration/oxidation of olefins. *Organic & biomolecular chemistry*, 13(13):3871–3877, 2015.

[36] J. F. Hartwig. Borylation and silylation of c-h bonds: a platform for diverse c-h bond functionalizations. *Accounts of chemical research*, 45(6):864–873, 2012.

[37] H. Braunschweig and F. Guethlein. Transition-metal-catalyzed synthesis of diboranes(4). *Angewandte Chemie International Edition*, 50(52):12613–12616, 2011.

[38] K. C. Lam, T. B. Marder, and Z. Lin. Mechanism of the palladium-catalyzed borylation of aryl halides with pinacolborane. *Organometallics*, 29(7):1849–1857, 2010.

[39] *Comprehensive organometallic chemistry III.* Elsevier, Amsterdam, 2007.

[40] G. A. Molander, S. L. J. Trice, S. M. Kennedy, S. D. Dreher, and M. T. Tudge. Scope of the palladium-catalyzed aryl borylation utilizing bis-boronic acid. *Journal of the American Chemical Society*, 134(28):11667–11673, 2012.

[41] H. Moody. Better borylation. *Nature Chemistry*, 5(2):78–79, 2013.

[42] M. B. Smith and J. March. *March's advanced organic chemistry: Reactions, mechanisms, and structure.* Wiley, New York and Weinheim, 6. ed. edition, 2007.

[43] H. C. Brown, N. R. de Lue, Y. Yamamoto, K. Maruyama, T. Kasahara, S. Murahashi, and A. Sonoda. Organoboranes. 23. reaction of organolithium and grignard reagents with .alpha.-bromoalkylboronate esters. a convenient, essentially quantitative procedure for the synthesis of tertiary alkyl-, benzyl-, propargyl-, and stereospecific allylboranes. *The Journal of Organic Chemistry*, 42(25):4088–4092, 1977.

[44] D. A. Shirley. The synthesis of ketones from acid halides and organometallic compounds of magnesium, zinc, and cadmium. In *Organic Reactions*, pages 28–58. John Wiley & Sons, Inc, Hoboken, NJ, USA, 2004.

[45] T. P. Povlock and W. T. Lippincott. The reaction of trimethoxyboroxine with aromatic grignard reagents. a new synthesis of borinic acids 1. *Journal of the American Chemical Society*, 80(20):5409–5411, 1958.

[46] K. Maruyama and T. Katagiri. Mechanism of the grignard reaction. *Journal of Physical Organic Chemistry*, 2(3):205–213, 1989.

[47] A. H. Allen and A. R. Tankard. The determination of boric acid in cider, fruits, etc. *The Analyst*, 29(October):301, 1904.

[48] K. Wolkenstein, H. Sun, H. Falk, and C. Griesinger. Structure and absolute configuration of jurassic polyketide-derived spiroborate pigments obtained from microgram quantities. *Journal of the American Chemical Society*, 137(42):13460–13463, 2015.

[49] J. Kohno, T. Kawahata, T. Otake, M. Morimoto, H. Mori, N. Ueba, M. Nishio, A. Kinumaki, S. Komatsubara, and K. Kawashima. Boromycin, an anti-hiv antibiotic. *Bioscience, biotechnology, and biochemistry*, 60(6):1036–1037, 1996.

[50] S. T. Miller, K. B. Xavier, S. R. Campagna, M. E. Taga, M. F. Semmelhack, B. L. Bassler, and F. M. Hughson. Salmonella typhimurium recognizes a chemically distinct form of the bacterial quorum-sensing signal ai-2. *Molecular cell*, 15(5):677–687, 2004.

[51] X. Chen, S. Schauder, N. Potier, A. van Dorsselaer, I. Pelczer, B. L. Bassler, and F. M. Hughson. Structural identification of a bacterial quorum-sensing signal containing boron. *Nature*, 415(6871):545–549, 2002.

[52] G. Feller and C. Gerday. Psychrophilic enzymes: hot topics in cold adaptation. *Nature reviews. Microbiology*, 1(3):200–208, 2003.

[53] C. Vieille and G. J. Zeikus. Hyperthermophilic enzymes: sources, uses, and molecular mechanisms for thermostability. *Microbiology and molecular biology reviews : MMBR*, 65(1):1–43, 2001.

[54] C. Wandrey, A. Liese, and D. Kihumbu. Industrial biocatalysis: Past, present, and future. *Organic process research & development*, 4(4):286–290, 2000.

[55] R. Mertens and A. Liese. Biotechnological applications of hydrogenases. *Current opinion in biotechnology*, 15(4):343–348, 2004.

[56] S. Davey. Enantioselectivity evolved. *Nature Chemistry*, 2008.

[57] R. Yuryev, S. Strompen, and A. Liese. Coupled chemo(enzymatic) reactions in continuous flow. *Beilstein journal of organic chemistry*, 7:1449–1467, 2011.

[58] J. Brummund, M. Müller, T. Schmitges, I. Kaluzna, D. Mink, L. Hilterhaus, and A. Liese. Process development for oxidations of hydrophobic compounds applying cytochrome p450 monooxygenases in-vitro. *Journal of biotechnology*, 233:143–150, 2016.

[59] A. G. McDonald and K. F. Tipton. Enzyme nomenclature and classification: the state of the art. *The FEBS journal*, 2021.

[60] M. Stelter, A. M. P. Melo, M. M. Pereira, C. M. Gomes, G. O. Hreggvidsson, S. HJORLEIFSDOTTIR, L. M. Saraiva, M. Teixeira, and M. Archer. A novel type of monoheme cytochrome c: biochemical and structural characterization at 1.23 a resolution of rhodothermus marinus cytochrome c. *Biochemistry*, 47(46):11953–11963, 2008.

[61] P. L. Yeagle. *The Membranes of Cells*. Elsevier Science, s.l., 3rd ed. edition, 2016.

[62] M. Negrerie, S. Cianetti, M. H. Vos, J.-L. Martin, and S. G. Kruglik. Ultrafast heme dynamics in ferrous versus ferric cytochrome c studied by time-resolved resonance raman and transient absorption spectroscopy. *The journal of physical chemistry. B*, 110(25):12766–12781, 2006.

[63] G. Battistuzzi, M. Borsari, and M. Sola. Redox properties of cytochrome c. *Antioxidants & redox signaling*, 3(2):279–291, 2001.

[64] R. M. Roat-Malone. *Bioinorganic chemistry: A short course*. Wiley-Interscience, Hoboken, New Jersey, 2002.

[65] S. B. J. Kan, R. D. Lewis, K. Chen, and F. H. Arnold. Directed evolution of cytochrome c for carbon-silicon bond formation: Bringing silicon to life. *Science (New York, N.Y.)*, 354(6315):1048–1051, 2016.

[66] P. S. Coelho, Z. J. Wang, M. E. Ener, S. A. Baril, A. Kannan, F. H. Arnold, and E. M. Brustad. A serine-substituted p450 catalyzes highly efficient carbene transfer to olefins in vivo. *Nature chemical biology*, 9(8):485–487, 2013.

[67] G. A. ALFREDSSON, J. K. Kristiansson, S. HJORLEIFSDOTTIR, and K. O. STETTER. Rhodothermus marinus, gen. nov., sp. nov., a thermophilic, halophilic bacterium from submarine hot springs in iceland. *Microbiology*, 134(2):299–306, 1988.

[68] M. Regitz and G. Maas. *Diazo compounds: Properties and synthesis*. Academic Press, Orlando, 1. print edition, 1986.

[69] S. P. Green, K. M. Wheelhouse, A. D. Payne, J. P. Hallett, P. W. Miller, and J. A. Bull. Thermal stability and explosive hazard assessment of diazo compounds and diazo transfer reagents. *Organic process research & development*, 24(1):67–84, 2020.

[70] V. Fasano and M. J. Ingleson. Expanding water/base tolerant frustrated lewis pair chemistry to alkylamines enables broad scope reductive aminations. *Chemistry (Weinheim an der Bergstrasse, Germany)*, 23(9):2217–2224, 2017.

[71] X. Li and D. P. Curran. Insertion of reactive rhodium carbenes into boron-hydrogen bonds of stable n-heterocyclic carbene boranes. *Journal of the American Chemical Society*, 135(32):12076–12081, 2013.

[72] Q.-Q. Cheng, Z.-F. Zhu, Y.-Z. Zhang, X.-L. Xie, and Q.-L. Zhou. Copper-catalyzed b-h bond insertion reaction: a highly efficient and enantioselective c-b bond-forming reaction with amine-borane and phosphine-borane adducts. *Journal of the American Chemical Society*, 135(38):14094–14097, 2013.

[73] Y. Wang, P. Xue, M. Cao, T. Yu, S. T. Lane, and H. Zhao. Directed evolution: Methodologies and applications. *Chemical Reviews*, 121(20):12384–12444, 2021.

[74] H. Renata, R. D. Lewis, M. J. Sweredoski, A. Moradian, S. Hess, Z. J. Wang, and F. H. Arnold. Identification of mechanism-based inactivation in p450-catalyzed cyclopropanation facilitates engineering of improved enzymes. *Journal of the American Chemical Society*, 138(38):12527–12533, 2016.

[75] Fundamentals of chemical reaction kinetics. In J. Ancheyta, editor, *Chemical Reaction Kinetics*, pages 1–53. John Wiley & Sons, Ltd, Chichester, UK, 2017.

[76] D. A. Vallero. Environmental biochemodynamic processes. In *Environmental Biotechnology*, pages 89–150. Elsevier, 2016.

[77] J. Gao, Y. Wang, Y. Ping, D. Hu, G. Xu, F. Gu, and F. Su. A thermodynamic analysis of methanation reactions of carbon oxides for the production of synthetic natural gas. *RSC Advances*, 2(6):2358, 2012.

[78] C. A. Lewis and R. Wolfenden. Influence of pressure on the equilibrium of hydration of aliphatic aldehydes. *Journal of the American Chemical Society*, 95(20):6685–6688, 1973.

[79] Y. Wang, M. Kunz, S. Siebers, H. Rollins, J. Gleaves, G. Yablonsky, and R. Fushimi. Transient kinetic experiments within the high conversion domain: The case of ammonia decomposition. *Catalysts*, 9(1):104, 2019.

[80] D. Vasic-Racki, J. Bongs, U. Schörken, G. A. Sprenger, and A. Liese. Modeling of reaction kinetics for reactor selection in the case of l-erythrulose synthesis. *Bioprocess and biosystems engineering*, 25(5):285–290, 2003.

[81] H. L. Le Chatelier. On a general expression of the laws of chemical equlibrium. *Comptes rendus de l'Académie des sciences*, (99):786–789.

[82] A. Cornish-Bowden. *Fundamentals of enzyme kinetics*. Wiley-Blackwell, Weinheim, 4., completely revised and greatly enlarged ed. edition, 2012.

[83] S. H. Hristova and A. M. Zhivkov. Isoelectric point of free and adsorbed cytochrome c determined by various methods. *Colloids and Surfaces B: Biointerfaces*, 174:87–94, 2019.

[84] J. C. Wilks and J. L. Slonczewski. ph of the cytoplasm and periplasm of escherichia coli: rapid measurement by green fluorescent protein fluorimetry. *Journal of bacteriology*, 189(15):5601–5607, 2007.

[85] J. L. Slonczewski, B. P. Rosen, J. R. Alger, and R. M. Macnab. ph homeostasis in escherichia coli: measurement by 31p nuclear magnetic resonance of methylphosphonate and phosphate. *Proceedings of the National Academy of Sciences of the United States of America*, 78(10):6271–6275, 1981.

[86] E. Laurenti, G. Suriano, E. M. Ghibaudi, and R. P. Ferrari. Ionic strength and ph effect on the fe(iii)-imidazolate bond in the heme pocket of horseradish peroxidase: an epr and uv–visible combined approach. *Journal of Inorganic Biochemistry*, 81(4):259–266, 2000.

[87] V. Gold, editor. *The IUPAC Compendium of Chemical Terminology*. International Union of Pure and Applied Chemistry (IUPAC), Research Triangle Park, NC, 2019.

[88] R. G. Duggleby and J. F. Morrison. Progress curve analysis in enzyme kinetics. model discrimination and parameter estimation. *Biochimica et Biophysica Acta (BBA) - Enzymology*, 526(2):398–409, 1978.

[89] N. Nikolova, K. Tenekedjiev, and K. Kolev. Uses and misuses of progress curve analysis in enzyme kinetics. *Central European journal of biology*, 3(4):345–350, 2008.

[90] Y.-S. Cho and H.-S. Lim. Comparison of various estimation methods for the parameters of michaelis-menten equation based on in vitro elimination kinetic simulation data. *Translational and clinical pharmacology*, 26(1):39–47, 2018.

[91] R. J. Leatherbarrow. Use of nonlinear regression to analyze enzyme kinetic data: Application to situations of substrate contamination and background subtraction. *Analytical Biochemistry*, 184(2):274–278, 1990.

[92] S. Li. *Reaction engineering*. Butterworth-Heinemann an imprint of Elsevier, Oxford, UK and Cambridge, MA, 2017.

[93] H. Chmiel. Bioreaktoren. In H. Chmiel, editor, *Bioprozesstechnik*, pages 197–236. Spektrum Akademischer Verlag, Heidelberg, 2011.

[94] Safety in chemical reaction engineering. In *Modeling of Chemical Kinetics and Reactor Design*, pages 910–1033. Elsevier, 2001.

[95] H. Chmiel, editor. *Bioprozesstechnik*. Spektrum Akademischer Verlag, Heidelberg, 2011.

[96] D. Bonvin. Optimal operation of batch reactors—a personal view. *Journal of Process Control*, 8(5-6):355–368, 1998.

[97] T. Yamanè and S. Shimizu. Fed-batch techniques in microbial processes. In *Bioprocess Parameter Control*, volume 30 of *Advances in Biochemical Engineering/Biotechnology*, pages 147–194. Springer-Verlag, Berlin/Heidelberg, 1984.

[98] C. Bideaux, S. Alfenore, X. Cameleyre, C. Molina-Jouve, J.-L. Uribelarrea, and S. E. Guillouet. Minimization of glycerol production during the high-performance fed-batch ethanolic fermentation process in saccharomyces cerevisiae, using a metabolic model as a prediction tool. *Applied and environmental microbiology*, 72(3):2134–2140, 2006.

[99] P. K. Robinson. Enzymes: principles and biotechnological applications. *Essays in biochemistry*, 59:1–41, 2015.

[100] P. de Santis, L.-E. Meyer, and S. Kara. The rise of continuous flow biocatalysis – fundamentals, very recent developments and future perspectives. *Reaction Chemistry & Engineering*, 5(12):2155–2184, 2020.

[101] H. S. Fogler. *Essentials of chemical reaction engineering*. Prentice Hall international series in the physical and chemical engineering sciences. Prentice-Hall, Upper Saddle River, NJ, 2011.

[102] S. Gardner, T. Kawamoto, and Dennis P. Curran. 1,3-dimethylimidazoyl-2-ylidene borane. *Organic Syntheses*, (92):342–335, 2015.

[103] M. M. Bradford. A rapid and sensitive method for the quantitation of microgram quantities of protein utilizing the principle of protein-dye binding. *Analytical Biochemistry*, 72:248–254, 1976.

[104] G. Rasul, G. K. S. Prakash, and G. A. Olah. Protonated borane−lewis base complexes bh 4 x + (x = nh 3 , ph 3 , h 2 o, h 2 s, co) 1. *Inorganic Chemistry*, 38(1):44–47, 1999.

[105] C. E. Mortimer and U. Müller. *Chemie: Das Basiswissen der Chemie ; 128 Tabellen*. Thieme, Stuttgart, 10., überarb. aufl. edition, 2010.

[106] D. P. Curran, A. Solovyev, B. M. Makhlouf, L. Fensterbank, M. Malacria, and E. Lacôte. Synthesis and reactions of n-heterocyclic carbene boranes. *Angewandte Chemie International Edition*, 50(44):10294–10317, 2011.

[107] M. Ferrer, T. N. Chernikova, M. M. Yakimov, P. N. Golyshin, and K. N. Timmis. Chaperonins govern growth of escherichia coli at low temperatures. *Nature Biotechnology*, 21(11):1267, 2003.

[108] A. Etoc, F. Delvigne, J. P. Lecomte, and P. Thonart. Foam control in fermentation bioprocess. *Applied Biochemistry and Biotechnology*, 130(1-3):392–404, 2006.

[109] M. Yoshino and K. Murakami. Analysis of the substrate inhibition of complete and partial types. *SpringerPlus*, 4:292, 2015.

[110] J.-B. Du Prel, G. Hommel, B. Röhrig, and A. Blettner. Confidence interval or p-value?: part 4 of a series on evaluation of scientific publications. *Deutsches Arzteblatt international*, 106(19):335–339, 2009.

[111] A. Liese, M. Karutz, J. Kamphuis, C. Wandrey, and U. Kragl. Enzymatic resolution of 1-phenyl-1,2-ethanediol by enantioselective oxidation: Overcoming product inhibition by continuous extraction. *Biotechnology and Bioengineering*, 51(5):544–550, 1996.

[112] S. Wu, R. Snajdrova, J. C. Moore, K. Baldenius, and U. T. Bornscheuer. Biocatalysis: Enzymatic synthesis for industrial applications. *Angewandte Chemie International Edition*, 60(1):88–119, 2021.

[113] W. Kühlbrandt. Structure and function of mitochondrial membrane protein complexes. *BMC biology*, 13:89, 2015.

[114] O. Levenspiel. *Chemical reaction engineering*. Wiley, Hoboken, NJ, 3. ed. edition, 1999.

[115] G. Emig and E. Klemm. *Technische Chemie: Einführung in die chemische Reaktionstechnik ; mit 47 Tabellen und 35 Rechenbeispielen*. Springer-Lehrbuch. Springer, Berlin and Heidelberg, 5., aktualisierte und erg. aufl. edition, 2005.

[116] H. S. Fogler and M. N. Gürmen. *Elements of chemical reaction engineering*. Prentice Hall PTR/Pearson Education Internat, Upper Saddle River, NJ, 4. ed. edition, 2006.

[117] K. L. Shaw, G. R. Grimsley, G. I. Yakovlev, A. A. Makarov, and C. N. Pace. The effect of net charge on the solubility, activity, and stability of ribonuclease sa. *Protein science : a publication of the Protein Society*, 10(6):1206–1215, 2001.

[118] P. Novák and V. Havlíček. Protein extraction and precipitation. In *Proteomic Profiling and Analytical Chemistry*, pages 51–62. Elsevier, 2016.

[119] J. Li, W. Han, and Y. Yu. Chromatography method. In T. Ogawa, editor, *Protein Engineering - Technology and Application*. InTech, 2013.

[120] C. S. Vestling and D. T. Warner. The isoelectric points of threonine and some related compounds. *Journal of Biological Chemistry*, 144(3):687–690, 1942.

[121] M. Lambros, X. Pechuan-Jorge, D. Biro, K. Ye, and A. Bergman. Emerging adaptive strategies under temperature fluctuations in a laboratory evolution experiment of escherichia coli. *Frontiers in microbiology*, 12:724982, 2021.

[122] C. A. White-Ziegler, A. J. Malhowski, and S. Young. Human body temperature (37degrees c) increases the expression of iron, carbohydrate, and amino acid utilization genes in escherichia coli k-12. *Journal of bacteriology*, 189(15):5429–5440, 2007.

[123] E. Z. Ron and B. D. Davis. Growth rate of escherichia coli at elevated temperatures: Limitation by methionine. *Journal of bacteriology*, 1971(2):391–396, 107.

[124] C. Fernandez-Lozano, M. Gestal, C. R. Munteanu, J. Dorado, and A. Pazos. A methodology for the design of experiments in computational intelligence with multiple regression models. *PeerJ*, 4:e2721, 2016.

[125] I. H. Sarker. Machine learning: Algorithms, real-world applications and research directions. *SN computer science*, 2(3):160, 2021.

[126] L. Arnaut. Elementary reactions in solution. In *Chemical Kinetics*, pages 263–293. Elsevier, 2021.

[127] G. B. Postnikova, S. V. Tselikova, and Sivozhelezov V. S. Study of electron transport in heme proteins. x. effect of ph, ionic strength, and zinc ions and the rate of ferricytochrome c reduction by oxymyoglobin from swine heart. *Molekularnaia biologiia*, 26(4):880–890, 1992.

[128] P. E. P. Burke, Campos, C. B. de L., L. F. Da Costa, and M. G. Quiles. A biochemical network modeling of a whole-cell. *Scientific reports*, 10(1):13303, 2020.

[129] L. G. Peeva, M. Sairam, and A. G. Livingston. Nanofiltration operations in nonaqueous systems. In *Comprehensive Membrane Science and Engineering*, pages 91–113. Elsevier, 2010.

[130] A. Ziaee, A. B. Albadarin, L. Padrela, T. Femmer, E. O'Reilly, and G. Walker. Spray drying of pharmaceuticals and biopharmaceuticals: Critical parameters and experimental process optimization approaches. *European journal of pharmaceutical sciences : official journal of the European Federation for Pharmaceutical Sciences*, 127:300–318, 2019.

[131] J. Romanos, M. Beckner, D. Stalla, A. Tekeei, G. Suppes, S. Jalisatgi, M. Lee, F. Hawthorne, J. D. Robertson, L. Firlej, B. Kuchta, C. Wexler, P. Yu, and P. Pfeifer. Infrared study of boron–carbon chemical bonds in boron-doped activated carbon. *Carbon*, 54:208–214, 2013.

[132] B. Smith. Organic nitrogen compounds, part i: Introduction: Organic nitrogen compounds, part i: Introduction. *Spectroscopy*, 34(1):10–15, 2019.